HOKKAIDO UNIVERSITY

Title	Characteristics of stiffness and strength mobilization in steel slag-mixed dredged clays from immediately after mixing
Author(s)	Weerakoon Mudiyanselage, Nilan Ranjana Weerakoon
Degree Grantor	北海道大学
Degree Name	博士(工学)
Dissertation Number	甲第13344号
Issue Date	2018-09-25
DOI	https://doi.org/10.14943/doctoral.k13344
Doc URL	https://hdl.handle.net/2115/71813
Type	doctoral thesis
File Information	Weerakoon_Mudiyanselage_Nilan_Ranjana_Weerakoon.pdf

Hokkaido University Collection of Scholarly and Academic Papers : HUSCAP

Characteristics of stiffness and strength mobilization in steel slag-mixed dredged clays from immediately after mixing

By

Weerakoon Mudiyanselage Nilan Ranjana Weerakoon

A thesis submitted in partial fulfillment of the requirements for the degree of Doctor of Philosophy

Examination Committee:

Supervisor: Assoc. Prof. Satoshi Nishimura (Hokkaido University)
Member: Prof. Tatsuya Ishikawa (Hokkaido University)
Member: Prof. Tsutomu Sato (Hokkaido University)
Member: Assoc. Prof. Koichi Isobe (Hokkaido University)

Division of Field Engineering for Environment
Graduate School of Engineering, Hokkaido University
September 2018

ABSTRACT

Dredged soils need to be pre-treated prior to reuse in construction due to its high water content and unfavorable engineering properties. A possible solution to improve the properties is solidification by mixing several binders such as cement, lime, and ground granulated blast furnace slag (GGBS). Reusing of the dredged soils, however, comes with technical and economic challenges and optimization in design requires further research. This study focuses on one such binders of waste origin, the steel slags deriving from steel processing plants, which are often used as a substitute of aggregates in road construction due to their durability. The presence of Portlandite ($Ca(OH)_2$) in steel slag leads to potential hydration capacity, and this can be exploited to improve engineering properties of high-water content dredged clays.

From previous research, the various factors affecting the strength mobilization at the stiff stage was identified; the slag content, the particle size of slag, curing time and addition of alkali activators such as NaOH and/or Na_2SiO_3. Despite these general pieces of knowledge, the continuous stiffness and strength mobilization and the correlation between them in different steel slag-mixed dredged clays from immediately after mixing have not been fully studied. Such a study will help find suitable materials and mixing conditions at an early stage of engineering work. There is still a lack of a guide to which kind of combination of steel slag and clay leads to greater strength development. Different types of dredged clay and steel slag, and their physico-chemical interactions that result in stiffness and strength mobilization need to be comprehensively and systematically studied.

The strength and stiffness mobilization characteristics of four dredged clays from Japan named A, B, C and D, mixed with two steel slags, S1 and S2, were continuously investigated from immediately after mixing to 28 days of curing by using direct shear apparatus and bender elements. In addition to the dredged clays, a non-marine clay, Kasaoka clay (K), was also used to further investigate the strength and stiffness mobilization. Unlike in more conventionally adopted unconfined compression testing, these tests could be applied to mixed specimens since initial un-cemented states, and are useful in detecting the transition of the slurry-like states to more solid states.

The stiffness and strength increase rates in the second, main stage of evolution in the clay-slag mixtures were found to be loosely correlated to the amorphous silica amount. The correlation was also influenced by the $Ca(OH)_2$ amount in slag. The results can be used to screen out clays that are hard to solidify in the medium term, based on quick on-site measurement of amorphous silica amount. For quality control in practice, the strength–stiffness relationship was critically examined as means to assess the strength with non-destructive stiffness probes. A close observation revealed that representing a wide range of curing time and mixing conditions by a single line, as proposed in existing studies, could be misleading. A new interpretation of the relationship is proposed.

The comparison of strength obtained by using two different test methods, direct shear test (DST) and unconfined compression test (UCT), was carried out on the specimen cured from 3 days to 28 days. The fair agreement of the strength from 3 days to 28 curing obtained by direct shear test (DST) and unconfined compression test (UCT) was identified. Further study was made on potential factors affecting the stabilization processes, such as the influence of water salinity and the grain size and shape. Although there is no significant influence of strength on pore water salinity, stiffness at initial curing may differ on the pore water salinity. Under the same gradation, the strength and stiffness induced by S1 and S2 were even more different, suggesting that the gradation is not the cause of the observed difference. The same circularity of the grains implies that the grain shape does not affect the difference in solidification performance between two slags. The investigation was conducted on the internal micro-structural characteristics in the steel slag-mixed clay specimen. By X-Ray Computed Tomography scanning on the specimen before and during the shear, the uniform distribution was identified to confirm the homogeneity of the specimen. It was clearly observed that soft specimen manifested ductile behavior while stiff specimen showed brittle behavior by the formation of the cracks.

TABLE OF CONTENTS

ABSTRACT ..... **II**

LIST OF TABLES ..... **VIII**

LIST OF FIGURES ..... **IX**

LIST OF NOTATIONS ..... **XII**

ACKNOWLEDGEMENTS ..... **XIV**

CHAPTER 1 – INTRODUCTION **1**

1.1 RESEARCH BACKGROUND **1**

1.2 PROBLEM STATEMENT **2**

1.3 RESEARCH OBJECTIVES **3**

1.4 STRUCTURE OF THE THESIS **4**

CHAPTER 2 - LITERATURE REVIEW **6**

2.1 DREDGED SOILS **6**

2.2 NEGATIVE IMPACTS CAUSED BY DUMPING OF DREDGED SOILS **9**

2.3 REUTILIZATION OF DREDGED SOILS **10**

2.4 SOLIDIFICATION OF DREDGED SOILS **11**

2.4.1 Cement **13**

2.4.2 Lime **19**

2.4.3 Fly ash **20**

2.4.4 Blast furnace slag **21**

2.5 SOLIDIFICATION BY STEEL SLAGS **23**

2.5.1 Alkali activators **25**

CHAPTER 3 - EXPERIMENTAL METHODOLOGY **27**

3.1 MATERIALS **27**

3.1.1 Dredged clays 27
3.1.3 Steel Slag 32
3.2 SAMPLE PREPARATION 34
3.2.1 Casting of specimens 34
3.3 pH CHANGES IN SLAG - DREDGED CLAY MIXTURE 36
3.4 MECHANICAL TESTING METHODS 37
3.4.1 Direct shear test (DST) 37
3.4.2 Defining undrained shear strength 39
3.4.3 Unconfined compression test (UCT) 41
3.4.4 Variability of unconfined compressive strength 42
3.4.5 Bender element test (BE) 44
CHAPTER 4 – EVALUATION OF HARDENING CHARACTERISTICS IN STEEL SLAG-MIXED DREDGED CLAYS AND NON-MARINE CLAY 47
4.1 STRENGTH MOBILIZATION IN DREDGED CLAYS 47
4.1.1 Patterns of strength mobilization with curing time 47
4.1.2 Correlation between strength increment coefficients and amorphous silica amount 49
4.2 STIFFNESS MOBILIZATION IN DREDGED CLAYS 51
4.2.1 Patterns of stiffness mobilization with curing time 51
4.2.2 Correlation between stiffness increment coefficients and amorphous silica amount 53
4.3 STRENGTH MOBILIZATION IN NON-MARINE CLAY 54
4.3.1 Patterns of strength mobilization with curing time 54
4.4 STIFFNESS MOBILIZATION IN NON-MARINE CLAY 57
4.4.1 Patterns of stiffness mobilization with curing time 57

4.5 CORRELATION BETWEEN STRENGTH AND STIFFNESS 60

4.5.1 Overall correlation for the whole set of data 60

4.5.2 Identification of an alternative interpretation by considering the evolution of strength and stiffness in the second stage of curing 62

4.6 SUMMARY 64

CHAPTER 5 – FURTHER INVESTIGATION OF THE FACTORS AFFECTING MEASURED STRENGTH AND STIFFNESS 66

5.1 INTRODUCTION 66

5.2. COMPARISON OF STRENGTHS OBTAINED BY DIRECT SHEAR AND UNCONFINED COMPRESSION TESTS 66

5.3 INFLUENCES OF PORE WATER SALINITY ON NON-MARINE KASAOKA CLAY MIXTURES 67

5.3.1 Effect of pore water salinity on the strength and stiffness mobilization in Kasaoka clay mixtures 68

5.4 INVESTIGATION OF EFFECT OF STEEL SLAG GRAIN SIZE ON STRENGTH AND STIFFNESS MOBILIZATION 69

5.4.1 Adjustment of different grain size of steel slags 69

5.4.2 Influence of different slag gradation on strength mobilization 70

5.4.3 Investigation of strength mobilization under the same gradation in both steel slag slag types 71

5.4.4 Influence of different slag gradation on stiffness mobilization 72

5.5 IDENTIFICATION OF STEEL SLAG GRAIN SHAPE IN S1 AND S2 73

5.5.1 Analysis of slag grain shape 73

5.6 SUMMARY 75

CHAPTER 6 – ASSESMENT OF INTERNAL MICRO-STRUCTURE BY THE X-RAY COMPUTED TOMOGRAPHY (X-Ray CT) ON DIRECT SHEAR

SPECIMENS 77

6.1 INTRODUCTION 77

6.2 INTERNAL SLAG GRAIN DISTRIBUTION PATTERN OBSERVED BY X-RAY COMPUTED TOMOGRAPHY (X-RAY CT) 78

6.2.2 Assessment of uniformity of the specimen 80

6.3 X-RAY COMPUTED TOMOGRAPHY DURING DIRECT SHEARING OF THE SPECIMEN 82

6.3.1 Identification of formation of crack during shearing 83

6.4 SUMMARY 84

CHAPTER 7 – CONCLUSIONS AND RECOMMENDATIONS 86

REFERENCES 88

LIST OF TABLES

CHAPTER 3

Table 3. 1: Physical properties of dredged clays..... 27

Table 3. 2: Representative measurements of organic and silica contents in dredged clays (Toda et al., 2018) 28

Table 3. 3: Physical properties of non-marine clay 31

Table 3. 4: Physical properties of two steel slags 33

Table 3. 5: Unconfined compressive tests results for dredged clays 43

Table 3. 6: Unconfined compressive tests results for non-marine clay, Kasaoka clay 44

LIST OF FIGURES

CHAPTER 2

Figure 2. 1: Dredging operation of the east coast at Nagoya port 6

Figure 2. 2: The volume of dumped wastes in Japanese ports (Tsuchida and Egashira, 2004) 7

Figure 2. 3: The volume of dredged soils from various regions in Japan (MLIT, 2008) 8

Figure 2. 4: Utilization and disposal percentage of dredged soil in Japan (MLIT, 2008) 8

Figure 2. 5: Associated problems regarding dumping of dredged soils 9

Figure 2. 6: Manmade Island by stabilizing dredged soils for airport in Japan (Watabe and Sassa, 2015) 11

Figure 2. 7: Improvement of dredged soils by various binders 12

Figure 2.8: Wide range correlation between stiffness and undrained strength for cement treated soils (Seng and Tanaka, 2011)……..18

Figure 2. 9: Fly ash stabilized soil blocks 21

CHAPTER 3

Figure 3. 1: Particle size distribution of dredged clays and steel slag 28

Figure 3. 2: The solubility of amorphous silica as a function of pH from Palmer and Palmer (1995) and Cui et al. (2017)..... 29

Figure 3. 3: Mineralogical compositions of dredged clays by X-Ray Diffraction (XRD) 30

Figure 3. 4: Particle size distribution of Kasaoka 31

Figure 3. 5: Mineralogical compositions of Kasaoka clay by X-Ray Diffraction (XRD) 32

Figure 3. 6: Photographs of steel slags..... 33

Figure 3. 7: Particle size distribution of steel slags 33

Figure 3. 8: Mineralogical compositions of steel slags by X-Ray Diffraction (XRD) . 34

Figure 3. 9: X-Ray CT scan images of slag-clay A mixture at α=30% (Specimen: 60mm diameter and 32mm thick)..... 35
Figure 3. 10: pH variation in slag-clay mixtures' pore water during curing..... 37
Figure 3. 11: Schematic diagram of direct shear apparatus employed in this study.. 38
Figure 3. 12: Frictional stress in the direct shear test..... 39
Figure 3. 13: Direct shear test results for clay A mixed with different slag contents of S1 and S2..... 40
Figure 3. 14: The relationship between unconfined compressive stress, σ and axial strain, ε for three independent tests under same conditions..... 42
Figure 3. 15: Schematic diagram of bender element system and travel time measurement method..... 45

CHAPTER 4

Figure 4. 1: Relationships between undrained strength (S_u) and curing time, with trend lines in log-log scale..... 48
Figure 4. 2: Variation of second-stage strength increment coefficient; a_2 with amorphous silica amount..... 50
Figure 4. 3: The relationship between shear modulus (G) and curing time, with trend lines in log-log scale..... 52
Figure 4. 4: Variation of second-stage stiffness increment coefficient; b_2 with amorphous silica amount..... 54
Figure 4. 5: The relationship between strength and curing time of Kasaoka clay mixed with S1 and S2, with trend lines in log-log scale..... 55
Figure 4. 6: The relationship between strength and curing time, with trend lines in log-log scale..... 56
Figure 4. 7: The relationship between shear modulus (G) and curing time of Kasaoka clay mixed with S1 and S2, with trend lines in log-log scale..... 58
Figure 4. 8: The relationship between shear modulus (G) and curing time, with trend lines in log-log scale..... 59
Figure 4. 9: Correlations between shear modulus (G) and shear strength, S_u..... 61

Figure 4. 10: Correlations between shear modulus (G) and shear strength, S_u 62

CHAPTER 5

Figure 5. 1: Correlation between undrained shear strengths obtained by direct shear and unconfined compression tests 67

Figure 5. 2: Strength and stiffness mobilization with curing time for Kasaoka clay-slag mixture prepared with both distilled water and seawater 68

Figure 5. 3: Adjustment of grain size of S1 steel slag 70

Figure 5. 4: Strength mobilization with curing time, according to different grain sizes of slag 70

Figure 5. 7: Image processing for circularity calculation by ImageJ application 74

Figure 5. 8: Circularity of slag grains according to four different of grain diameters 74

CHAPTER 6

Figure 6. 1: Diagram of direct shear apparatus with X-Ray CT scanning technology 78

Figure 6. 2: Diagram of typical X-Ray configuration..... 79

Figure 6. 3: Steps sequence conducted in ImageJ application 80

Figure 6. 4: A typical example of an image processed by ImageJ application..... 81

Figure 6. 5: Coordinates of centre in three-dimensional sectional views for AS1-30% 82

Figure 6. 6: Formation of cracks during shearing from 0 mm to 7 mm 83

Figure 6. 7: Relationship between shear stress and shear displacement obtained by direct shear test discussed in chapter 3 (First test) and X-Ray CT direct shear test in Port and Airport Research Institute (Second test) 84

LIST OF NOTATIONS

a_1: Strength increment coefficient at first stage of curing

a_2 : Strength increment coefficient at second stage of curing

A_{Si}: Non-biogenic amorphous silica

b_1: Stiffness increment coefficient at first stage of curing

b_2: Stiffness increment coefficient at second stage of curing

B_{Si}: Biogenic amorphous silica

e_{max}: Maximum void ratio

e_{min}: Minimum void ratio

G: Shear modulus

n: Number of slag grains

N_i: Pixel value of each slag grain

q_u: Unconfined compressive strength

S_u: Undrained shear strength

TOC: Total Organic Carbon

T_{Si}: Total amorphous silica

V_C: Volume of wet dredged clay

V_S: Volume of dry steel slag

V_s: Shear wave velocity

X_c: X coordinate of center of gravity

X_i: X coordinate of center of slag grain

X_s: X coordinate of mass-center

Y_c: Y coordinate of center of gravity

Y_i: Y coordinate of center of slag grain

Y_s: Y coordinate of mass-center

Z_c: Z coordinate of center of gravity

Z_i: Z coordinate of center of slag grain

Z_s: Z coordinate of mass-center

α: Slag content

τ: Shear stress

τ_f: Maximum shear stress

σ_v: Vertical reaction stress

ρ: Mass density

ACKNOWLEDGEMENTS

I would like to express my gratitude to everyone who has inspired and supported me during the work on my Doctoral thesis.

This research would not have been possible without the support of many people. First and foremost, my genuine appreciation goes to my supervisor, Associate Professor Satoshi Nishimura for his all guidance, support, sharing off valuable knowledge and experiences. He was an excellent advisor to me during my three years at Hokkaido University. Absolutely he was an integral part of my success and supervised me to come up with good findings, read my numerous revisions and helped make some sense of the confusion. I had the good fortune to be one of the students under his supervision. This work was funded by Steel Foundation for Environmental Protection Technology. Nippon Steel & Sumitomo Metal Corporation provided the dredged clays and slag for testing. Their aids are sincerely acknowledged.

My sincere thanks go to the other members of my examination committee, Associate Professor Tatsuya Ishikawa and Professor Tsutomu Sato who offered great guidance, support and valuable instruction during three years, and Associate Professor Koichi Isobe who also offered guidance and support. I am grateful to Dr. Fumihiko Fukuda who offered great support and valuable instruction and Mr.Yutaka Kudoh who provided considerable instructions for the lab works. I would like to acknowledge Ms. Haruna Sato and Ms. Kanako Toda, for their great support, team work, and sharing the findings, and my lab-mates who endured this long process with me, always offering support and great assistance. Heartfelt gratitude is extended for the entire family members of the e3 program.

I would like to acknowledge to the coordinator of the e3 program, Mrs. Natalya Shmakova, for her kind support, and encouragement. I pay my grateful thank to the Government of Japan, for providing me a MEXT scholarship to pursue the degree of Doctor here at Hokkaido University, Japan. Last but not least I would like to thank, father, mother, and sister for always encouraging and supporting me.

Thank you!

CHAPTER 1 – INTRODUCTION

1.1 RESEARCH BACKGROUND

Dredged clays are conventionally considered as a slurry-like fluid. In Japan, a large amount of dredged soil is produced due to the development in coastal areas, such as navigation channels, port facilities, large vessel seaports, breakwaters and land reclamation. Dredged clays are conventionally considered as waste materials to be disposed of in either offshore locations or inland facilities. Therefore, if a reuse potential can be derived for the dredged soils, environmental and ecological impacts by dumping can be avoided by giving a second life to these dredged clays as alternative green products for the construction industry.

These soils are generally low in bearing capacity and have high compressibility, making them unsuitable for use as a sound geo-material in civil engineering applications, such as backfilling. Thus, the dredged soils need to be pre-treated prior to application, and a possible solution is to improve the strength properties by solidification. The solidification technique is not novel and widely adopted to improve soft soils by admixing several binders such as cement, lime, fly ash and ground granulated blaster furnace slag. Many researchers have worked with cement treated soils to introduce construction uses to the dredged clays. From past studies, several factors influencing strength mobilization of cement or lime treated soils have been found (**Seng and Tanaka, 2011**; **Toohey et al., 2013**; **Xiao et al., 2014**). Meanwhile, some researchers have proposed empirical formulae based on various indices to predict the strength of cement treated soils for long-term curing time (**Kasama et al., 2006**; **Kang et al., 2014**; **Sasanian et al., 2014**).

From a sustainability point of view, the reuse of these wastes can be more popularized, if the binding agents are retrieved from another source of waste too, hence reducing the costs and enhancing the 'green' sustainability appeal. One of such materials is the steel slag found in steel processing plants, which is often used as a substitute of aggregates in road construction due to their durability. Another reason for selecting steel slag is the presence of high Portlandite ($Ca(OH)_2$) content. It indicates potential binding capacity similar to that widely recognized in manufactured cement. Recently dredged clay

is mixed with steel slag to improve their engineering properties and is used for several engineering applications such as backfill materials, embankment, sub-base in road construction, land reclamation and etc.

Some researchers have worked on this topic to understand the strength mobilization after 3-day curing time. From them, various factors for strength mobilization after 3-day curing time were identified, such as the optimum content of slag, the particle size of slag, curing time and chemical interaction between slag and clay (**Sun et al., 2009**; **Chan et al., 2012**; **Chan et al., 2014**). The potential cementing property of steel slag can be greatly activated by the addition of proper activators. Therefore, steel slag mixed with alkali activators such as NaOH and/or Na_2SiO_3 can exhibit an acceleration of the hydration, with higher strength than those obtained from pure slag (**Shi et al., 2004**; **Poh et al., 2006**; **Chan et al., 2014**). From a viewpoint of chemistry, the formation of Calcium Silicate hydrate (C-S-H), Alumina Ferric Oxide monosulfate (AFm), or Friedel's salt was considered as causes for strength development by reaction between $Ca(OH)_2$ in steel slag and silica in dredged clays (**Kiso et al., 2008**). However, the continuous stiffness and strength mobilization and their correlation in different steel slag-mixed dredged clays from immediately after mixing have not been fully studied. Such a study will help find suitable materials and mixing conditions at an early stage of engineering work.

1.2 PROBLEM STATEMENT

Despite these general pieces of knowledge, there is still a lack of a guide to which kind of combination of steel slag and clay leads to greater strength development. Clays with apparently similar properties in terms of gradation and plasticity often indicate significant differences in solidification processes when mixed with the same slag. Different types of dredged clay and steel slag, and their chemical-physical interactions that result in stiffness and strength mobilization need to be comprehensively and systematically studied. In practice, however, precisely predicting the eventual strength of a slag-clay mixture solely based on the constituents' (i.e. slag and clay) properties will still be difficult, considering the complexity of the involved stabilization processes. The focus, therefore, should also be laid on how any sign of eventual solidification can be detected empirically at early stages

of curing. This would facilitate the laboratory mix tests and initial design, by curtailing the standard 28-day curing and instead conducting many shorter-period trials.

Immediately after mixing, the sample still remained very soft. Therefore conventional laboratory tests such as unconfined compression tests and triaxial compression tests could not be carried out for initial curing time because the specimen was not strong enough to stand by itself. But immediately after mixing, the mixture can be poured and cured in the direct shear box. Therefore, direct shear tests were adopted for specimens at a wide range of curing times, from 0.5 hours to 28 days. However, the comparison of strength obtained by using two different tests method such as direct shear test (DST) and unconfined compression test (UCT) was carried out on the specimen cured from 3 days to 28 days. Further study was made on potential factors affecting the stabilization processes, such as the influence of pore water salinity and the grain size and shape. In this study, it is focused on the further investigation of the internal micro-structural characteristics in the steel slag-mixed clay specimen. Therefore image-based analysis of failure patterns was performed aided by X-Ray Computed Tomography (X-Ray CT) tests.

In addition to these geotechnical engineering aspects, this project has been undertaken as a joint investigation by geotechnical and geochemistry research teams, intending to obtain deeper understanding into fundamental physico-chemical processes of clay-slag solidification while approaching to mechanical characterization with appropriate geotechnical laboratory expertise. The main findings by the latter team, who analyzed geochemical processes in the same clay-slag mixtures presented in this thesis, are summarized by **Toda et al. (2018)**. Their findings are important in directing us to focus on differences of readily soluble amorphous silica amount in the clays in explaining the observed differences in solidification degree.

1.3 RESEARCH OBJECTIVES

In this study, the stiffness and strength mobilization characteristics in eight combinations of steel slag and dredged clay at three different slag proportions each were investigated from early stages of curing time by using direct shear apparatus and bender elements.

Unlike in more conventionally adopted unconfined compression testing, these tests could be applied to mixed specimens since initial uncemented states, and are useful in detecting the transition of the slurry-like states to more solid states. The strengths at the stiff stage, from 3 days to 28 days were compared with unconfined compressive strengths obtained by unconfined compression tests. Effects of grain size and shape on stiffness and strength mobilization were studied. Image-based analysis of failure patterns was performed aided by X-Ray Computed Tomography (X-Ray CT) tests. The main objectives under this study are listed from 1 to 5.

1. To comprehensively characterize the strength–time and stiffness–time curves from early stages and understand the influencing factors.

2. To identify any relation between the stiffness and strength that serves as a useful tool for monitoring the quality of steel slag-clay mixtures in practice. It allows the strength to be assessed with non-destructive stiffness probes in the field.

3. To find out the differences in the strength obtained by using two different tests method such as direct shear test (DST) and unconfined compression test (UCT) on the specimen cured from 3 days to 28 days.

4. To discover the potential factors affecting the stabilization processes, such as the influence of pore water salinity, and the grain size and shape.

5. To understand the internal micro-structural characteristics in the steel slag-mixed clay specimen through image-based analysis of failure patterns aided by X-Ray Computed Tomography (X-Ray CT).

1.4 STRUCTURE OF THE THESIS

Chapter 1 summarizes the broad background and the research questions addressed in this study. A detailed literature review pertaining to the research area is given in Chapter 2. Chapter 3 presents experimental materials and methodology used in this study. Evaluation

of hardening characteristics in dredged clays and non-marine clay mixed with steel slags is discussed in chapter 4. Chapter 5 shows the further investigation of the factors affecting measured strength and stiffness based on different test method and grain size and shape. The image-based analysis on the specimen before and during the shear aided by X-Ray Computed Tomography (X-Ray CT) tests was explained in Chapter 6. After Chapter 6, the main contributions of this research are described under conclusions in Chapter 7.

CHAPTER 2 - LITERATURE REVIEW

2.1 DREDGED SOILS

Sedimentation is a natural process wherein suspended particulates are deposited in environments of decreasing energies. Anthropogenic changes to natural waterways, i.e., dam creation, levees, manmade channels change the dynamics of fluvial environments, sometimes accelerating sedimentation which can limit the depth or close navigational channels. The excavation of materials from subaqueous environments has been carried out for centuries by a process known as dredging; the excavated sediment removed by dredging operations is considered as dredged materials. The dredging process is crucial to our nation's shipping, recreational boating, defense, ecosystem preservation and flood prevention, and has the following three stages: dredge planning, dredging operations, and management of the removed dredged materials by effective transportation.



Figure 2. 1: Dredging operation of the east coast at Nagoya port (*http:// www.kk-kojimagumi.co.jp)*

The dredging operation is the physical removal of sediments for new construction, maintenance or restoration of navigable channels, expanding of existing port facilities (**Fig.2.1**) and shoreline protection. For an example in Japan, yearly water channel

maintenance and marine construction have resulted in 10-15 millions m^3 of dredged soils for disposal (**Japan Port and Airport Association, 1999**). In one estimate, soil obtained from dredging in Japan exceeds 20 million m^3 annually (**Mitarai et al., 2008**; **Yamagoshi et al., 2015**).

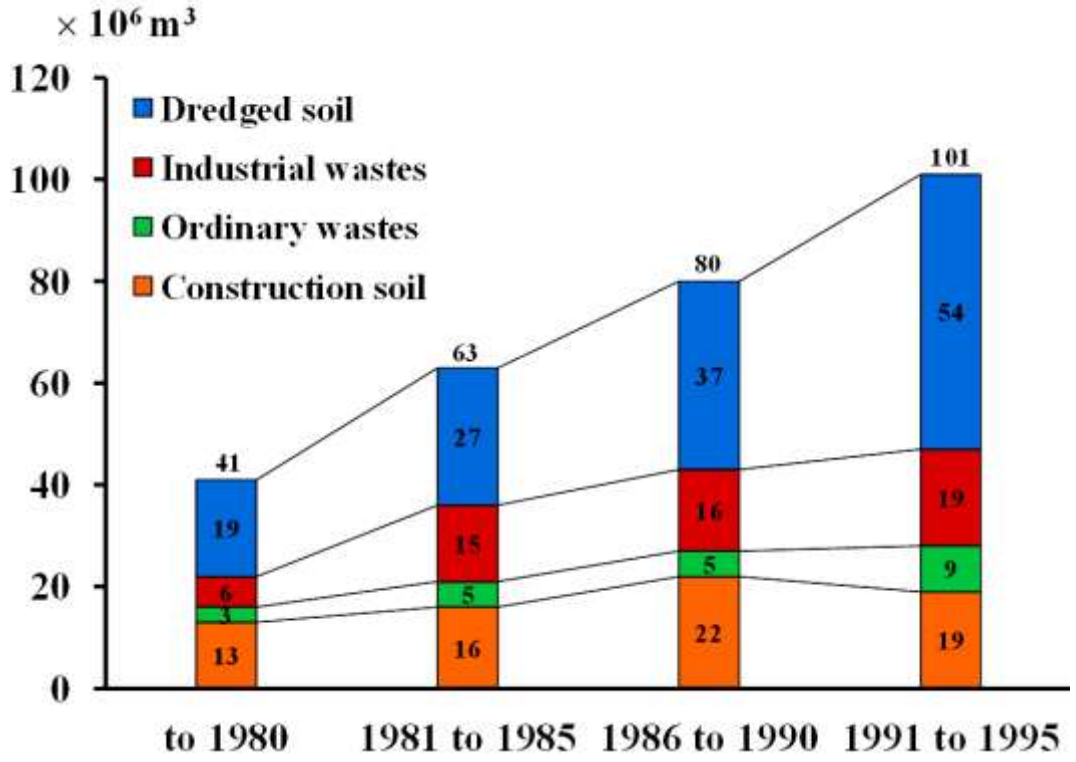


Figure 2. 2: The volume of dumped wastes in Japanese ports (Tsuchida and Egashira, 2004)

The amount of dumped wastes in Japanese ports during 1980 to 1995 is illustrated in **Fig.2.2**, as taken from **Tsuchida** and **Egashira** (**2004**). To keep these wastes properly, it costs 30 billion yen annually for the construction of seawall structures. The majority of wastes are dredged soils and surplus soils from constructions. It was reported by **Miki et al., 2005** that approximately 208 million m^3 of soils were generated from construction work around the country for the fiscal year 2000 and only about 30% was reused, that means about 145 million m^3 of soils were dumped. Another interesting report from Ministry of Land, Infrastructure, Transport, and Tourism (MLIT) of Japan in 2008 focused mainly on dredged soil waste in several industrial cities, and, as indicated in **Fig.2.3** and **Fig.2.4,** shows its percentage of recycling and disposal. The important fact is that a large amount of dredged soil concentrated mostly in a small area, for instance, Kanto (Tokyo

Bay) and Kinki (Osaka Bay).

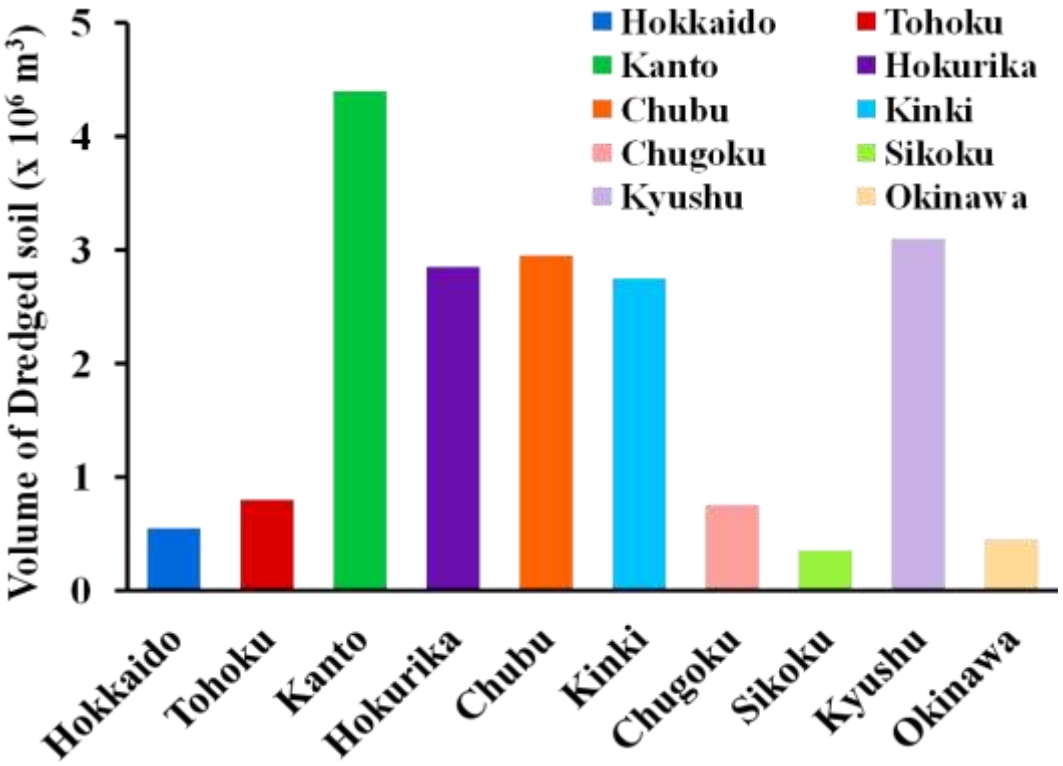


Figure 2. 3: The volume of dredged soils from various regions in Japan (MLIT, 2008)

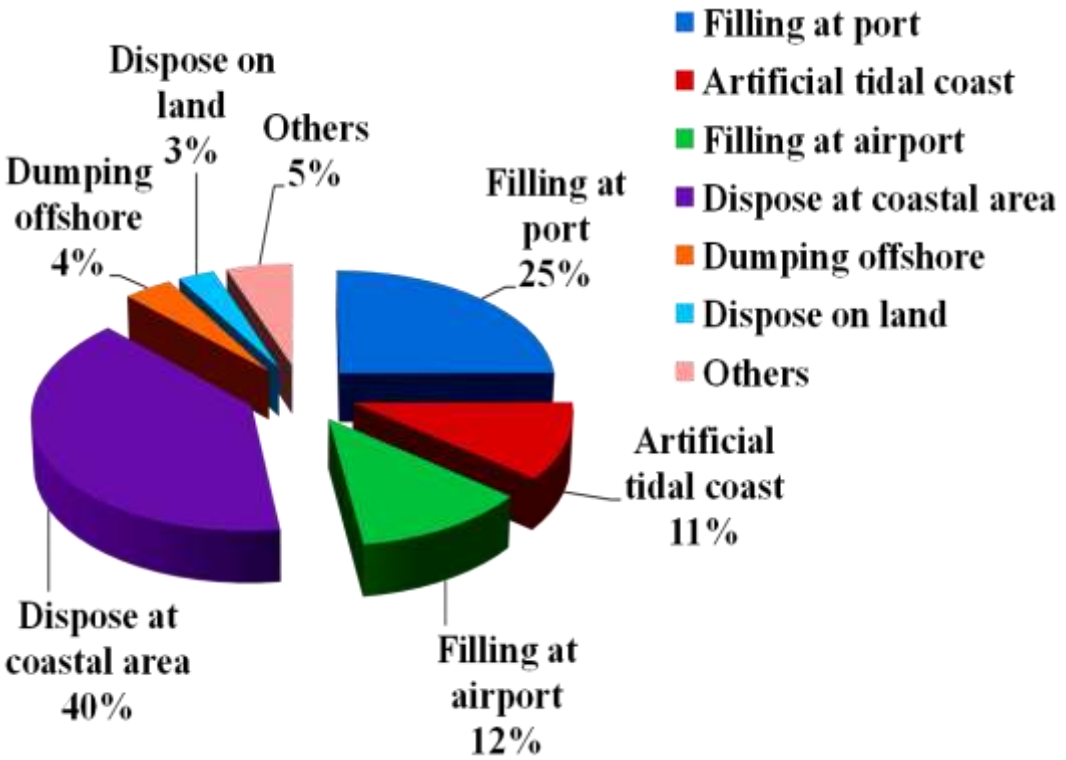


Figure 2. 4: Utilization and disposal percentage of dredged soil in Japan (MLIT, 2008)

Since this material is large in volume, heavy and not valuable, it cannot be transported to other larger cities. From **Fig.2.4**, only 48% of total volume was used in various applications while another 47% was dumped or disposed. The management issues of these wastes are concerned not only in Japan but also in most developed countries such as the United States, Europe, China, South Korea and so forth. The available lands for disposing of this material are limited and also environmental aspect is concerned.

2.2 NEGATIVE IMPACTS CAUSED BY DUMPING OF DREDGED SOILS

Dredged clays are conventionally considered as waste materials for disposal in either offshore locations or inland facilities. Either of these measures incurs costs, time, labour and some risk for sustainable developments. As shown in **Fig.2.5**, the dredging process can also cause negative impacts on the environment, especially when the dredged soils are dumped into offshore waters and disposal environment on inland.

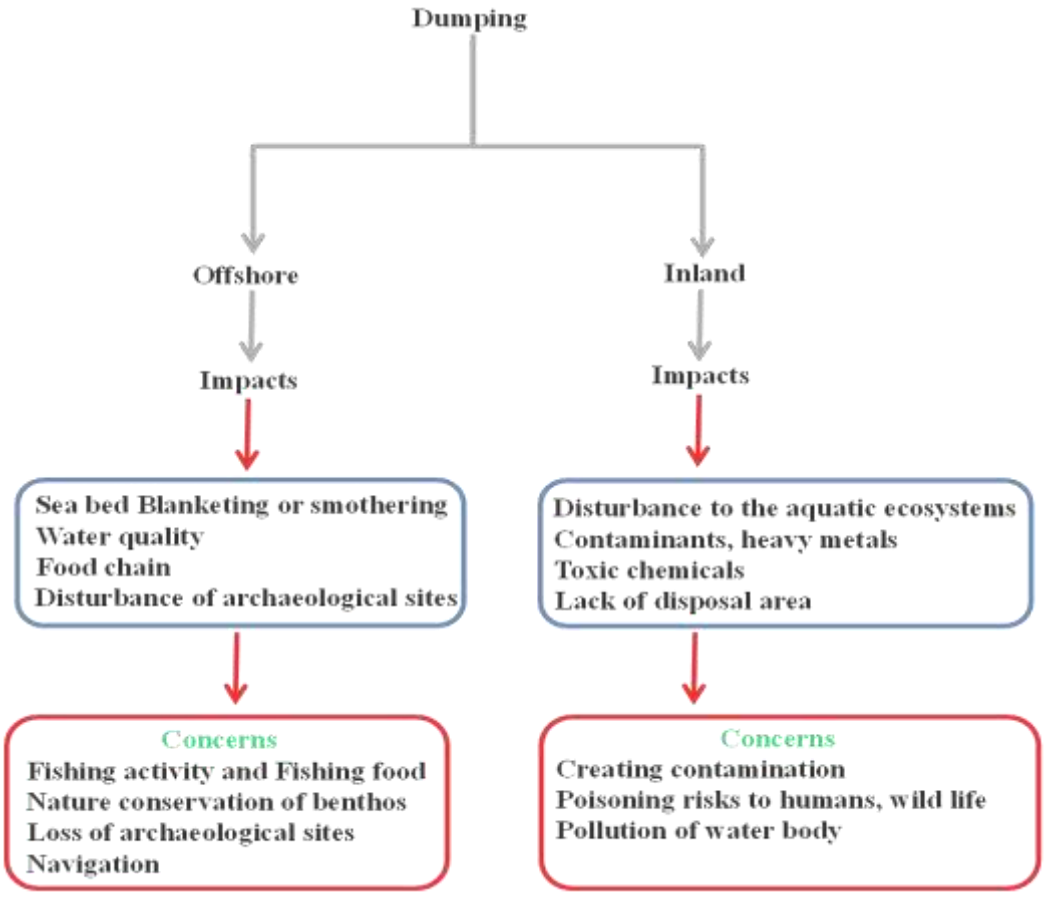
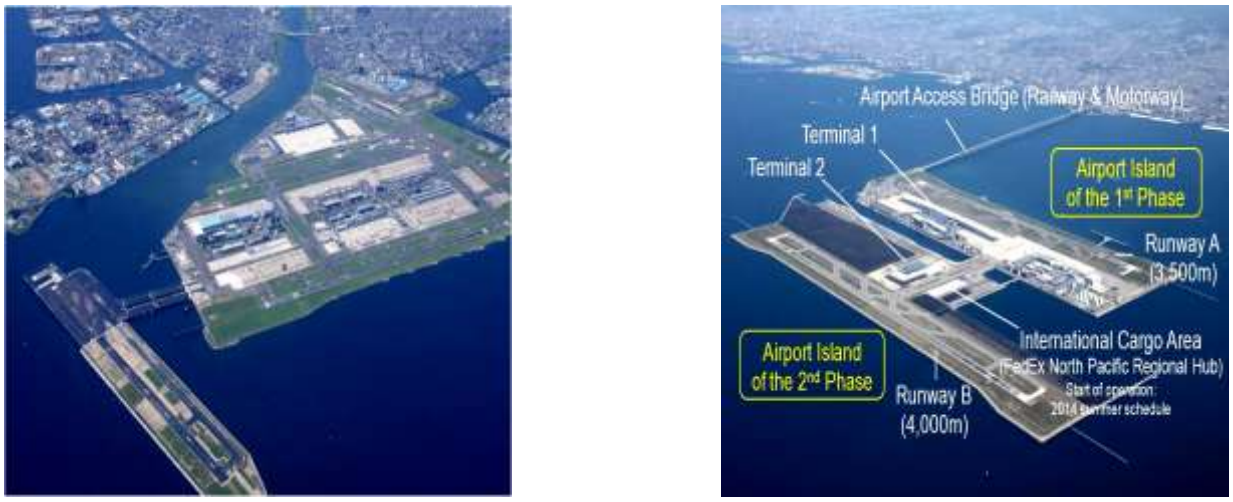


Figure 2. 5: Associated problems regarding dumping of dredged soils

Dumping activities from the dredging works could adversely affect the physical and biological elements of the sea. Contaminated dredged soils are harmful and could degrade the marine environment and result in long-term, irreversible damages. Dumping of contaminated dredge soil has a variable impact on the ecosystems, depending on the nature and amount of the contaminants (**Reish, 1980** and **1981**). Dumping of non-contaminated sediments, however, may also have adverse effects on the functioning of the aquatic ecosystem. Suspension of fine sediments may influence nutrient dynamics in estuaries, affect growth of filter-feeding organisms and impair the performance of visual predators. At dump sites, local benthos may be affected by burial and by changing sediment properties. For many years, the question of where to dump dredged sediments was mainly determined by two items of economical nature. One being related to the cost of shipping the dumped sediments to the dump site, the other related to the chance of recirculation of dumped sediments to the original dredge site. Since 1990, environmental effects have become more and more important in the policy regarding dumping of dredged sediments (**Essink, 1999**). The professionals from Geotechnical Engineering understood that if a reuse potential can be derived for the dredged soils, the environmental and ecological impact by dumping can be avoided.

2.3 REUTILIZATION OF DREDGED SOILS

The preferable solutions to the problem are to recycle it as reclamation material or apply it to another construction uses in effective ways. A reuse potential has been sought actively for in these dredged clays on the sustainability ground, as the capacity of dumping sites is dwindling (**Tang et al., 2001**). Natural properties of the dredged soil are unsuitable for such purposes, with high water content, high compressibility, and low strength. Proper understanding of such soils' properties, both at natural and improved states, will lead to stabilizing the supply of sustainable reclamation materials for coastal development (**Fig.2.6**), as well as helping management of surplus, dredged soils, thus contributing substantially to infrastructure development while imposing minimum stress to the environment.



(**a**) Aerial photo of Tokyo Haneda airport (**b**) Aerial photo of Kansai airport

Figure 2. 6: Manmade Island by stabilizing dredged soils for airport in Japan (Watabe and Sassa, 2015)

Towards such fundamental understanding, in this thesis, suitable experimental testing methods and frameworks for interpretation have been implemented that serve to engineering practice as well as are academically novel. Generally, there are two ways of using dredged soils or very soft clays as fill material, i.e. directly applied to reclamation site or pre-treated prior to reutilization (**Brils et al., 2014**). A possible solution is solidification by binders (**Grubb et al., 2010**; **Chan et al., 2015**; **Watabe and Sassa, 2015**) to improve the engineering properties for construction.

2.4 SOLIDIFICATION OF DREDGED SOILS

Soil stabilization aims at improving soil strength and increasing resistance to softening by swelling through bonding the soil particles together, waterproofing the particles or combination of the two (**Sherwood, 1993**). The simplest stabilization process is consolidating the soft soils. Another process is by improving gradation of particle size and further improvement can be achieved by adding binders to the weak soils (**Rogers et al, 1993**). Soil stabilization can be accomplished by several methods. All these methods fall into two broad categories namely;

1. Mechanical stabilization

Under this category, soil stabilization can be achieved through the physical process

by altering the physical conditions of native soil particles by either induced vibration or compaction or by incorporating other structures such as barriers and nailing. Mechanical stabilization is not the main subject of this review and will not be further discussed.

2. Chemical stabilization or solidification

Under this category, soil stabilization/solidification depends mainly on chemical reactions between stabilizer (cementitious material) and soil minerals (pozzolanic materials) to achieve the desired effect. A chemical stabilization/solidification method is the main theme of this thesis.

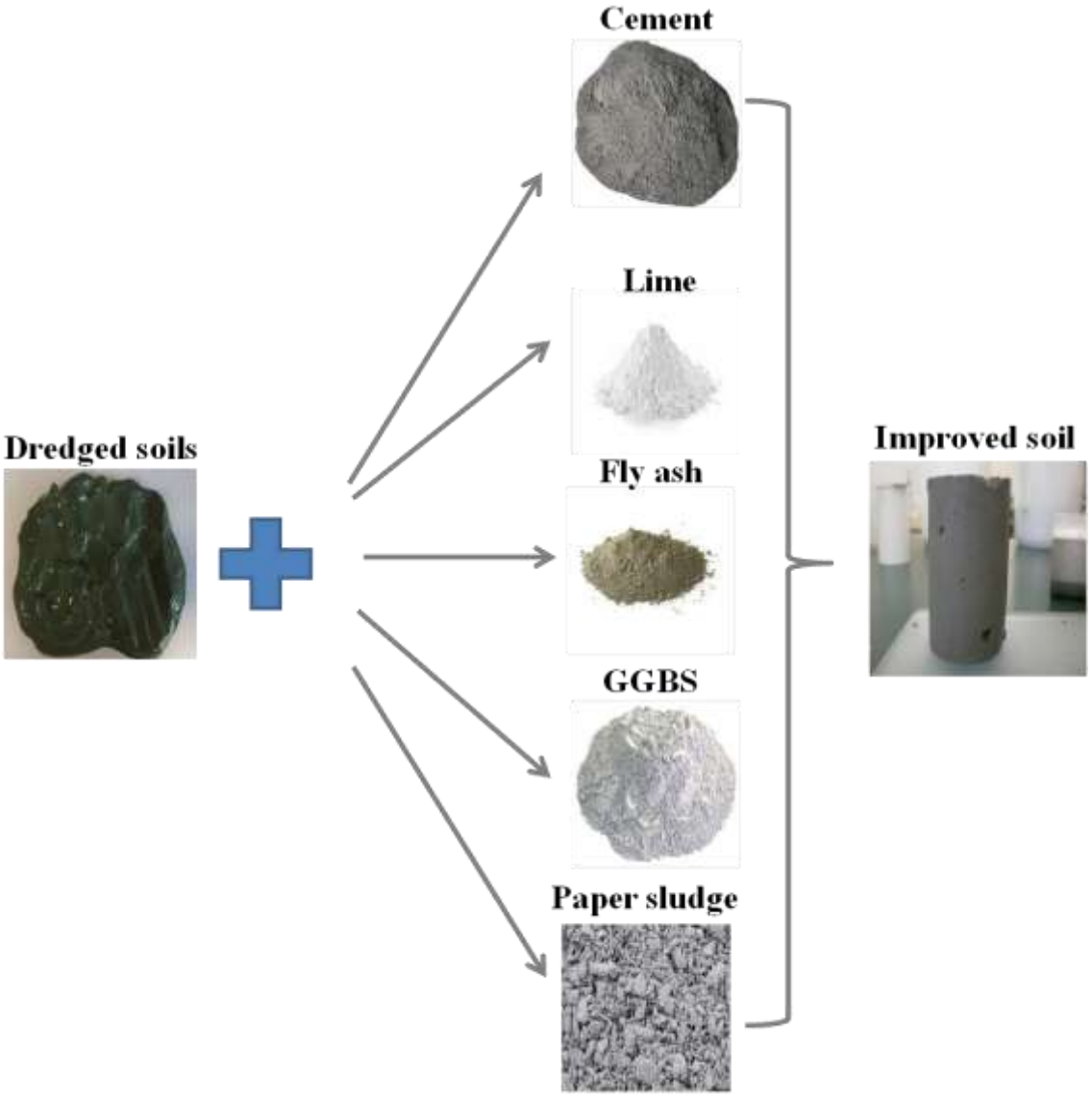


Figure 2. 7: Improvement of dredged soils by various binders

The solidification technique is not novel and widely adopted to improve soft soil or weak soils by admixing with several binders (**Fig.2.7**) such as cement, lime, fly ash, Ground Granulated Blast furnace Slag (GGBS), paper sludge or combination of these. The solidified soil materials have a higher strength, lower permeability, and lower compressibility than the native soil. The method can be achieved in two ways, namely; (1) in situ stabilization/solidification and (2) ex-situ stabilization/solidification. The decision to technological usage depends on which soil properties have to be modified.

The chief properties of soil which are of interest to engineers are volume stability, strength, compressibility, permeability and durability (**Sherwood, 1993**). For a successful solidification, laboratory tests followed by field tests may be required in order to determine the engineering and environmental properties. Laboratory tests may produce higher strength than in field, but will help to assess the effectiveness of solidified materials. Results from the laboratory tests will enhance the knowledge on the choice of binders and amounts. These binders promote the chemical hardening of the mixture, transforming the low strength material to one with sufficiently increased strength and stiffness, as required of a usable material in the construction. Lime and cement are the effective admixtures for solidification. Adding lime or cement to soft clay improves its engineering properties such as index properties, strength, and resistance to compressibility. The successful application of lime and lime mixed with waste materials such as fly ash, ark shell ash and foamed waste glass stabilized soft Ariake clay were reported by **Nanri** and **Onitsuka (1996)** and **Onitsuka** and **Shen (1998, 2000)**. The lime and cement solidified surplus clays are normally utilized as engineering materials for backfill and pavement.

2.4.1 Cement

Soil-cement solidification technique has also been in existence for a long time. A construction project near Johnsonville, South Carolina in 1935 was one of the first controlled construction projects in which cement was used as a soil binder in the United States (**Das 1990**). Cement treatment causes a chemical reaction similar to a lime and can be used for both modification and solidification purposes such as in a road construction.

Numerous types of cement are available in the market; these are ordinary Portland cement, blast furnace cement, sulfate resistant cement and high alumina cement. Usually, the choice of cement depends on the type of soil to be treated and desired final strength.

Hydration process is a process under which cement reaction takes place. The process starts when cement is mixed with water and other components for the desired application resulting in hardening phenomena. The hardening (setting) of cement will enclose soil as glue. The hydration reaction is slow proceeding from the surface of the cement grains and the center of the cement grains may remain un-hydrated (**Sherwood, 1993**). Cement hydration is a complex process with a complex series of unknown chemical reactions (**MacLaren** and **White, 2003**). However, this process can be affected by

1. Presence of foreign matters or impurities
2. water-cement ratio
3. Curing temperature
4. Presence of additives
5. The specific surface of the mixture

Depending on factor(s) involved, the ultimate effect on setting and gain in strength of cement stabilized soil may vary. Therefore, this should be taken into account during mix design in order to achieve the desired strength. Calcium silicates, C_3S and C_2S are the two main cementitious materials of ordinary Portland cement responsible for strength development (**Al-Tabbaa** and **Perera, 2005**). Calcium hydroxide is another hydration product of Portland cement that further reacts with pozzolanic materials available in the stabilized soil to produce further cementitious material (**Sherwood, 1993**). Normally the amount of cement used is small but sufficient to improve the engineering properties of the soil and further improve by substituting lime or fly ash. Cement stabilized soils have the following improved properties:

- Increase in strength
- Increase in stiffness
- Decrease in volume expansion potential or compressibility

The strength development of cement and lime stabilized clay are mainly obtained by formation of cementing products ($CaO\text{-}SiO_2\text{-}H_2O$, $CaO\text{-}Al_2O_3\text{-}H_2O$) that were investigated by X-ray diffraction and scanning electron microscope (SEM) (**Kawamura** and **Dimond 1975**; **Kamon** and **Nontananandh 1991**; **Rajasekaran et al., 1997**). It is clearly shown that the cementing products cause the strength of stabilized clay to increase. There are many factors such as differences in soil gradation, types of clay minerals, organic matter, pH, sulphate and etc., (**Sherwood 1958**, **1962**; **Moh 1962**; **Mateos 1964**; **Thompson 1966** and **Miura et al., 1988**) that significantly influence the ability of clay to react with cement and lime to achieve a strength increase.

Some studies were conducted on cement or lime-treated soils to comprehensively understand the physical properties such as the mobilization of strength and stiffness. The influence of clay water content, cement content, and curing time on the strength and the compressibility of cement-treated clay were studied by using cement-treated remolded soft Bangkok clay (**Lorenzo and Bergado, 2004**). The ratio of after-curing void ratio to cement content was proven to be an effective independent parameter to obtain a unique relationship of unconfined compressive strength (q_u). This ratio combined together the influence of clay water content, cement content, and curing time on the strength of treated clay and higher cement content induces higher compression index. **Horpibulsuk et al. 2011** also found that for the water content varies in the range of liquidity index between 1 and 2, the ratio of clay water content to cement content is the prime parameter governing the strength and the compressibility at the pre-yield state.

An experimental study on the primary yielding and post-yield behavior of cement-treated Singapore marine clay were studied by conducting unconfined compression tests and triaxial tests (**Xiao et al., 2014)**. The study was. The results show that all the primary yield loci for the cement-treated marine clay have a consistent shape regardless of the mix ratio, curing stress or curing period. The cement-treated soil under curing stress was investigated by (**Consoli et al., 2000**; **Rotta et al., 2003**). The application of confining stress, caused a reduction in stiffness with increase of the initial mean effective stress for the specimens cured without confining stress, while for those cured under stress the opposite behavior was observed. The importance of the void ratio

during the formation of cement bonds and also of the degree of cementation for the compressive behavior of the cemented soil, and demonstrated that the variation in yield stress with void ratio and cement content is dependent on the curing stress and independent of the stress history. The sample size is also found to have a considerable influence on the mixing quality (**Larsson, 2001**).

Meanwhile, some researchers have proposed empirical formulae to predict the strength of cement-treated soils for long curing time based on various indices (**Chiu et al., 2008**; **Sasanian et al., 2014**), such as cement content, cement-water ratio, and normalized water content**. Kasama et al.** (**2006**) found that the yield stress ratio determined by using initial relative density and cement content can be used to estimate the strength. Several equations defined by some researchers are mentioned as follows. **Mitchell et al. (1974)** proposed a relationship between the unconfined compressive strength of cement treated soils and the curing time, as given in the following equation:

$$q_D = q_{D_0} + K \log\left(\frac{D}{D_0}\right) \tag{2.1}$$

where, q_D is the unconfined compressive strength at curing after D days, q_{D_0} is the unconfined compressive strength at curing after D_0 days, and K = 480 c for coarse-grained soils and K = 70 c for fine-grained soil, and c is the cement content determined by the mass ratio of cement to dried soil. **Tang et al. (2001)** conducted a series of strength tests for 28 marine clay samples treated with cement and proposed an equation considering the water content and the cement content as given in the following equation:

$$q_u = \frac{K(C-C_0)}{(\frac{G_S w}{100}+1)^2} \tag{2.2}$$

where K is the strength coefficient, C is the amount of cement: the weight of cement per unit volume, C_0 is the minimum amount of cement required for strength mobilization, and w is the water content of original soils. **Tsuchida and Tang (2012)** proposed an equation, in which the gel-space ratio theory of hardened cement paste is considered, to predict the unconfined compressive strength of cement-treated clays, as given in the following equation:

$$\boldsymbol{q_u} = \boldsymbol{k_c^*}(\boldsymbol{c^*} + \boldsymbol{c_0^*})\boldsymbol{Y^N} \quad (2.3)$$

where $\boldsymbol{k_c^*}$ is the coefficient of strength increment, $\boldsymbol{c^*}$ is the cement content, $\boldsymbol{c_0^*}$ is the minimum cement content required for strength mobilization, Y is the volumetric solid content (solid particles of cement, and soil), and N is the exponential parameter for the effect of void structure of soil and cement content to all solid material of soil. **Kang et al. (2015a and b)** proposed using a specific volume ratio, defined by considering the cement volume as part of the skeletal volume, for the prediction. Two equations were proposed to estimate the strength of cement treated dredged clays as follows.

$$q_u = \exp(c_1)\left(\frac{w'}{w_L}\right)^{-c_2} \times t^{e_1 \ln(c^*+e_2)+ e_3} \quad (2.4)$$

where, c_1 and c_2 are strength parameters normalized to water content related to 1 hour curing after mixing with cement. The parameter e_1 is constant, 0.234 and the parameter e_2 is minimum cement content to develop strength. Parameter e_3 is the strength increment coefficient within 3 days. In this study, the cement content c^* (%) is defined as the ratio of mass of cement to the mass of solid particles in cement and soil. Therefore the development of equation for the prediction of strength at early stages is important for many civil engineering projects, which deals with the transport of treated soils. As mentioned, many researchers have proposed equations based on various indices to predict the strength mobilization of cement-treated soils through laboratory tests. However, the equations to estimate unconfined compressive strength are based on curing times of more than 3 days. In addition, since the strength of 14 or 28 days is used as a reference, the equations used to evaluate the unconfined compressive strength during the early stages of curing for less than 3 days are not applicable.

In addition to the strength, the correlation between strength and stiffness for cement-mixed soil possessing relatively high levels of strength has already been studied by many researchers (**Terashi et al. 1983; Lee et al. 2005; Flores et al. 2010**). **Seng and Tanka, (2011)** examined the behavior of cement treated soils according to different mixtures of water and cement contents and also soil properties, mainly focusing on undrained shear strength (S_u) and stiffness (G) during the initial stages of curing or a lower

strength range. **Fig.2.8** shows the correlation between G and the shear strength derived from the present study, together with the results of tests conducted by **Terashi et al. (1983)**. It is of interest that a linear relation between G and S_u also exists over 4 orders of magnitude for G and S_u, i.e., S_u ranges between approximately 0.2 kPa and 2000 kPa. It is found that the relation can be fitted quite well by a power function with a regression coefficient of about 94%, as expressed in Eq.2.5.

$$G=310S_u^{1.06} \tag{2.5}$$

It should be noted that the power of S_u is very close to 1.0, indicating that G is about 300 times greater than S_u, regardless of the strength magnitude or G. The proposed correlation can be used to estimate the strength based on non-destructive stiffness probes in practice.

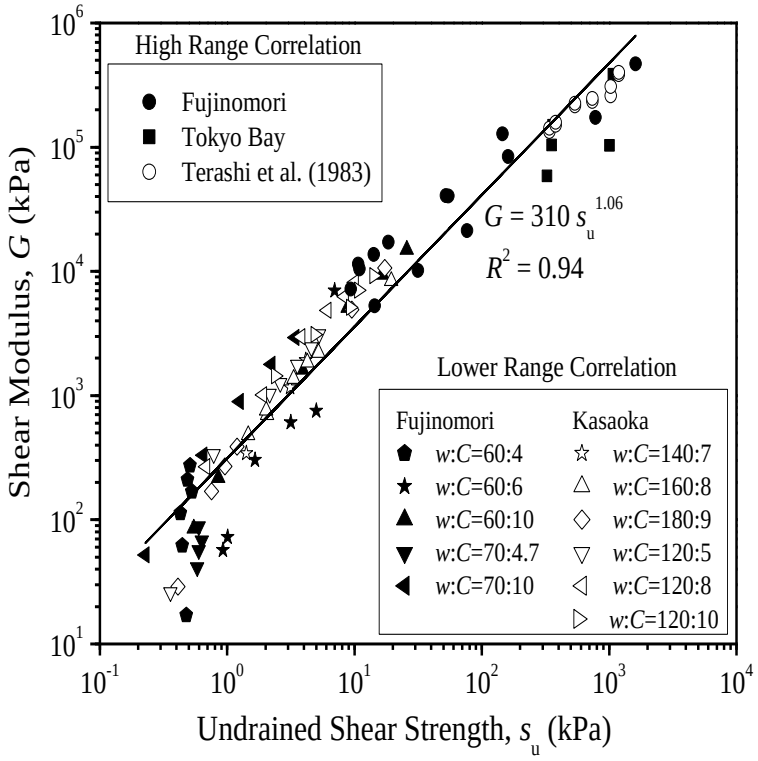


Figure 2. 8: Wide range correlation between stiffness and undrained strength for cement treated soils (Seng and Tanaka, 2011)

To the author's knowledge, there is no equation to determine the strength of steel slag-treated clays during the early stages of curing based on the physicochemical characteristics.

2.4.2 Lime

Lime is one of the oldest and still popular additives used to improve fine-grained soils. Construction of Denver International Airport is an example of using lime stabilization/solidification method. Following are the four major lime-based additives used in geotechnical construction; hydrated high calcium lime $Ca(OH)_2$, Calcitic quicklime CaO, monohydrated dolomitic lime $Ca(OH)_2$ MgO and dolomitic quicklime CaO MgO. Lime treatment of soil facilitates the construction activity in three ways (**Mallela et al. 2004**). First, a decrease in the liquid limit and an increase in the plastic limit results in a significant reduction in plasticity index. Reduction in plasticity index facilitates higher workability of the treated soil. Second, as a result of chemical reaction between soil and lime, a reduction in water content occurs. This facilitates compaction of very wet soils. Further, lime addition increases the optimum water content but decreases the maximum dry density and finally immediate increase in strength and modulus results in a stable platform that facilitates the mobility of equipment.

When lime is mixed with the clayey material in the presence of water several chemical reactions take place. They include cation exchange, flocculation-agglomeration, pozzolanic reaction, and carbonation (**Mallela et al. 2004**). These reactions contribute to immediate changes in plasticity index, workability, and strength gain. The pozzolanic reaction occurs between lime and, the silica and alumina of the clay mineral and produces cementing material including calcium-silicate-hydrates and calcium alumina hydrates. The basic pozzolanic reactions are as follows:

$$Ca(OH)_2 + SiO_2 \rightarrow CaO\text{-}SiO_2\text{-}H_2O \quad (2.5)$$

$$Ca(OH)_2 + Al_2O_3 \rightarrow CaO\text{-}Al_2O_3\text{-}H_2O \quad (2.6)$$

Pozzolanic reactions are time- and temperature-dependent and may continue for a long period of time. Addition of lime to soil increases its pH; studies have shown that when the pH of the soil increases to 12.4, which is the pH of saturated limewater, the solubility of silica and alumina increase significantly. Therefore, as long as sufficient calcium from the lime remains in the mixture and the pH remains at least 12.4, the pozzolanic reaction will continue. In some instances, lime reacts with carbon dioxide to

produce calcium carbonate instead of calcium-silicate-hydrates and calcium alumina hydrates. Such carbonation is an undesirable reaction from the point of soil improvement (**Bergado et al. 1996**; **Mallela et al. 2004**).

Lime treatment reduces maximum dry density and increases optimum water content (**Mallela et al. 2004**; **Thompson 1966**). Increase in optimum water content facilitates compaction of soils which are wet of optimum in their natural condition. Results of studies have also revealed that optimum water content increases with increasing lime content (**Mallela et al. 2004**; **Thompson 1966**). The drying of wet soil and the increase in soil workability is attributed to the immediate treatment, whereas the increase in soil strength and durability is associated with the long-term treatment (**Locat et al., 1990**; **Wild et al., 1996**; **Mallela et al., 2004**; **Kassim et al., 2005**; **Geiman, 2005**). **Toohey et al. 2013** found that stress-strain behavior after 41°C curing is similar to that observed after 23°C curing, only at an accelerated curing time. It appears from stress-strain behavior that 41°C curing does not induce any influential chemical reactions that are not present during 23°C curing. Specimens cured at 41°C reached q_u values equivalent to 28 day 23°C q_u after 1.8–5.9 days. The evolution of stress-strain-strength in lime-stabilized soil is influenced by a number of variables including temperature, soil and mineral type, lime concentration, and preparation (moisture, compaction). As such, an equivalent accelerated curing regime (temperature and duration) will always vary.

2.4.3 Fly ash

Fly ash is a by-product of coal combustion in power plants. Fly ash contains silica, alumina, and different oxides and alkalis in its composition, and is considered as a pozzolanic material (**Das, 1990**). The most common elemental compositions of fly ash include SiO_2, TiO_2, Al_2O_3, Fe_2O_3, MnO, MgO, CaO, Na_2O, K_2O, P_2O_5, SO_3 and organic carbons. A guideline for selecting fly ash as soil stabilizing agent is provided in **ASTM-D593 (2011)**. There are two types of fly ash, type “C” and type “F”. This classification is based on the chemical composition. Fly ash type “C” contains a significant amount of free lime. This type of fly ash produces pozzolanic and cementitious reactions. **Cockrell et al. (1970)** have shown that the lighter color fly ash indicates the presence of high calcium

oxide and the darker color reflects the high organic content. However, it must be noted that fly ash properties are highly variable and depend on the chemical composition of coal and combustion technology.



Figure 2. 8: Fly ash stabilized soil blocks (http://www.hydraformasia.com/wp-content/uploads/2011/07/banner2.jpg)

As shown in **Fig.2.9**, fly ash can improve the engineering properties of soil by making stiff blocks and utilize in different constructions. Class C fly can be used on its own to solidify moderately plastic soils (**Ferguson et al., 1993**) with no addition of activators like lime and Portland cement. As reported by the same author, fly ash treatment can also reduce the swell potential for fat clays and increase the strength of pavement subgrades. In coarser aggregates, fly ash functions both as a pozzolanic and/or filler to reduce the void spaces among the aggregate particles. **Chan et al. (2014)** found that addition of fly ash to the dredged sediments results in pH reduction and the consumption of CH from the hydration of cement. As identified by the same author, a higher amount of fly ash substitution for cement and prolonged curing time was found to be beneficial for strength enhancement and better bonding of the soil binder, to form stiffer structure. Fly ash dose leads to lower void ratio and as results of that it increases strength at 28 days curing (**Grubb et al., 2010**).

2.4.4 Blast furnace slag

These are the by-product in pig iron production. The chemical compositions are similar to that of cement. It is, however, not cementitious compound by itself, but it possesses latent hydraulic properties which upon addition of lime or alkaline material the hydraulic properties can develop (**Sherwood, 1993**; **Åhnberg et al, 2003**). Depending on the cooling

system adopted in the manufacturing processes, **Sherwood (1993)** itemized slag in three forms, namely:

1. Air-cooled slag

   Hot slag after leaving the blast furnace may be slowly cooled in open air, resulting in crystallized slag which can be crushed and used as aggregate.

2. Granulated or Pelletized slag

   Quenching (i.e. sudden cooling with water or air) of hot slag may result in the formation of vitrified slag. The granulated blast furnace slag or Merit 5000 (commonly known in Sweden) is a result of the use of water during quenching process, while, the use of air in the process of quenching may result into formation of pelletized slag.

3. Expanded slag

   Under certain conditions, steam produced during cooling of hot slag may give rise to expanded slag.

Among these three types of slag, the use of Ground Granulated Blast Furnace Slag (GGBFS), an industrial by-product, is well established as a binder in many cement applications where it provides enhanced durability and high resistance to sulfate attack (**Wild et al., 1999**). The soil stabilized with lime-activated slag has shown significant strength enhancement relative to lime-stabilized soil and also very good volume stability when subjected to water in presence of the aggressive sulfates (**Green et al., 2000**). The changes in the chemical structure of the clays are examined and the fact that the slag decreases the swelling potential of the clays and increases strength (**Wild et al., 1996**; **Wild et al., 1999**; **Green et al., 2000). Kavak and Bilgen (2016)** found that grain size of the slag directly affects the reactions in the soil. Although it is impossible to use the slag without any operation like pulverizing or sieving as an additive for soil, it can be used directly as a granular road material in places close to the factory. The same author identified that although slag–lime and clay mixtures do not affect optimum water contents of clay significantly, slag-lime decreases the dry density and leads to a smooth proctor curve.

2.5 SOLIDIFICATION BY STEEL SLAGS

In addition to cement or lime, using other waste materials such as steel slag is an economical and sustainable solution in recycling the surplus soil. Steel slag is a material retrieved from a source of waste in steel processing plants and, due to the high $Ca(OH)_2$ content, a potential hydration capacity similar to that in manufactured cement exists. Dredged clays are hence sometimes mixed with steel slag to improve their engineering properties. Concerning the basic properties of CaO-improved soil as a civil engineering material, **Yamagoshi et al. (2015)** obtained the following knowledge based on characteristic of strength development and impact on water environment.

1. When a mixture of CaO-improved soil and dredged soil is aged in seawater, Ca from the CaO-improved soil and SiO_2 and Al_2O_3 from the dredged soil form certain hydrates like calcium silicate-based hydrate (C-S-H) and calcium aluminate-based hydrate (AFm), causing the mixture to solidify.
2. The development of strength of CaO-improved soil becomes conspicuous with the lapse of time of aging. It was confirmed that the strength development continues up to 91 days curing.
3. The development of strength of CaO-improved soil is enhanced as the mixing ratio of CaO improver is increased. It was confirmed that the strength improving effect continues to increase till the mixing ratio of CaO improver was raised to 40%.
4. It was experimentally verified that by mixing the CaO improver in dredged soil, it is possible to restrain not only the elution of phosphorus and sulfides from the dredged soil but also the multiplication of algae.

Several studies have been carried out to understand the strength of mobilization with curing time in steel slag-mixed clays. Various factors affecting the strength mobilization after 3-day curing time were identified; slag content, the particle size of slag, curing time and fines content. Few findings by **Chan et al. (2012)** are drawn, which demonstrates the potential of reviving dredged marine clay to useful geo-materials by solidification with steel slag.

1. Higher slag portion in the dredged clay induces greater strength improvement. The fines portion present in the slag was found to have a significant influence on the solidification effect. This is attributed to the larger specific surface of the finer particles.

2. Prolonged curing showed increased solidification, and the time effect was more pronounced with higher slag percentage and fines content. Bulk density of the solidified clay was dependent on the slag dosage, primarily due to the self-weight of the slag.

3. Plotting young's modulus (E) against unconfined compressive strength (q_u), will yield the following equation:

$$E = 151 q_u \quad (2.7)$$

4. The water consumption rate, as reflected in the final water content measured, suggests that approximately 40 % of mixing water is necessary for every part of dry slag added to the clay.

Chan et al. (2014) identified that the reduction of organic content in the dredged material is attributed to entrapment by the cementitious products from the chemical reactions of the binders. The steel slag functions both as a binder and filler, simultaneously bonding the soil and slag particles, while stiffening the structure of the mixture by its own larger particle size and denser form. The correlation between stiffness and strength was proposed by following equation to make quick estimation of the strength, especially in the design mix stage of a dredged sediments solidification exercise.

$$q_u = 0.4 V_p^{1.05} \quad (2.8)$$

where V_p is the P- wave velocity.

For several high-water-content soils stabilized by cement, cement-lime, and cement-slag, clear relationships between shear modulus normalized by bulk density and unconfined compressive strength were observed (**Åhnberg** and **Holmén, 2008**). The cementation process generated by the various binders in the specimens showed an increase

in stiffness similar to that of strength with time. The correlation can approximately be expressed as:

$$G_0 = 82\rho q_{uc}^{1.2} \quad (2.9)$$

where G_0 is the small strain modulus, ρ is the bulk density, and q_{uc} is the unconfined compressive strength of the specimens.

The strength increment of steel slag-mixed clay is attributed to the formation of cementitious hydrates such as Calcium Silica hydrates (C-S-H), alongside Alumina Ferric Oxide monosulfate (AFm), Friedel's salt, etc. The C-S-H is thought to be particularly important, produced by the reaction between $Ca(OH)_2$ in steel slag and silica in dredged clays (**Kiso et al., 2008**; **Yamagoshi et al., 2015**).

2.5.1 Alkali activators

Since the early of the 1990s (**Davidovits, 1991**), the alkali-activated aluminosilicate-based material has been shown to exhibit a wide range of physical properties that allow them to be applied in many industries. The potential of alkali-activated material for the utilization in high-temperature exposure has become one of the research interests. The use of this cementitious materials could also be used to reduce industrial waste for instance ashes (**Temuujin, et al., 2010**), slag (**Wang et al., 1994**; **Cheng** and **Chiu, 2003**), water glass (**Bădănoiu et al., 2015**), copper mining (**Ahmari** and **Zhang, 2012**).

Their versatilities come from many excellent engineering properties, including a high compressive strength and light weight. The cementing potential of fly ash and slag can be greatly activated by addition of appropriate activators (**Phetchuay et al., 2014**; **Arulrajah et al., 2016**). The sodium hydroxide (NaOH), potassium hydroxide (KOH), sodium water glass (Na_2SO_3) and potassium water glass (K_2SO_3) is most commonly used as alkaline activators (**Al Bakri et al., 2011**). Steel slag mixed with alkali activators such as NaOH and/or Na_2SiO_3 can exhibit acceleration of the hydration, with higher strength than those obtained with slag and clay only (**Shi et al., 2004**; **Poh et al., 2006**; **Chan et al., 2014**; **Gao et al., 2015**). Based on the preliminary test results in the reusing of dredged marine soils with admixing activated steel slag by **Chan and Abdul Jalil, (2011)**, the

optimum molarity for NaOH was found to be 4 Mol. The strength of the soil without slag addition was barely 60 kPa, and the increment at 5:5 mix ratio after 7 days was more than double, that is, 120 kPa. Higher concentration of NaOH appeared to be detrimental to the strength enhancement of the soil-slag mixture, possibly due to the unfavorable pH for solidification to take place effectively. Indeed, specimens with 9 Mol NaOH and above suffered dramatic drop in strength. By 12 Mol, it has reverted to the untreated soil's strength of about 60kPa, clearly indicating the negative impact of excessive concentration of the activator used.

CHAPTER 3 - EXPERIMENTAL METHODOLOGY

3.1 MATERIALS

3.1.1 Dredged clays

Four different types of dredged clays from Japanese ports were used in this study, named A, B, C and D in this thesis. Obtained as dredged, they were firstly sieved through 425μm to remove coarser inclusions such as large sea shells to ensure the specimen homogeneity. At the sampled states, all the clays were slurry with their natural water contents greater than the liquid limits. Their properties are summarized in **Table 3.1**. Clay C is a low plasticity clay (ML), while the others are classified as high plasticity clays (CH). Clay D is coarser when compared with other three clays as shown in particle size distributions in **Fig.3.1**. From **Table 3.2**, the ignition loss for all the dredged clays was found to be between 4.2% and 7.9%, suggesting the presence of a relatively low amount of organic matters. According to **Chan et al. (2013)**, there is no strong influence of ignition loss on mechanical characteristics when it is less than 20%. The Total Organic Carbon (TOC) was less than 2%, and consistent with the low ignition loss values.

Table 3. 1: Physical properties of dredged clays

Clay	Plastic limit (%)	Liquid limit (%)	Plasticity index	Particle density (g/cm^3)
A	28.4	73.4	45.0	2.78
B	37.1	89.8	52.7	2.74
C	29.1	44.1	15.0	2.71
D	30.7	66.2	35.5	2.71

The primary cause of the strength and stiffness increases in slag-clay mixtures is the formation of cementitious hydrates (C-S-H), resulting from the reaction between $Ca(OH)_2$, supplied mainly from the slag, and the silica, mainly from the clay minerals. The factors influencing C-S-H formation include solubility of silica, clay mineralogy, curing

conditions and pH level that affects the silica solution processes, among others (**Solanki and Zaman, 2012**).

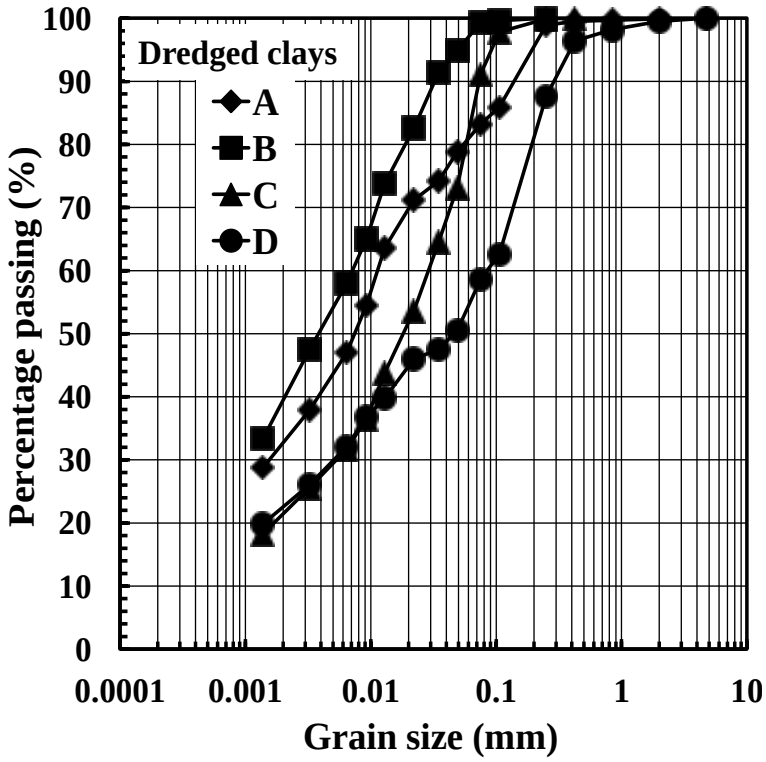


Figure 3. 1: Particle size distribution of dredged clays and steel slag

Table 3. 2: Representative measurements of organic and silica contents in dredged clays (Toda et al., 2018)

Clay	Ignition loss (%)	Total organic carbon, TOC (%)	Humic acid content (mg/g)	Biogenic amorphous silica, B_{Si} (mg/g)	Non-biogenic amorphous silica, A_{Si} (mg/g)	Total amorphous silica, T_{Si} (mg/g)
A	7.5	1.5	1.02	24.0	12.3	36.3
B	7.9	2.0	0.74	26.2	7.2	33.4
C	4.2	1.2	1.23	15.4	5.3	20.7
D	6.7	0.6	2.05	15.3	2.5	17.8

In particular, a continuation of a highly alkaline environment that induces dissolution of the silica from the clay is important to keep the silica supply to the pore spaces. **Toda et**

al. (2018) found that the silica contained in the clay, amorphous silica, in particular, plays a crucial role in the early solidification, as they have significantly higher solubility than crystalline counterparts at given pH, as shown in **Fig.3.2**. **Toda et al**. quantified the amorphous silica of both biogenic and non-biogenic origins in clays A-D. As shown in **Table 3.2**, different amounts of amorphous silica were identified, in terms of biogenic amorphous silica (B_{Si}) and non-biogenic amorphous silica (A_{Si}). Biogenic amorphous silica is produced in surface waters of the world's oceans mostly by diatoms, sponge spicules, and silicate minerals (**Conley et al., 1993**; **Nelson et al., 1995**), while the non-biogenic amorphous silica is transformed by solution and dehydration of volcanic glass (**Aoyagi, 1985**; **Sarmiento and Gruber, 2006**).

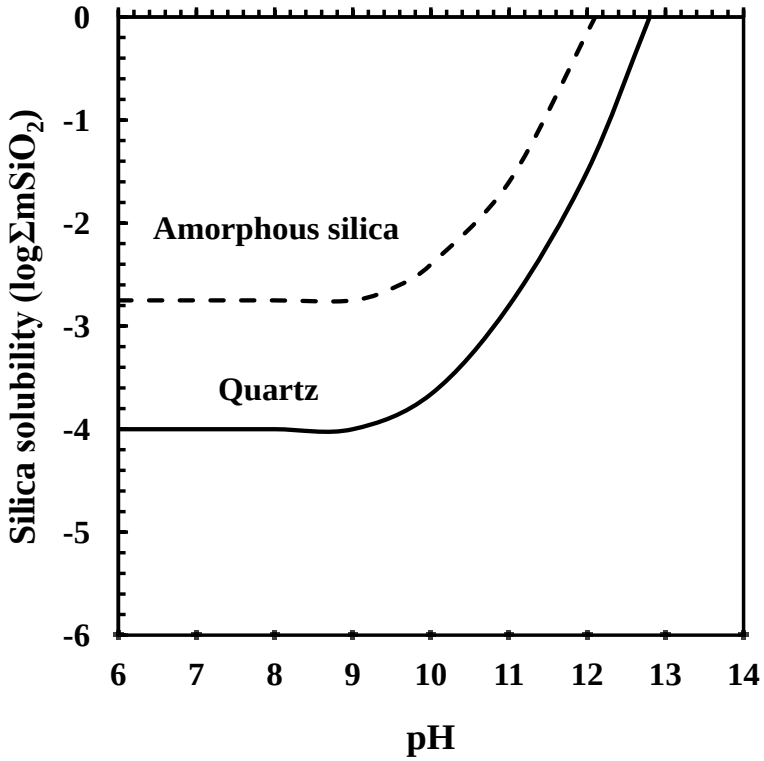


Figure 3. 2: The solubility of amorphous silica as a function of pH from Palmer and Palmer (1995) and Cui et al. (2017)

The Na_2CO_3 method was used to extract the biogenic amorphous silica in the dredged clays. 50mg of dredged clay was added to 2 mol/l of the Na_2CO_3 solution and it is digested at 85°C for 5 hours after which the amount of silica extracted was measured (**Mortlock and Froelich, 1989**). The NaOH extraction is the most commonly used method to assess the non-biogenic amorphous silica in soils. 50 mg of dredged clay was added into

0.5 mol/l of NaOH and digested at 100°C for 2.5 minutes. The amount of extracted silica was then measured (**Kodama and Ross, 1991**; **Kodama et al., 1995**). The B_{Si} content in clays C and D are nearly half of those in clays A and B. The significant differences of the A_{Si} content were also detected in clay A to D. The total amorphous silica amount, T_{Si}, was broadly in proportion to B_{Si}, due to the relatively smaller amount of A_{Si}.

Another well-recognized factor that hinders the C-S-H formation is the existence of organic acids, such as humic acid, in clay that buffers the alkalization of the mixture and prevents silica dissolution. The humic acid was quantified in **Toda et al. (2018)** and shown in **Table 3.2**, along with the ignition loss and TOC, which are broader indices of organic content. The measured amount of humic acid was eventually considered minor in this study, as the pH buffer effect was small in all the tested slag-clay mixtures. The pH measured in some of the dredged clay-slag mixtures is discussed in section **3.2.2**. Right after the mixing, all the clays exhibited similarly high pH, sufficient to cause amorphous silica dissolution (see **Fig.3.2**).

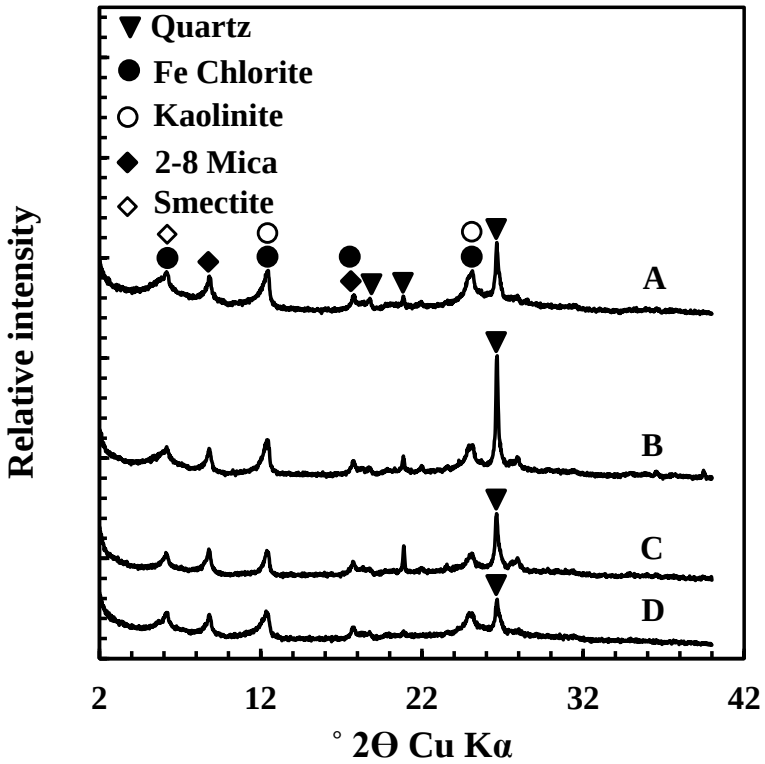


Figure 3. 3: Mineralogical compositions of dredged clays by X-Ray Diffraction (XRD)

X-Ray Diffraction (XRD) analysis was conducted on the four dredged clays to identify and compare the mineralogical phases. The RIGAKU XRD analysis Multiflex was used

with a tube voltage and tube current of 30kV and 20mA, respectively. The XRD spectra for the mineralogical phases of the four dredged clays are shown in **Fig.3.3**. From the XRD tests results, broadly identical mineralogical compositions were identified for all the clays, while the peaks of the quartz (SiO_2) show some differences between them. However, note that the XRD spectra reflect only crystalline minerals, not amorphous ones. The amorphous silica, both biogenic and non-biogenic, is not captured in these spectra.

3.1.2 Non-marine clay

In this study, a non-marine clay was also tested: Kasaoka (K). Their index properties are summarized in **Table 3.3**. Kasaoka clay available in dry powder condition was mixed with required distilled water and kept about one day for the soil particle to be hydrated well.

Table 3. 3: Physical properties of non-marine clay

Clay	Plastic limit (%)	Liquid limit (%)	Plasticity index	Particle density (g/cm^3)
Kasaoka (K)	22.5	59.6	37.1	2.70

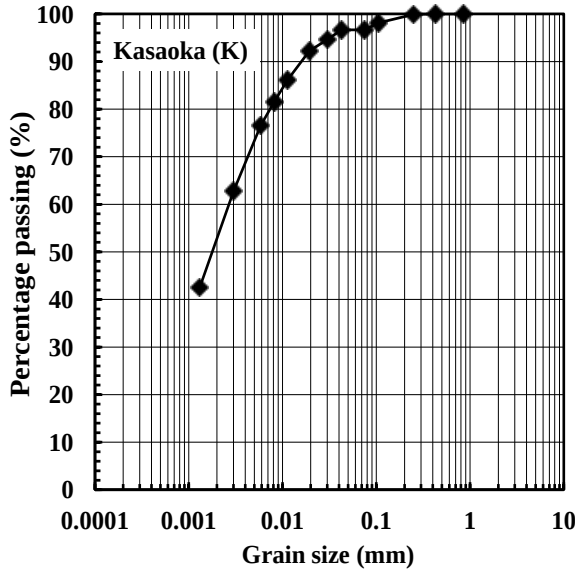


Figure 3. 4: Particle size distribution of Kasaoka

The physical properties of Kasaoka clay are summarized in **Table 3.3**. It can be classified as high plasticity clays (CH). Kasaoka clay is finer when compared with dredged clays as shown in particle size distributions in **Fig.3.4**. X-Ray Diffraction (XRD)

analysis was conducted on Kasaoka clay similar to the four dredged clays to identify and compare the mineralogical phases.

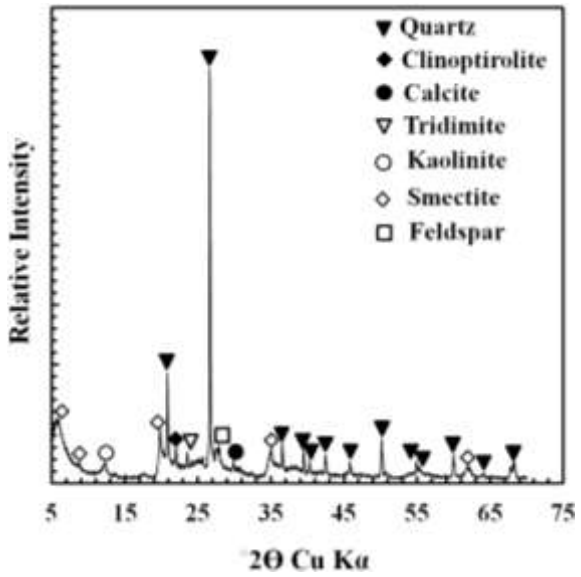


Figure 3. 5: Mineralogical compositions of Kasaoka clay by X-Ray Diffraction (XRD)

The XRD spectrum for the mineralogical phases of the Kasaoka clay is shown in **Fig.3.5**. From the XRD tests results, although different mineralogical compositions were identified for Kasaoka clay compared to the dredged clays, the peaks of the quartz (SiO_2) show some differences between them. However, the amorphous silica, both biogenic and non-biogenic, is not captured in these spectra. Both biogenic and non-biogenic amorphous silica amounts were measured by following the same methods (**Mortlock and Froelich, 1989**; **Kodama and Ross, 1991**; **Kodama et al., 1995**) as used in measurements of dredged clays. Different amounts of biogenic amorphous silica and non-biogenic amorphous silica were identified in the pore fluid of the Kasaoka clay-water mixture. Biogenic amorphous silica amount was less than clay A, i.e., 18.3 mg/g. But significant differences of non- biogenic amorphous silica amount, in particular, can be detected between Kasaoka clay and all dredged clays, i.e., 20.3 mg/g of A_{Si} in Kasaoka clay is the highest amount among all clays. However, total amorphous silica amount is larger.

3.1.3 Steel Slag

Two steel slags, S1 and S2, from difference iron works in Japan were used in this study. They are shown in **Fig.3.6**. Their dry particle densities and minimum (e_{min}) and maximum (e_{max}) void ratios are summarized in **Table 3.4**. The slag, as received from the steel

manufacturer, contained particles of irregular shapes and different sizes. The largest particles in S1 and S2 passed 9.5 mm and 4.75 mm sieves, respectively, as shown in **Fig.3.7**. The XRD spectra for the mineralogical phases of the slags are shown in **Fig.3.8**. Slag S1 contained a notably higher $Ca(OH)_2$ amount than S2, as indicated by the higher spectral peak.



(a) S1 steel slag **(b)** S2 steel slag

Figure 3. 6: Photographs of steel slags

Table 3. 4: Physical properties of two steel slags

Type of slag	Particle density (g/cm^3)	e_{min}	e_{max}
S1	3.5	0.869	1.238
S2	3.8	0.771	1.167

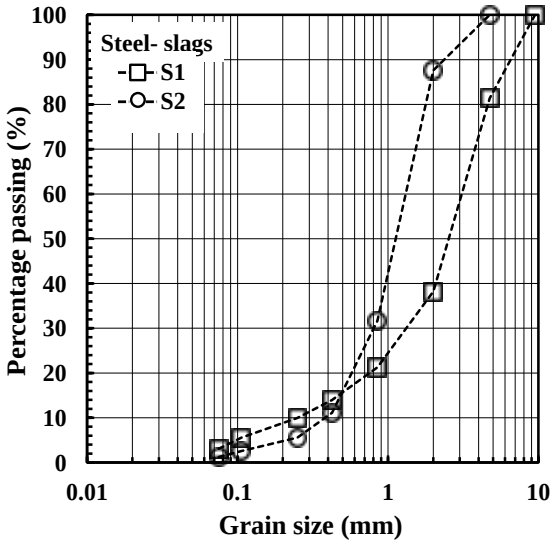


Figure 3. 7: Particle size distribution of steel slags

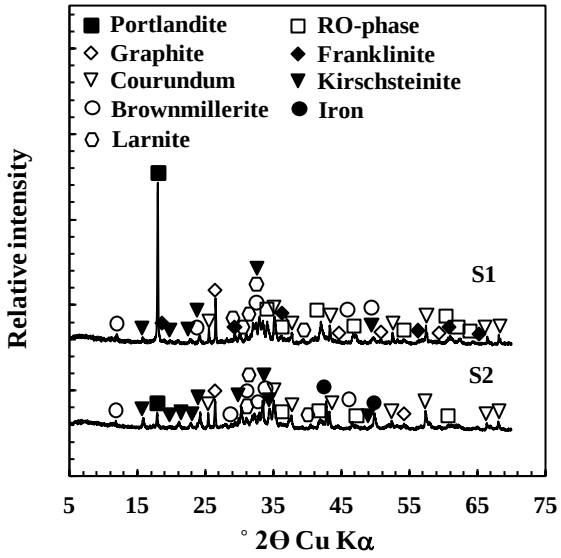


Figure 3. 8: Mineralogical compositions of steel slags by X-Ray Diffraction (XRD)

3.2 SAMPLE PREPARATION

3.2.1 Casting of specimens

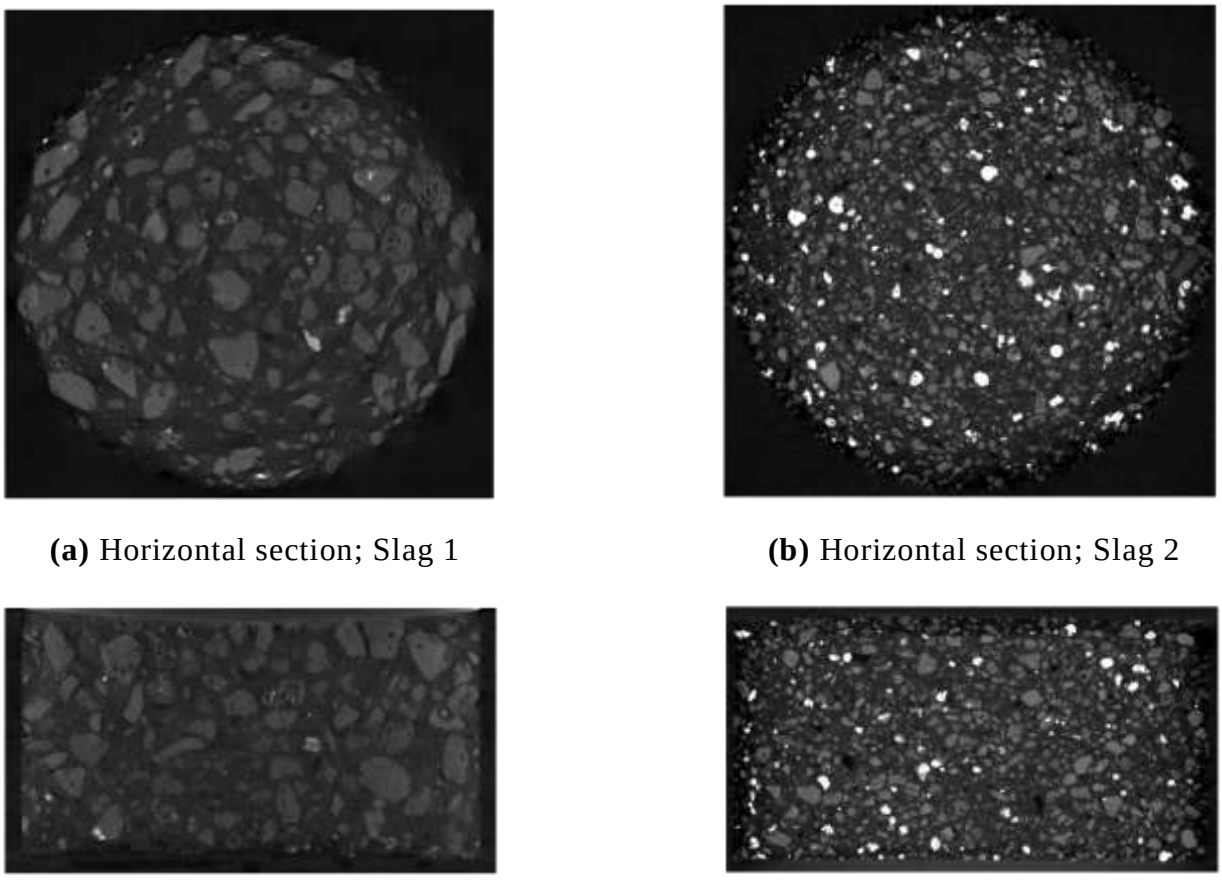
The samples for the mechanical tests were prepared by mixing the four clays and the two slags at different proportions. The slag content, α, is defined as a volume-based ratio, as expressed as;

$$\alpha = \frac{V_S}{V_S + V_C} \times 100\ \% \tag{3.1}$$

where V_S and V_C are the volumes of dry slag and wet dredged clay, respectively. Three values, 20%, 30% and 40%, for α were adopted in this study to understand the influence of different steel slag content on the strength and stiffness of the slag-clay mixture. In Japan, 30% is a standard ratio often adopted in practice. The equivalent void ratios for these three steel slag contents, calculated by considering V_C as the volume of voids and V_S as the volume of solid, are well above e_{max}, causing 'floating slag particle' structures.

In preparing specimens, the water content of a dredged clay sample was firstly adjusted by adding artificial seawater to be 1.5 times its liquid limit. Kasaoka clay sample was prepared by adding distilled water to maintain similar normalized water content as dredged clays. Then by adding the required slag amount into the dredged clay, it was thoroughly mixed for 3 minutes by using a spatula. Immediately after mixing, the sample

still remained very soft. Conventional laboratory tests such as unconfined compression tests (UCTs) and triaxial compression tests could not be carried out for initial curing time, because the specimen was not strong enough to stand by itself. Therefore, direct shear tests (DSTs) were adopted for specimens at a wide range of curing times, from 0.5 hours to 28 days. This was made possible by using the shear box as a curing mold by closing the upper and lower halves together. Typically for the tests after 0.5 hours to 1 day curing time (more for some mixtures), the specimen was prepared in the shear box having a diameter of 60 mm and a height of 32 mm. For the rest of samples at longer curing time, the slag-clay mixture was cured in a separate cylindrical mold having the same dimensions as the shear box and then transferred to it. In both methods, the samples were cured at a room temperature (25^{o}C) hermetically.



(a) Horizontal section; Slag 1 **(b)** Horizontal section; Slag 2

(c) Vertical section; Slag 1 **(d)** Vertical section; Slag 2

Figure 3. 9: X-Ray CT scan images of slag-clay A mixture at α=30% (Specimen: 60mm diameter and 32mm thick)

ASTM D3080-98 recommends that the ratio of the maximum particle size to the shear box diameter should not be greater than 0.1. The ratio for slag S1 was 0.16 and slightly exceeds this criterion. However, **Fakhimi and Hosseinpour (2011)** found that a ratio of 0.2 could be used in direct shear testing with only minor loss of accuracy in shear strength measurement when the Questa rock pile material was tested under low normal stresses. In addition to the DSTs, a series of unconfined compression tests (UCTs) and bender elements tests were carried out for determining the strength and stiffness, respectively. The samples were cast in cylindrical molds with a diameter of 50 mm and a height of 100 mm. For all the specimens described above, the samples were tapped while casting to remove any air bubbles trapped within the mixture. A three-dimensional X-Ray CT scan revealed that there is no segregation of slag and clay due to tapping, and the sample remained almost perfectly uniform, as shown in **Fig.3.9**. In the X-Ray CT images, black indicates void while grayscale provides solid particles. The explanation regarding on the segregation is further discussed in Chapter 5.

3.3 pH CHANGES IN SLAG - CLAY MIXTURE

Observed pH changes are illustrated in **Fig.3.10** for all five clays mixed with 30 % of S1 from immediately after mixing to 91 days. For the pH measurement, HANNA soil direct pH/^{o}C meter HI9912N was used. The pH of the mixtures immediately after mixing (1 hour curing) was 12.3-12.8, indicating that it was strongly alkaline. As discussed earlier, organic content and acid in the dredged clays were limited to buffer the pH rise significantly. After 8 hours, substantial pH reduction started in clay A and clay B mixtures, followed by clay C and clay D mixtures. For clay A, for example, the pH decreased to 10.6 by 28 days. Clays C and D indicated no significant changes in pH even after 28 days, remaining above 12 until at least 91 days. As similar way as clays A and B, pH reduction started after 1 day curing in Kasaoka clay mixtures under both mixing water conditions, i.e., distilled water and seawater. For both mixing water conditions of Kasaoka clay, the pH decreased to 10.9-11.1.

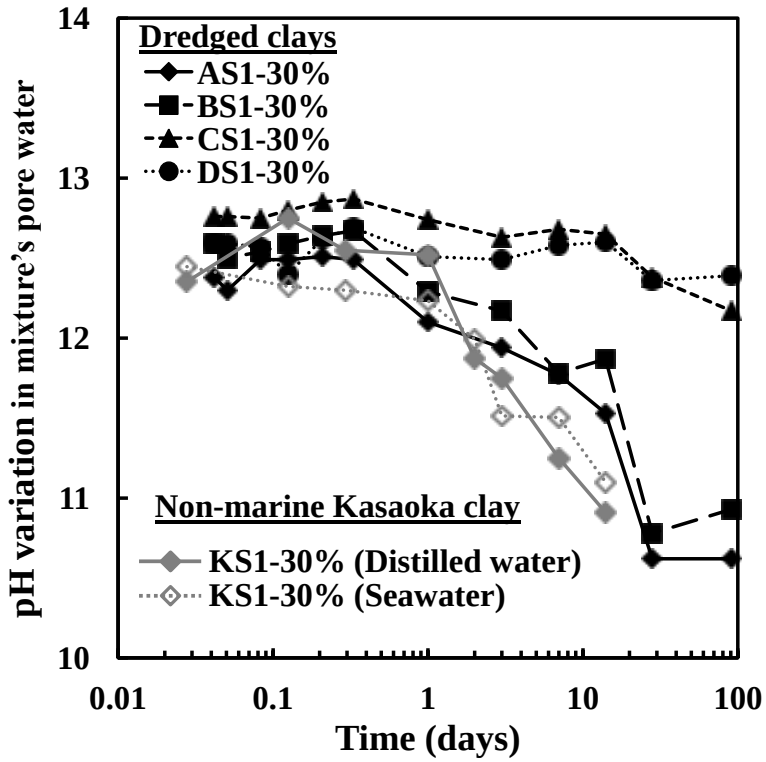


Figure 3. 10: pH variation in slag-clay mixtures' pore water during curing

The decline of the alkalinity of the pore solution is likely to be associated with the consumption of $Ca(OH)_2$ due to the hydration process. The significant pH reduction in clay A, clay B and Kasaoka mixtures are then consistent with the strong development of strength observed in these mixtures compared with clay C and clay D mixtures, as described later. It is important to notice that the initial pH of 12.3-12.8 is considered sufficiently high to dissolve amorphous silica, as **Fig.3.2** suggests. It is then inferred that the low strength, or subdued C-S-H formation process, seen in clay C and clay D mixture is due to a lack of amorphous silica itself, and not insufficiency of pH, often attributed to organic contents.

3.4 MECHANICAL TESTING METHODS

3.4.1 Direct shear test (DST)

The adopted direct shear apparatus is capable of performing tests in both constant-volume and constant-pressure conditions by servo-controlling with a computer or by mechanical fixation of the vertical ram. As shown in **Fig.3.11**, the apparatus comprises a bellofram cylinder on the top for vertical loading and a direct-drive motor on the side for horizontal

shearing. The horizontal displacement was applied to the lower half of the shear box resting on linear roller sliders.

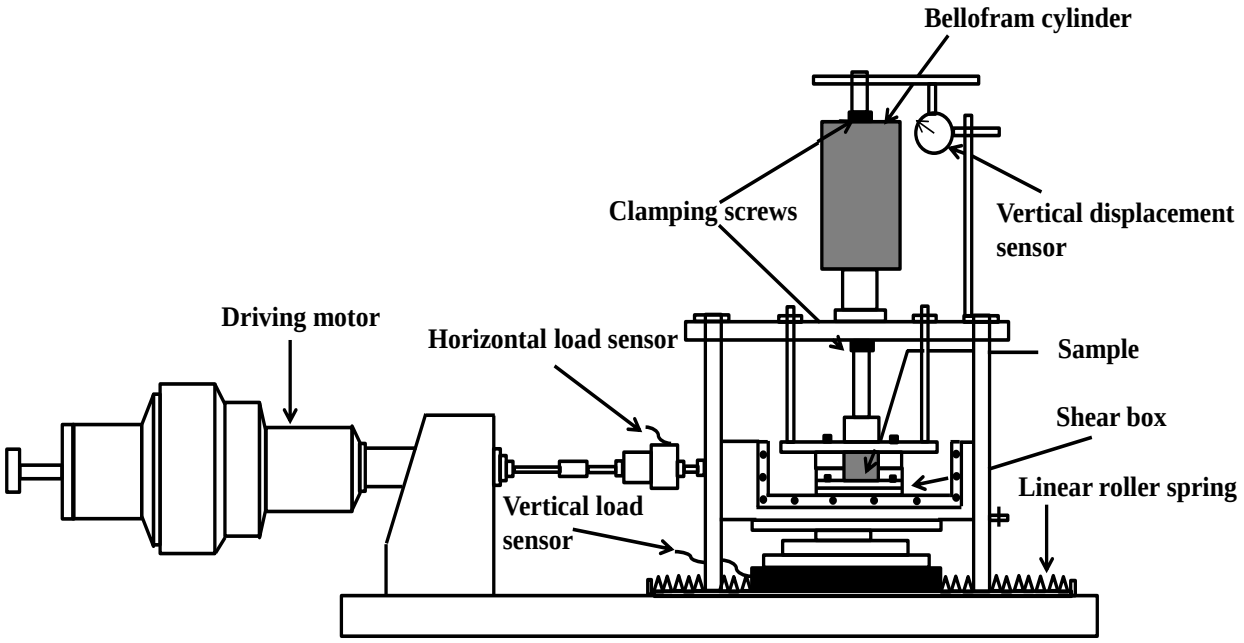


Figure 3. 11: Schematic diagram of direct shear apparatus employed in this study

After setting up the specimen inside the shear box, a low vertical pressure of 2-3 kPa was applied to the top of the specimen to ensure a contact between the top surface of the specimen and the loading platen. After this, to maintain the constant-volume condition, the loading ram of the bellofram cylinder was mechanically clamped and fixed. This is equivalent to an undrained condition similar to unconfined compression tests. Since the strength immediately after mixing can be very low, a correction was made for the friction along the roller sliders by measuring it without a specimen in place. The accuracy of the stress measurement after the correction was +/-0.8kPa. In this study, constant-volume DSTs were carried out by shearing at a quick, constant horizontal displacement rate of 2 mm/min up to a displacement of 7 mm, without submerging the specimens under water.

Since strength at immediately after mixing can be very low, the correction was made for the friction along the slider (**Fig.3.11**) by performing several DSTs without specimen at a shearing rate of 2 mm/min. In these tests, three different vertical loads of 0, 5 and 10 N were used to investigate the influence of vertical loads applied to the tank.

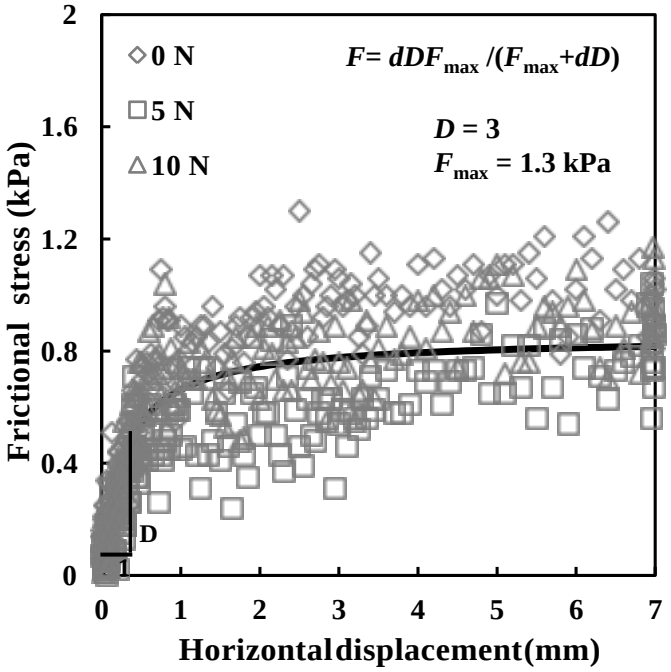


Figure 3. 12: Frictional stress in the direct shear test

Fig.3.12 shows relationship between the frictional stress and horizontal displacement for three vertical loads. For all vertical loads, the frictional stress increased linearly until the displacement of 1 mm and then it reached a constant value with some scatters. Eq.3.2 was proposed to model the relationship between the frictional stress and horizontal displacement and the determined frictional stress was subtracted from the measured shear stress in a specimen.

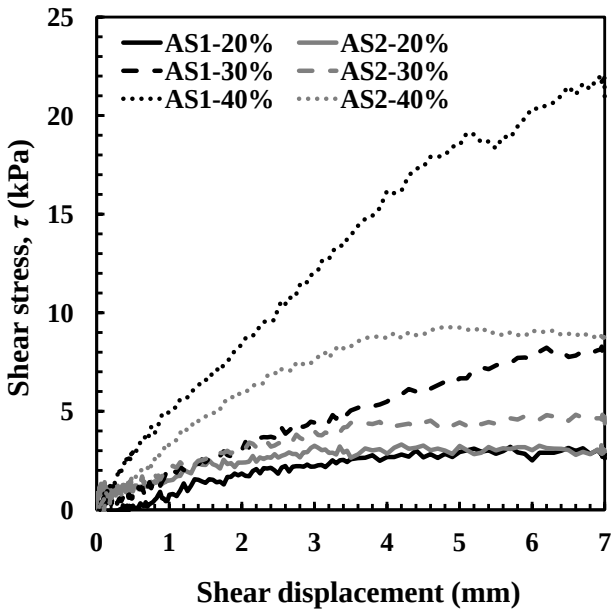
$$F = \frac{dDF_{max}}{F_{max}+dD} \tag{3.2}$$

where F and $F_{\max}$ are the frictional stress and the maximum fictional stress respectively, d is horizontal displacement and D is the gradient of the initial linear part of this relationship.

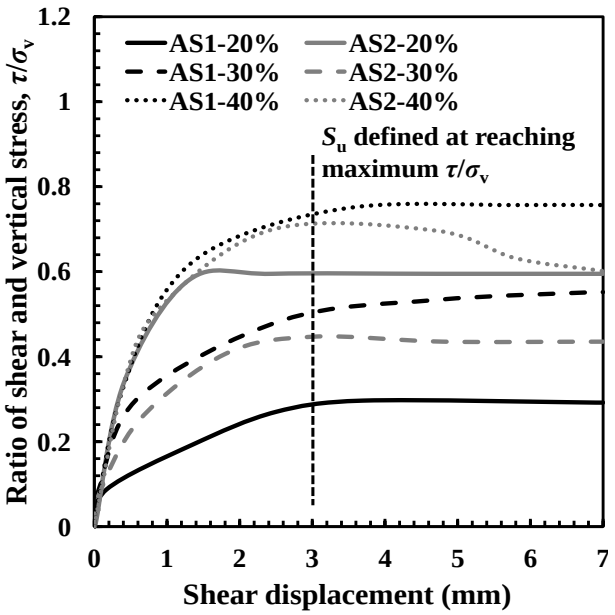
3.4.2 Defining undrained shear strength

As typical examples, six shear stress, τ, and the shear displacement relationships obtained from the DSTs on clay A mixed with slags S1 and S2 are shown in **Fig.3.13(a)** for 2-hour curing periods. In this paper, a test case is named by clay type, followed by slag type and then by the slag content. There are two distinct stress - displacement patterns between the different slags. S2 led to the clear occurrence of the failure (maximum) shear stress, τ_f.

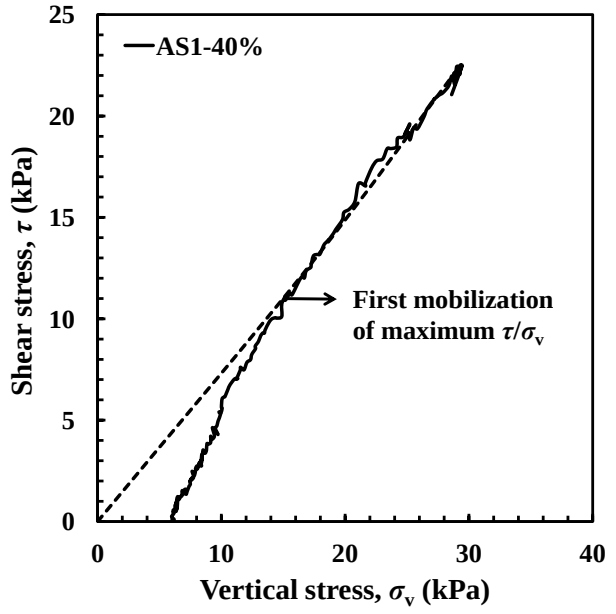
After that, the shear resistance remains approximately constant. The mixtures with S1 showed a similar tendency to this when the slag content is low (20%). For these cases, the undrained shear strength, S_u, can be defined at τ_f.



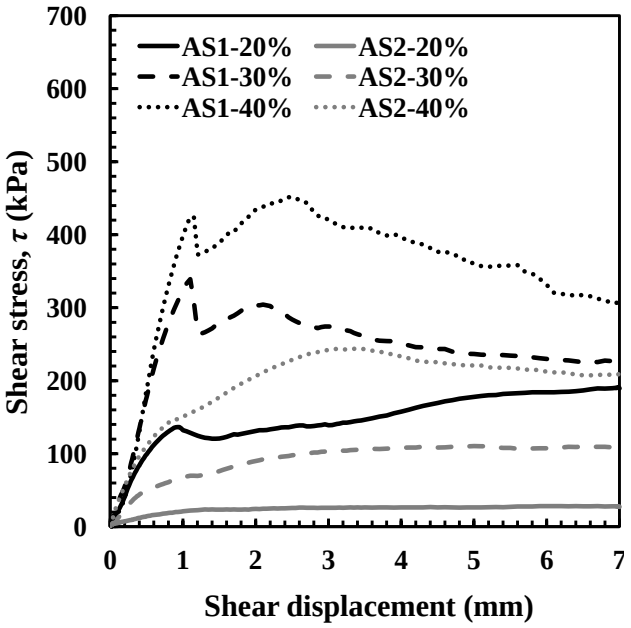
(a) Shear stress, τ, with shear displacement at 2 hours curing



(b) τ/σ_v with shear displacement at 2 hours curing



(c) Shear stress, τ, with vertical stress, σ_v



(d) Shear stress, τ, with shear displacement at 7 days curing

Figure 3. 13: Direct shear test results for clay A mixed with different slag contents of S1 and S2

In contrast to this, the mixtures with S1 at slag contents of 30% and 40% showed the continuous development of the shear resistance to the maximum applied displacement. This is considered to be due to the role of the coarser particles in causing the dilatancy in the mixtures. This behavior led to the absence of the peak shear strength, as the vertical reaction stress, σ_v increased in proportion to the shear stress as the constant volume is kept. To define the strength objectively for such cases without any clear τ– shear displacement peak, the τ value at the maximum τ/σ_v point was chosen as a lower estimate of the undrained shear strength. The stress ratio, τ/σ_v, – shear displacement plots for the data shown in **Fig.3.13(a)** are presented in **Fig.3.13(b)**. The normalized shear stress curves show a similar tendency for all the conditions. Although the stress ratio increases until a displacement of 3 mm, the shear stress only increases after that in proportion to the vertical stress by keeping a constant stress ratio. This stress ratio corresponds to the failure line in the stress space, as shown in **Fig.3.13(c)**, and defining strength at first mobilization of this ratio is a conservative and objective approach for such dilatants materials.

The τ– shear displacement relationships for 7-day curing are shown in **Fig.3.13(d)**. Significant strength development and post-peak brittleness are clear compared with the results for 2-hour curing. For many of the clay-slag combinations, the peak strength is well defined at this curing age. After the peak stress is attained, the shear stress shows a quick decrease and then an increase again in some cases. For these cases, S_u was defined by the initial peak strength, as this point registered higher τ/σ_v than in the following strain-hardening stage. Similar patterns of strength mobilization were observed in the other slag mixed-dredged clays.

3.4.3 Unconfined compression test (UCT)

The unconfined compression test is by far the most common method of soil shear testing because it is one of the fastest and cheapest methods of measuring shear strength. In the unconfined compression test, we assume that no pore water is lost from the sample during set-up or during the shearing process. A saturated sample will thus remain saturated during the test with no change in the sample volume, water content, or void ratio.

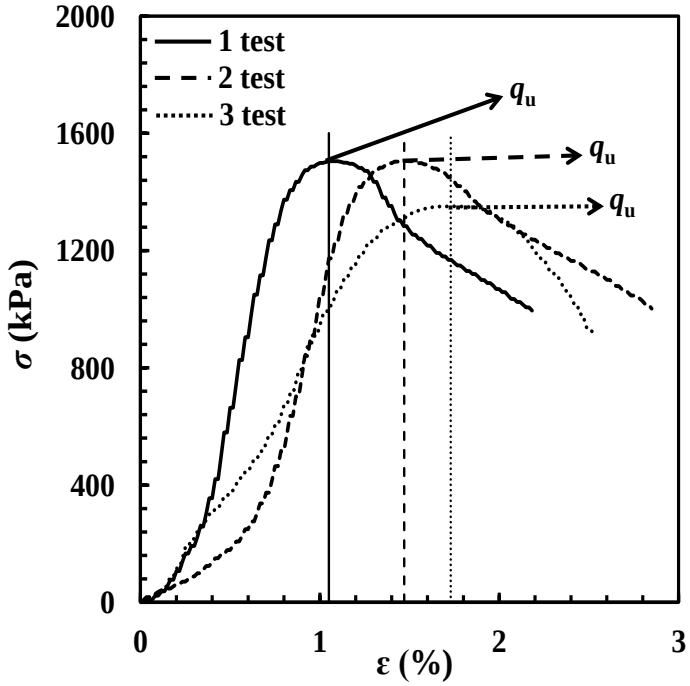


Figure 3. 14: The relationship between unconfined compressive stress, σ and axial strain, ε for three independent tests under same conditions

Pore pressures are not measured in an unconfined compression test; consequently, the effective stress is unknown. Hence, the undrained shear strength measured in an unconfined test is expressed in terms of the total stress. The UCT was conducted according to the procedures prescribed by the Japanese Industrial standards JISA 1216 (**JISA1216, 2009**). The loading rate was 1 % per minute, where the load-displacement data was automatically logged for subsequent analysis and processing. The basic parameters derived from the test were the unconfined compressive strength, q_u and the failure strain at peak stress or q_u. As shown in **Fig.3.14**, q_u is defined as peak stress during unconfined compression.

3.4.4 Variability of unconfined compressive strength

The unconfined compression tests (UCTs) were carried out on the specimens having the strength to stand on its own, i.e., curing time greater than 3 days. In this tests series, three independent tests for each slag-clay mixtures were conducted and their mean, range (max-min) and standard deviation are listed in **Table 3.5** and **3.6**. The most of clay C mixtures and all clay D mixtures were not strong enough to perform the unconfined compressive test. In **Table 3.6**, an abbreviation **"**NC" means the unconfined compressive

test for that mixture “not conducted”. All mixtures show strength increase with steel slag contents and curing time.

Table 3. 5: Unconfined compressive tests results for dredged clays

Sample	Mean (kPa)				Range (Max-Min) (kPa)				Coefficient of variation (%)			
	Curing day (Days)				Curing day (Days)				Curing day (Days)			
	3	7	14	28	3	7	14	28	3	7	14	28
AS1-20%	248	334	381	420	20	27	71	48	4.03	4.19	9.71	5.71
AS1-30%	450	723	786	1074	32	96	155	108	3.78	6.78	11.32	10.98
AS1-40%	602	1144	1646	1941	39	102	82	148	3.32	4.46	2.49	4.28
AS2-20%	64	77	93	110	7	9	1	8	6.25	5.19	0.64	3.63
AS2-30%	187	242	282	303	8	12	3	14	2.14	2.48	0.53	2.31
AS2-40%	341	547	663	775	51	44	59	63	7.62	4.20	4.52	4.51
BS1-20%	136	202	221	282	16	30	32	23	5.88	7.92	8.14	4.25
BS1-30%	230	406	556	812	15	44	50	15	3.47	5.42	5.03	0.98
BS1-40%	275	470	652	992	17	39	9	132	3.27	4.25	0.76	6.65
BS2-20%	45	55	65	77	3	18	10	13	4.44	16.36	9.23	9.09
BS2-30%	105	147	162	198	8	13	6	15	3.80	4.76	2.16	4.04
BS2-40%	241	343	422	540	7	41	49	38	1.66	6.12	6.16	3.52
CS1-20%		44	42	52		6	7	4		6.82	9.52	3.84
CS1-30%		127	200	254		79	13	43		32.28	4	8.66
CS1-40%	124	273	427	627	18	33	126	56	7.25	6.59	16.62	4.94
CS2-20%												
CS2-30%												
CS2-40%		42	44	59		1	6	19		1.43	6.82	16.95

Table 3. 6: Unconfined compressive tests results for non-marine clay, Kasaoka clay

Sample	Mean (kPa)				Range (Max-Min) (kPa)				Coefficient of variation (%)			
	Curing day (Days)				Curing day (Days)				Curing day (Days)			
	3	7	14	28	3	7	14	28	3	7	14	28
KS1-20%	221	NC	735	NC	56		71		16.29		4.89	
KS1-30%	188	356	669	959	33	41	93	97	9.57	5.89	7.62	5.00
KS1-40%	156	NC	649	NC	10		27		3.85		2.31	
KS2-20%	40	NC	122	NC	3		7		3.75		2.86	
KS2-30%	176	269	378	476	9	7	10	114	2.55	1.30	1.32	12.18
KS2-40%	228	NC	477	NC	18		25		3.95		2.73	

Out of four dredged clays, clay A mixtures showed higher strengths than others. Kasaoka clay mixtures also give similar tendency in solidification by increasing strength of all mixtures. However, these tables present the dominance of homogeneity in the variation of the mixtures unconfined compressive strength. The strength values can range from 40 kPa at lowest to 1941 kPa at highest, and their Coefficient of variation are 3.75 % to 4.28 % respectively. The variations of strengths in 40% slag content mixtures are largest with a coefficient of variation of 1.43 % to 16.62 % due to the poor homogeneity. In addition to that, some of higher strengths show a significant variation of ranges and coefficient of variation. The reason may be due to inhomogeneous solidification in higher strength level.

3.4.5 Bender element test (BE)

A bender element is a piezoelectric transducer composed of two conductive outer electrodes, two ceramic plates and a conductive metal shim at the center. When a bender element is deformed, the lattice distorts the dipole moment of the crystal and a voltage is generated. Conversely applying a voltage potential causes a bender element to deform. Hence bender elements can be used as either shear wave sources or receivers. A series of bender elements tests were simultaneously conducted. Bender element testing has been extensively adopted in geotechnical research involving cement-treated soils as a non-destructive testing method (**Consoli et al., 2009**; **Seng and Tanaka, 2011**; **Dong et al.,**

2017; **Xiao et al., 2017**).

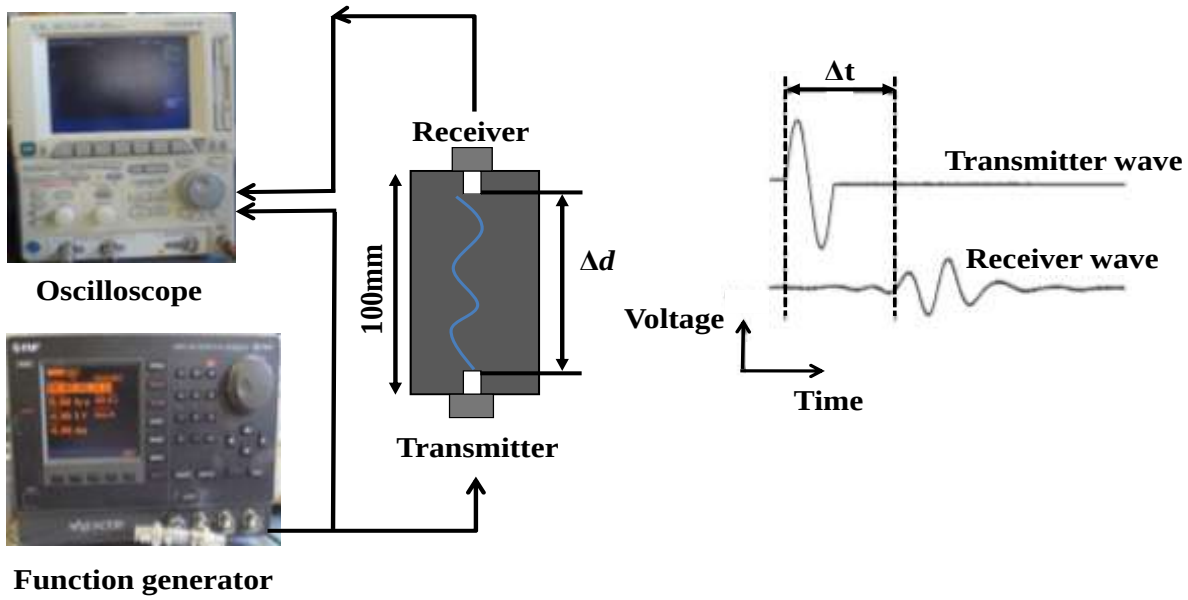
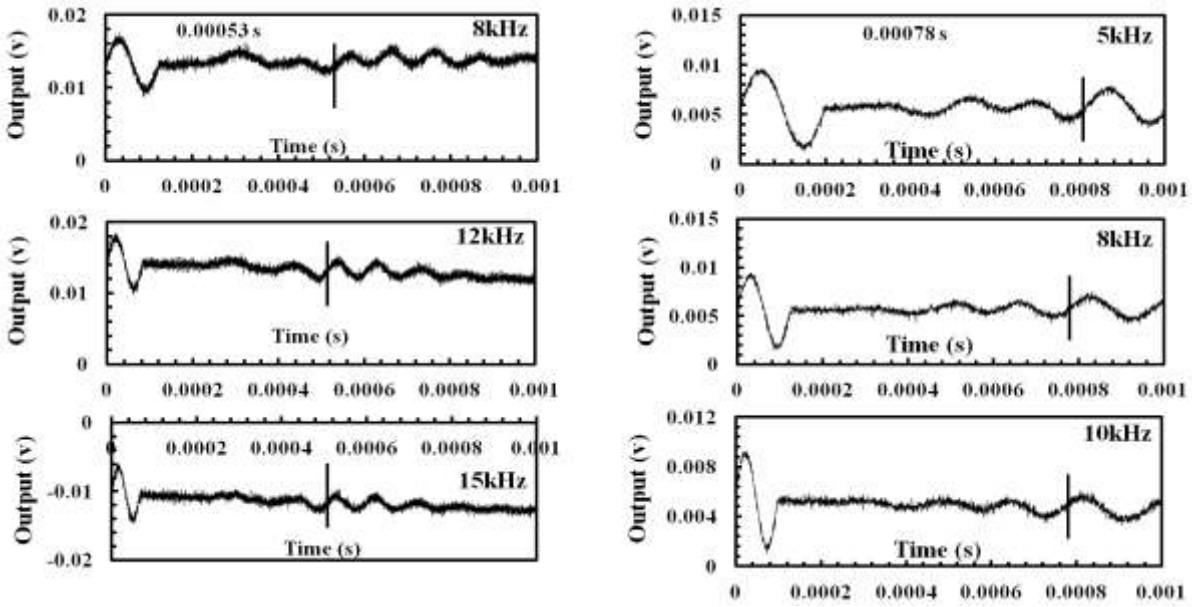


Figure 3. 15: Schematic diagram of bender element system and travel time measurement method



(a) Clay A mixed with 20% of S1 **(b)** Clay A mixed with 20% of S2

Fig.3.16. The relationship between the Output signal and travel time of shear wave for three different frequencies in 14 days curing specimens

It allows measuring shear wave velocity, V_s, or shear modulus, G, of a specimen at any specific curing time. As shown in **Fig.3.15**, a bender element of the parallel type 10 mm in length, 10 mm in width, and 0.5 mm in thickness was used as the transmitter and a

series type with a length of 13 mm, a width of 10 mm, and a thickness of 0.5 mm was the receiver. The transmitter element was assembled with a light metal cap while the receiver was attached to a brass pedestal where the protrusion length was approximately 7 and 9 mm, respectively. It is important that the protrusion length is sufficient to allow the bender element to penetrate into the soil sample to generate or receive shear waves.

The input frequency was varied according to the samples' stiffness by following the criteria suggested by **Yamashita et al. (2008)**. As shown in **Fig.3.16**, by using a function generator, high-frequency waves are created for the testing stiff soils (curing time greater than 3 days) and lower frequency waves are required for the soft soils (curing time form 0.5 hours to 3 days). Both transmitting and receiving signals are displayed in a digital oscilloscope. The shear wave velocity was determined based on the tip-to-tip travel distance and the arrival time evaluated by the start-to-start method. The typical example of determination of the travel time is illustrated in **Fig.3.16**. The small strain shear modulus was computed from the shear wave velocity and the mass density, ρ, as $G = \rho V_s^2$. As the measurement was non-destructive, a single specimen was used for each mixing condition and tested at various curing time.

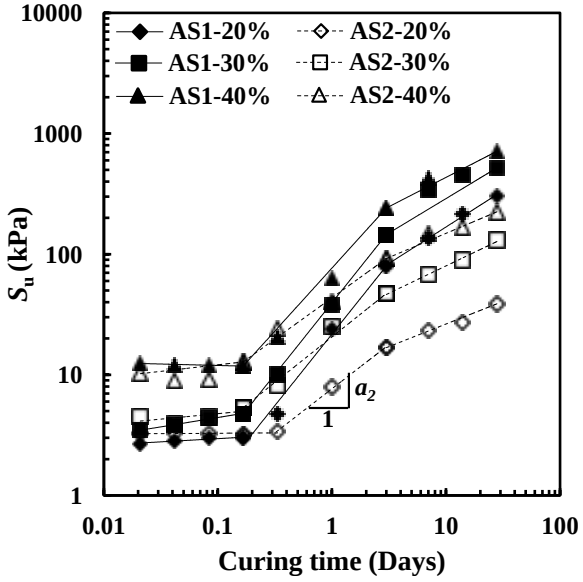
CHAPTER 4 – EVALUATION OF HARDENING CHARACTERISTICS IN STEEL SLAG-MIXED DREDGED CLAYS AND NON-MARINE CLAY

4.1 STRENGTH MOBILIZATION IN DREDGED CLAYS

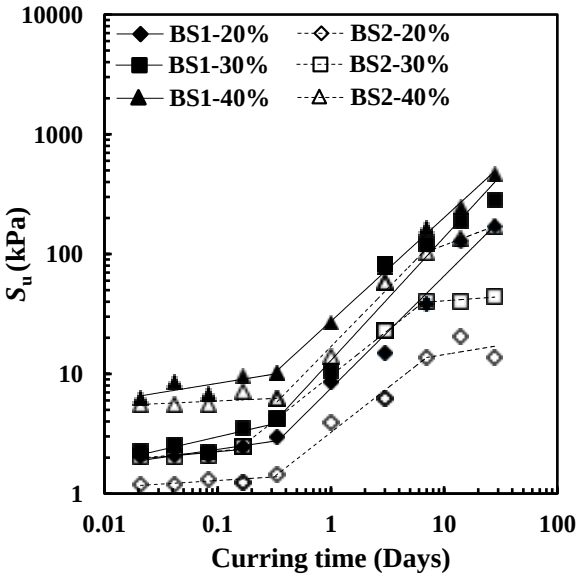
4.1.1 Patterns of strength mobilization with curing time

Fig.4.1 shows undrained strength, S_u, mobilization at different slag contents (20, 30 and 40%), with curing time, ranging from 0.5 hours to 28 days on a log-log scale. Based on the trends in each series, the strength mobilization can be divided into distinct stages. The strength mobilization can be clearly divided into three stages for the mixtures with clay A (called mixtures A for short; similar for the others) and BS2, but BS1, C, and D indicates only two stages. The first stage shows practically no strength improvement, lasting to approximately 4 hours for mixtures A, 8 hours for mixtures B, and 1 day for mixtures C and D. This stage might reflect a process of initial dissolution and diffusion of calcium and silica in the pore spaces. The end of this stage broadly corresponded to the onset of pH decline shown in **Fig.3.10,** indicating that the significant consumption of $Ca(OH)_2$ started after this stage. At this initial stage, there is no obvious influence of slag types on the strength, only affected by the slag content. The constant values of S_u were observed for both cases as the constituent grains remained unbonded. For cement-treated soils, a similar tendency was observed by **Seng and Tanaka (2011)**.

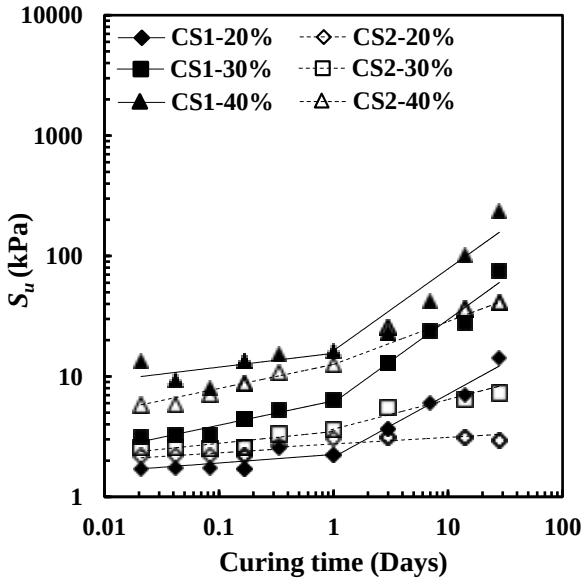
The second stage period observed was approximately 4 hours to 3 days for mixtures A, 8 hours to 28 days or more for mixtures BS1, 8 hours to 7 day for mixtures BS2 and 1 day to 28 days or more for mixtures C and D. Significant strength development was seen in this second stage as the C-S-H formation progressed, as reflected in the declining pH. In this stage, the mixtures with S1 show a tendency of greater strength increase than those with S2. Such differences between S1 and S2 are likely to be due to the higher $Ca(OH)_2$ amount in S1, as shown in **Fig.3.8**, providing a greater hydration capacity and rate than S2. To account for the difference in the gradation between S1 and S2, and for its potential influence on the results, the additional tests were performed in which the slag gradations were adjusted.



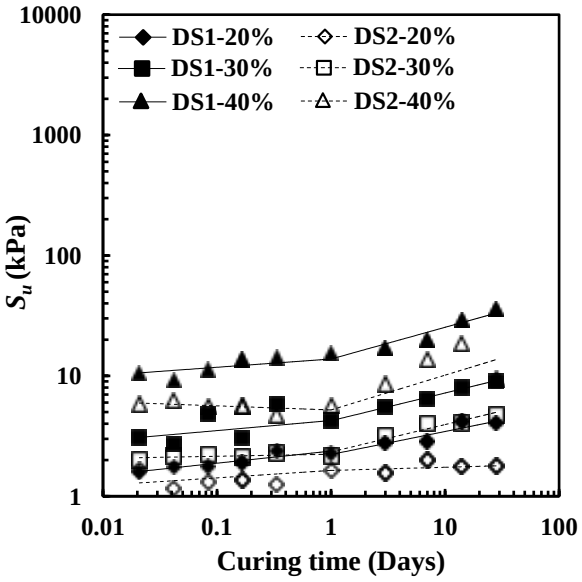
(a) Clay A mixed with S1 and S2



(b) Clay B mixed with S1 and S2



(c) Clay C mixed with S1 and S2



(d) Clay D mixed with S1 and S2

Figure 4. 1: Relationships between undrained strength (S_u) and curing time, with trend lines in log-log scale

Under the same gradation, the strength increase rates induced by S1 and S2 were even more different, suggesting that the gradation is not the cause of the observed difference. Detailed discussion on gradation was mentioned in the Chapter 5. The formation of cementitious C-S-H by the pozzolanic reaction, which occupies the voids within the soil and binds them together, was observed directly with scanning electron microscopy in

slag-clay mixtures by **Chan et al. (2014)**. The observed second stage may correspond to this mechanism. This is a mechanism common to other soil-pozzolanic mixtures (**Nakarai and Yoshida, 2015**; **Kavak and Bilgen, 2016**; **Ho et al., 2017**).

One of the major interests in practice is whether it is possible to foresee conditions that lead to reasonable strength after a standard curing period, such as 28 days, by observing the initial strength development. The patterns seen for the 24 mixtures in **Fig.4.1** suggest that 1 day of curing might reveal such groups; 9 of the 10 conditions that led to S_u of more than 100kPa by 28 days entered the second stage by 1 day. On the contrary, only one of the 12 conditions (mixtures C and D) that did not enter the second stage by 1 day attained S_u=100kPa by 28 days. This empiricism, possibly with further expansion of the data set, will be a useful first guide.

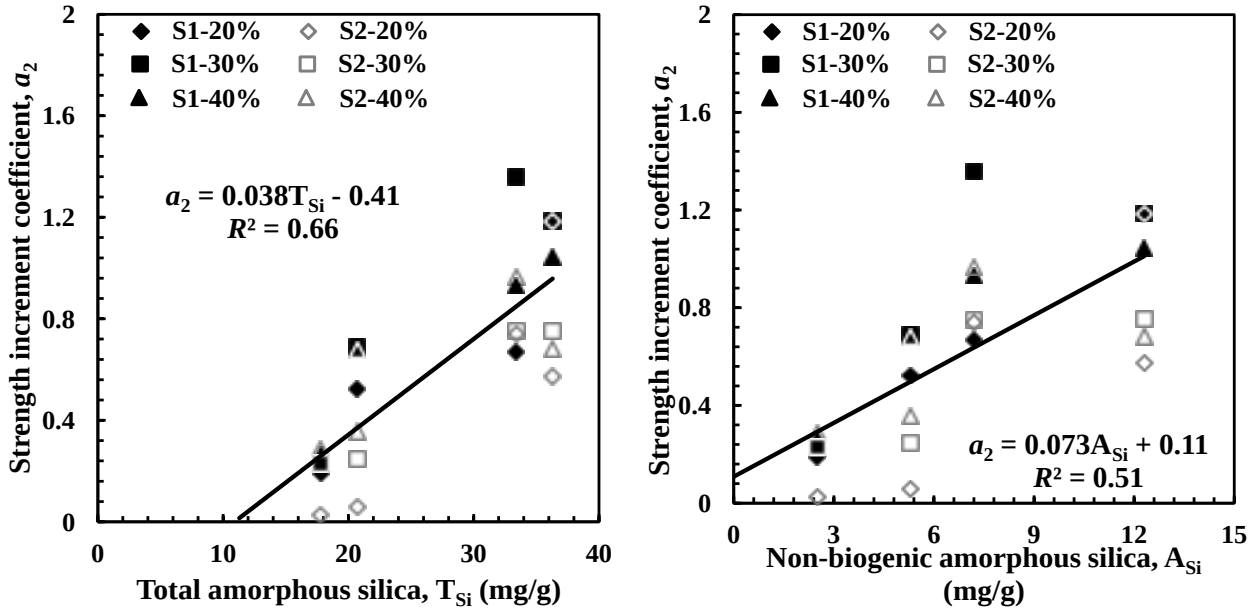
The third stage, observed for mixtures A and BS2, is characterized by the decelerated strength increase. The pH decreased by this stage to below 12, suggesting a considerable consumption of calcium and a less favorable environment for silica dissolution (see **Fig.3.10**). The C-S-H formation may still progress, but at reduced rates in this stage. This stage was not recognized for clays with much less amorphous silica (clays C and D) within the tested 28 days.

4.1.2 Correlation between strength increment coefficients and amorphous silica amount

Estimation of the strength increment rate based on chemical and other properties of dredged clays is helpful to predicting a 28-day S_u, a standard design parameter in practice, from early-age strength. To discuss the characteristics in the second stage quantitatively, the strength increment coefficient, a_2, was defined as the rate of the undrained shear strength increase against time in log-log scales, as illustrated in **Fig.4.1(a)**. Since the dissolution of both biogenic and non-biogenic amorphous silica contributes to C-S-H formation, a_2 is plotted against the total amorphous silica amount in the clays in **Fig.4.2**. The values of a_2 for most of the mixtures are not strongly affected by the slag content except in some cases. This may be because the $Ca(OH)_2$ supply was already in excess at this relatively early stage against the amount of silica, as suggested by the initial high pH

(**Fig.3.10**). However, the $Ca(OH)_2$ amount still seems to have moderate influence, as the generally lower values of a_2 seen for slag S2 suggest.

In **Fig.4.2(a)**, a loose linear correlation between a_2 and the total amorphous silica, T_{Si}, common to all the slag contents is considered. The moderate influence of slag contents makes the overall correlation too poor to be a prediction tool, but they suggest an overall trend of higher a_2 for greater T_{Si}. A similar correlation was considered between a_2 and the non-biogenic amorphous silica, A_{Si}, as shown in **Fig.4.2(b)**. Although the plots show a similar degree of scattering as in **Fig.4.2(a)**, the correlation seems to pass closely to the origin, while **Fig.4.2 (a)** shows T_{Si} offsets of 11.5 mg/g. This suggests that some part of initially existing biogenic silica is either not present or not contributing to strength development in this second stage. Biogenic silica, due to its greater specific surface area deriving from the organisms' geometry, is particularly quick to dissolve in an alkaline environment. A possibility is that it might have been partially consumed in the first stage. However, this mechanism remains hypothetic and needs to be confirmed.



(a) All mixtures of S1 and S2 with total amorphous silica **(b)** All mixtures of S1 and S2 with non-biogenic amorphous silica

Figure 4. 2: Variation of second-stage strength increment coefficient; a_2 with amorphous silica amount

Overall, the amorphous silica amount is likely to influence the rate of solidification and can decide whether a particular clay-slag mixture undergoes improvement in real time scale (typically 28 days). It can be used to screen out clays that are hard to solidify, such as clay D, based on the amorphous silica amount. Improving the correlation will require quantifying the influence of $Ca(OH)_2$, with further tests on different slags.

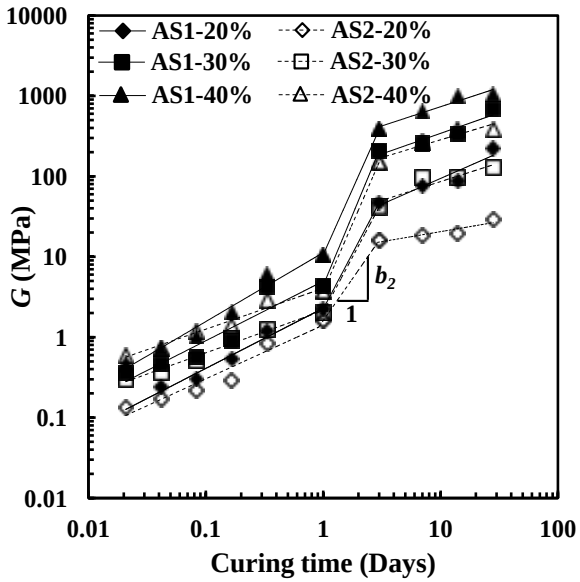
4.2 STIFFNESS MOBILIZATION IN DREDGED CLAYS

4.2.1 Patterns of stiffness mobilization with curing time

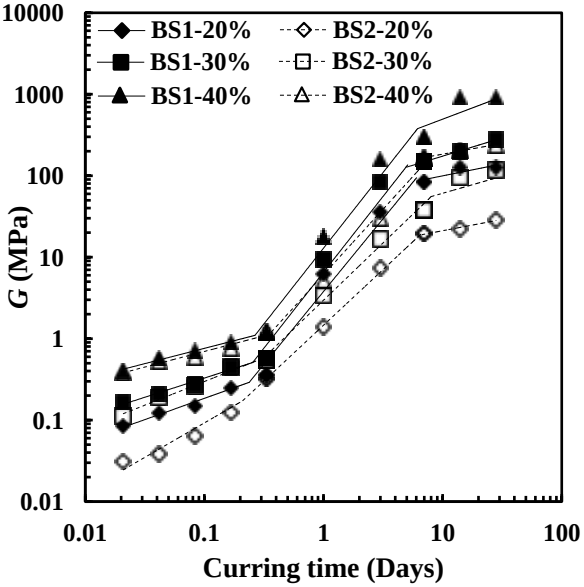
Fig.4.3 shows the shear stiffness (G) mobilization for all the mixtures with curing time ranging from 0.5 hours to 28 days on a log-log scale. Data are not shown for mixtures CS2-20% and DS2-20% from immediately after the mixing of approximately 2 hours of curing, as no clear shear wave signal was received. Similarly to the undrained strength, the stiffness mobilization can be divided into distinct stages based on the trends in each series; three stages for mixtures A and B, and two stages for C. Mixtures D indicate only a single stage and no significant development of stiffness throughout the tested curing time. Such different trends of stiffness mobilization for each mixture may reflect the same physico-chemical processes as discussed for the strength development. Different amounts of soluble silica in pore water supplied from the dredged clays possibly affected the formation rate of cementitious hydrates.

The initial stage lasted to approximately 1 day for the mixtures A, 8 hours for the mixtures B, 7 days for the mixtures C and for all the 28-day test duration for mixtures D. This initial stage is not concurrent with the initial stage identified for the undrained strength, and a slight increase in the stiffness was detected at the initial stage, in contrast to no strength development (**Fig.4.1**). The reason for this discrepancy may be remolding effect in the DST in quantifying S_u. **Seng and Tanaka (2011)** demonstrated that G in remolded clays can increase threefold in 24 hours of curing even without cement, due to thixotropy, whose effect is deleted upon remolding. The data shown in **Fig.4.3** indicate even greater increases, reflecting the initial hydration. However, this initial structure is fragile and not retained to the large strains at which S_u was evaluated. The initially flat S_u–time curves are explained by this mechanism; however, the mechanism for the delayed

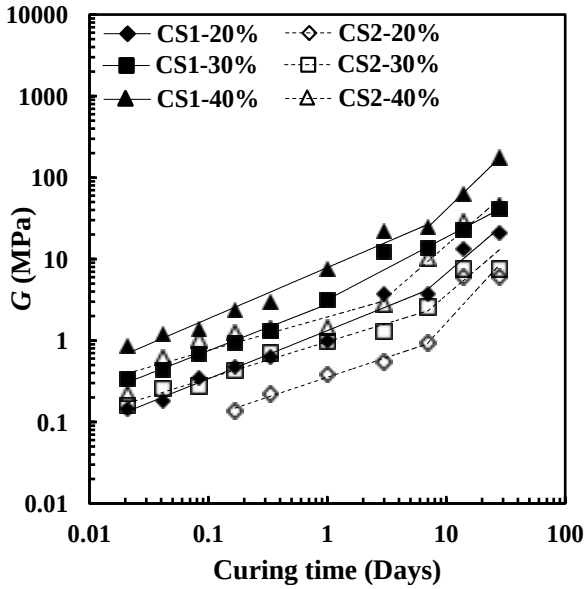
arrival of the second stage in G compared to S_u is not currently clear. At the initial stage, stiffness mobilized in most of the mixtures clearly depends on slag content but not much on its type, in a similar way as for the undrained strength.



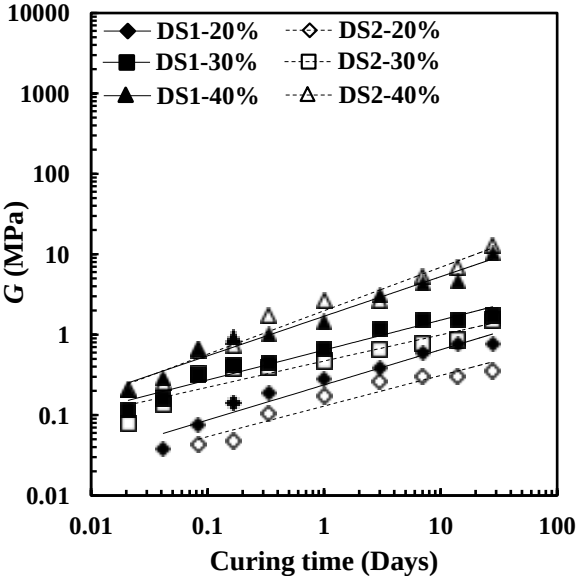
(a) Clay A mixed with S1 and S2



(b) Clay B mixed with S1 and S2



(c) Clay C mixed with S1 and S2



(d) Clay D mixed with S1 and S2

Figure 4. 3: The relationship between shear modulus (G) and curing time, with trend lines in log-log scale

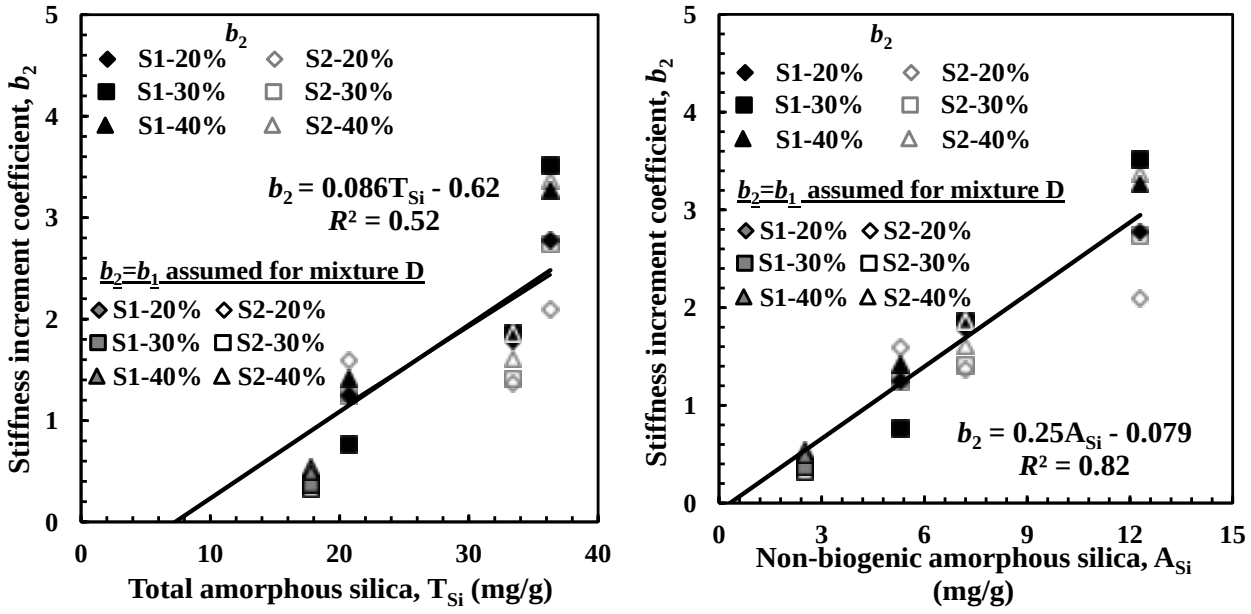
The second and the third stages are explained in the same way as for those in S_u. The second stage was observed for mixtures A, B, and C identified approximately from 1 day to 3 days, 8 hours to 7 days and 7 days to 28 days or more, respectively. The second stage

with rapid stiffness development was seen for these mixtures in the same way as the undrained strength. In this stage, the mixtures with S1 show a tendency of greater stiffness increase than those with S2, probably due to the larger amount of $Ca(OH)_2$ in S1. The third stage, observed for mixtures A and B, is characterized by the decelerated stiffness increase. The earlier discussion on the reduced pH by this stage is also relevant here.

4.2.2 Correlation between stiffness increment coefficients and amorphous silica amount

The stiffness increment coefficient, b_2, was defined for the second stage as the rate of the stiffness increase against time in log-log scales, as illustrated in **Fig.4.3(a)**. The relationships between b_2 with the steel slag contents and the amorphous silica amount, among other factors, are discussed again along a similar line as for the strength increment coefficient, a_2. The relationship between b_2 and the total amorphous silica, T_{Si}, is shown in **Fig.4.4(a)**. Mixtures D showed only the first stage within the tested 28 days, so b_2 is tentatively assumed same as b_1, the coefficient for the first stage. This assumption is based on the observation that a_2 was not significantly greater than a_1, the strength increment coefficient for the first stage.

Apart from a few outliers in mixtures A, b_2 is less affected by the slag content than a_2. **Fig.4.4(a)** shows that b_2 is fairly correlated to the clays' total amorphous silica amount. Although the b_2 values for mixture D had to be assumed, they are aligned close to the correlation line, and this would remain true unless b_2 turned out to be unrealistically greater than b_1. Extrapolation of the correlation line meets offsets of about 8.0 mg/g for T_{Si}; a similar value for a_2, as identified in **Fig.4.2(a)**. As seen for a_2, the offset disappears when b_2 is plotted against the non-biogenic amorphous silica amount, A_{Si}, and the correlation becomes stronger, as shown in **Fig.4.4(b)**. This observation leads to the same discussion as to the role of biogenic and non-biogenic amorphous silica, as described for the strength. Some part of biogenic silica seems to be absent or not contributing directly to the second-stage stiffness development.



(a) All mixtures of S1 and S2 with total amorphous silica **(b)** All mixtures of S1 and S2 with non-biogenic amorphous silica

Figure 4. 4: Variation of second-stage stiffness increment coefficient; b_2 with amorphous silica amount

In a similar way as for the strength, the earlier argument that the amorphous silica amount is a good indicator of clays that give favorable solidification results when mixed with steel slags was also demonstrated in terms of stiffness. Stiffness measurement has a virtue of being non-destructive and quick to perform on a single specimen during curing. The approach shown above can be extended to more varieties of clays and slags in future to corroborate the influence of the amorphous silica amount.

4.3 STRENGTH MOBILIZATION IN NON-MARINE CLAY

4.3.1 Patterns of strength mobilization with curing time

Fig.4.5 shows the undrained strength of Kasaoka clay mixtures mobilized at different slag contents (20, 30 and 40%), with curing time ranging from 0.5 hours to 28 days in a log-log scale. In a similar way as for the dredged clays, based on the trends in each series, the strength mobilization can be divided into distinct stages. The strength mobilization can be clearly divided into three stages for the all mixtures as seen for mixtures A. The first stage

shows practically no strength improvement, lasting to approximately 2 hours for all mixtures. This stage might reflect a process of initial dissolution and diffusion of calcium and silica in the pore spaces as similar to the process seen in the dredged clays. After this stage, there is an increase of strength in all the mixtures, indicating that the significant consumption of $Ca(OH)_2$ started after this stage. Although there is a slight influence of slag types on the strength, it is mainly affected by the slag content as similar way as dredged clays.

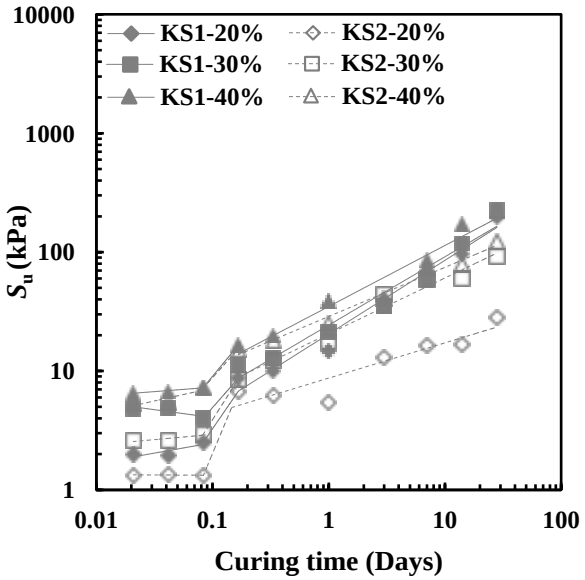
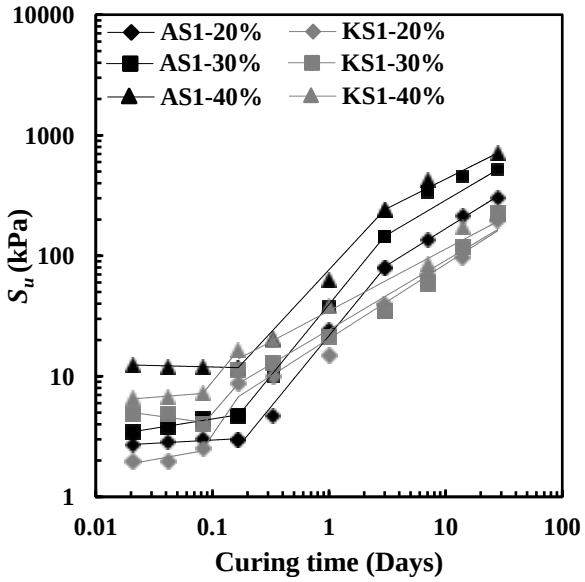


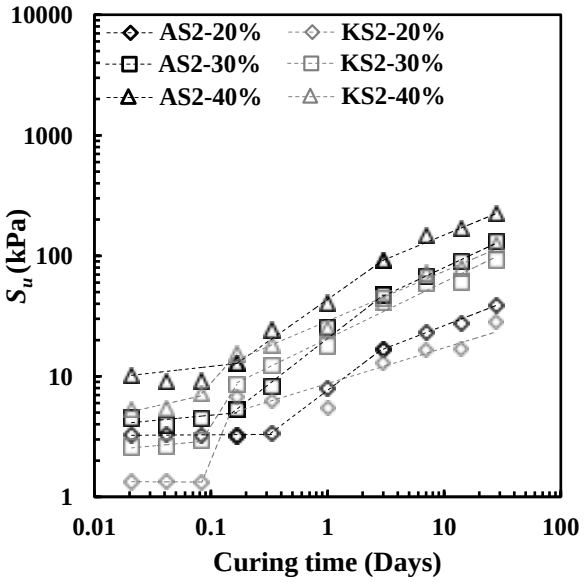
Figure 4. 5: The relationship between strength and curing time of Kasaoka clay mixed with S1 and S2, with trend lines in log-log scale

The second stage period observed was approximately 2 hours to 4 hours for all mixtures. The sudden strength development was seen in this stage and their strength values vary between 5 kPa to 20 kPa which is smaller development compared to strength development in clay A mixtures at this stage. In this stage, the mixtures with S1 show a tendency of slight strength increase than those with S2. Such differences between S1 and S2 are likely to be due to the higher $Ca(OH)_2$ amount in S1. The third stage, strength development may still progress, but at reduced rates compared to the second stage. Except KS2-20% mixture, there is no significant different in the strength enhancement between the mixtures at each curing days. Similar to dredged clays, the mixtures gained 100 kPa except KS2-20% mixtures by 28 days curing. Therefore this investigation provides a hint which is even non-marine clay produces the acceptable strength for the practical

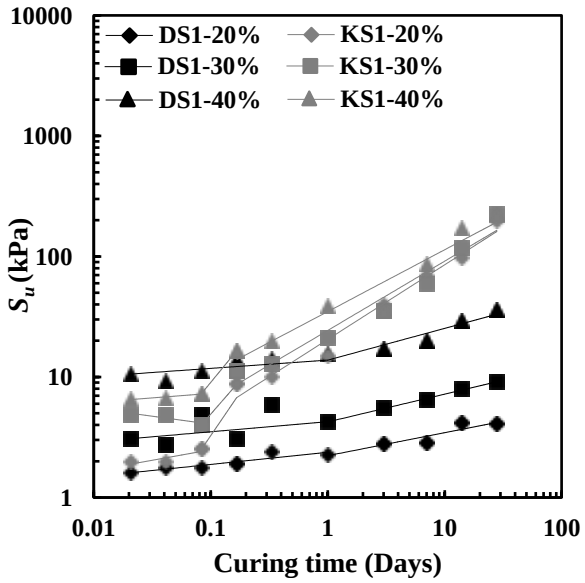
application in solidification process.



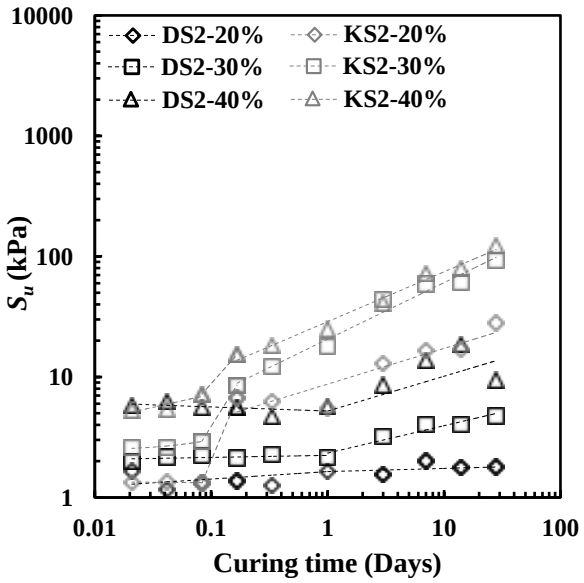
(a) Clays A and Kasaoka mixed with S1



(b) Clays A and Kasaoka mixed with S2



(a) Clays D and Kasaoka mixed with S1



(b) Clays D and Kasaoka mixed with S2

Figure 4. 6: The relationship between strength and curing time, with trend lines in log-log scale

The strength mobilization in clay A and D mixtures is selected as the strongest and weakest mixtures to compare with strength mobilization in all the Kasaoka clay mixtures. **Fig.4.6** shows comparison of strength mobilization with curing time between Kasaoka clay mixtures and clays A and D mixtures. Although there is no significant strength difference in clays A, D and Kasaoka at first stage, strength development of Kasaoka clay mixtures

starts much earlier than the dredged clays, i.e., 2 hours earlier than clay A mixtures. The second stage of Kasaoka clay mixtures is very short, i.e., within 2 hours, while clay A mixtures keep approximately 3 days in the second stage.

Strength development in Kasaoka mixtures at second stage has a considerable difference when compared with those in mixtures A and D. Even though Kasaoka clay contains highest amorphous silica amount among other clays, clay A mixtures shows greater strength development than Kasaoka clay under same steel slag type. Similar tendency was observed until 28 days curing. From the understanding of the strength mobilization in dredged clays, highest amorphous silica amount in clays were the one of key component for strong development of the mixture. But it cannot be clearly reflected in strength development of the Kasaoka clay mixtures. The reason for this case may be different pore water salinity between Kasaoka clay and clay A, i.e., seawater environment in clay A mixture may enhance dissolution of steel slag for hydration process. However, the influence of pore water salinity is further discussed in the Chapter 5. The obvious difference in strength development between Kasaoka and clay D mixtures was detected, which Kasaoka clay mixtures give greater solidification performance. The reason for this kind of discrepancies is because of higher amorphous silica amount in Kasaoka clay.

For the quantitative assessment, similar way as dredged clays, strength increment coefficient at third stage was defined by a_3. The strength increment coefficients at the third stage, a_3 is slightly higher in Kasaoka mixtures. The a_3 values of KS1 and KS2 mixtures are from 0.51 to 0.62 and from 0.30 to 0.47 respectively. It implies that greater strengths can be identified at longer curing times. However, the amorphous silica amount is likely to influence the rate of solidification and can decide whether a particular clay-slag mixture undergoes improvement in real time scale (typically 28 days).

4.4 STIFFNESS MOBILIZATION IN NON-MARINE CLAY

4.4.1 Patterns of stiffness mobilization with curing time

Fig.4.7 shows the shear stiffness (G) mobilization for all the mixtures with curing time ranging from 0.5 hours to 28 days on a log-log scale. Similarly to the undrained strength, the stiffness mobilization can be divided into distinct stages based on the trends in each

series; three stages for all mixtures. The initial stage lasted to approximately 1 day for the mixtures. This initial stage is not concurrent with the initial stage identified for the undrained strength, and a slight increase in the stiffness was detected at the initial stage, in contrast to no strength development (**Fig.4.5**). In a similar way as for the dredged clays, the reason for this discrepancy may be remolding effect in the DST in quantifying S_u. At the initial stage, stiffness mobilized in most of the mixtures clearly depends on slag content but not much on its type, in a similar way as for the undrained strength.

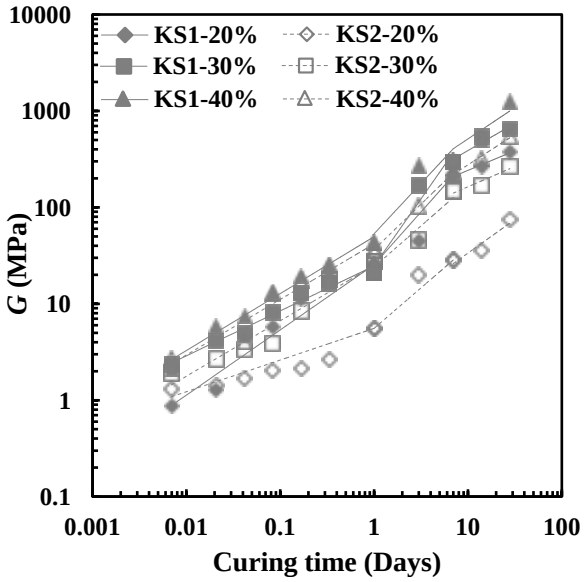
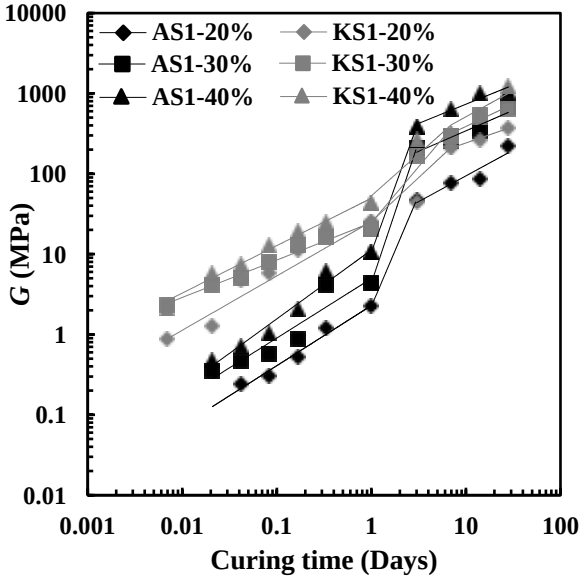
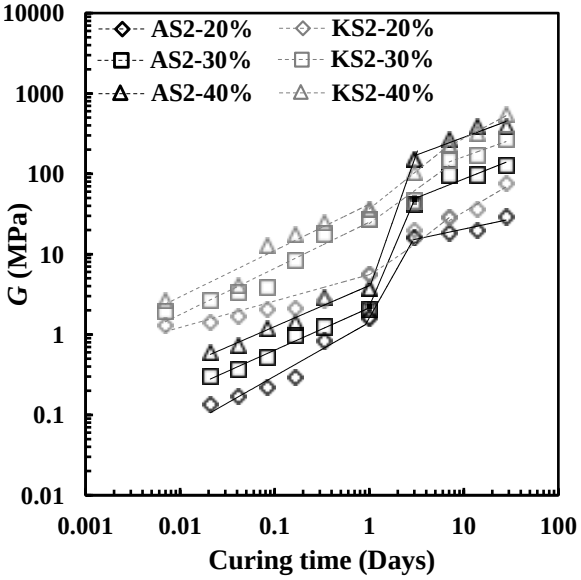


Figure 4. 7: The relationship between shear modulus (*G*) and curing time of Kasaoka clay mixed with S1 and S2, with trend lines in log-log scale

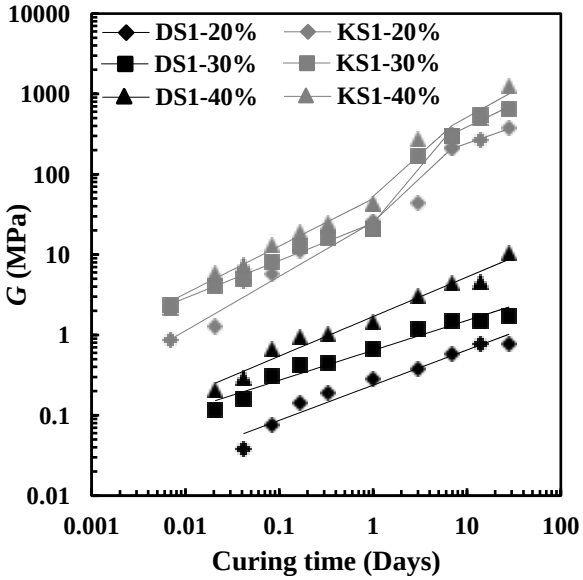
The second and the third stages are explained in the same way as for those in S_u. The second stage was observed for mixtures, identified approximately from 1 day to 7 days. The second stage with rapid stiffness development was seen for these mixtures in the same way as the undrained strength. In this stage, the mixtures with S1 show a tendency of greater stiffness increase than those with S2, probably due to the larger amount of $Ca(OH)_2$ in S1. The third stage, it is characterized by the decelerated stiffness increase.



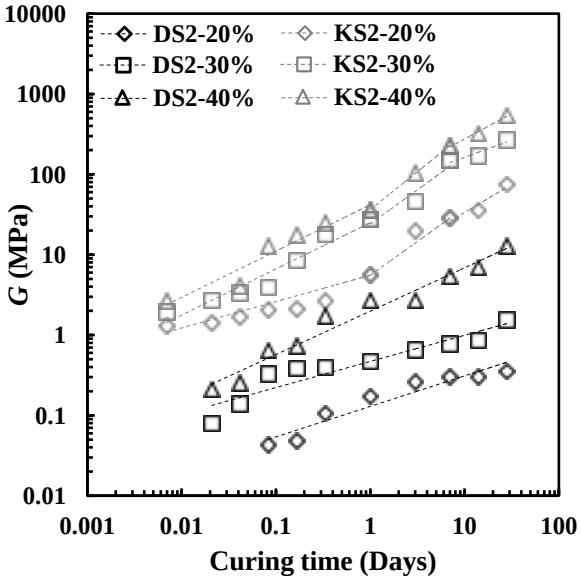
(a) Clays A and Kasaoka mixed with S1



(b) Clays A and Kasaoka mixed with S2



(a) Clays D and Kasaoka mixed with S1



(b) Clays D and Kasaoka mixed with S2

Figure 4. 8: The relationship between shear modulus (*G*) and curing time, with trend lines in log-log scale

In a similar way as **Fig.4.6**, the stiffness mobilization in clay A and D mixtures are selected as the strongest and weakest mixtures to compare with stiffness mobilization in all Kasaoka clay mixtures. **Fig.4.8** shows comparison of stiffness mobilization with curing time between Kasaoka clay mixtures and clay A and D mixtures. Kasaoka clay mixtures show higher stiffness from the first stage when compared to the stiffness in clay A and D

mixtures, by a factor of more than 10. This different solidification at initial stage of curing can be attributed by different characteristics in pore water salinity of the Kasaoka clay and some other factors such as the fineness, no organic matters. Even though the stiffness increment rates at this stage is lower than clay A mixtures, the stiffness of Kasaoka mixtures is slightly higher than those in clay A mixtures. But the stiffness increment rate and magnitude are obviously higher than those in clay D mixtures. For such a enhancement of the stiffness can be caused by higher amorphous silica consumption during hydration process.

For the quantitative assessment, similar way strength, stiffness increment coefficient at third stage was defined by b_3. For the comparison, the b_3 values for KS1 and AS1 mixtures are from 0.41 to 0.65 and from 0.48 to 0.64, and same values for KS2 and AS2 mixtures are from 0.42 to 0.70 and from 0.25 to 0.47, respectively. From the previous discussion of stiffness development in dredged clay mixtures, the clay A mixtures was identified as strong tendency in solidification by providing higher stiffness performance with support of high amorphous silica. The stiffness increment coefficients at the third stage, b_3 is slightly higher in Kasaoka mixtures. Therefore, in a similar way as strength, the greater stiffness can be identified at longer curing time. The earlier argument that the amorphous silica amount is a good indicator of clays that give favorable solidification results when mixed with steel slags was also demonstrated in terms of stiffness.

4.5 CORRELATION BETWEEN STRENGTH AND STIFFNESS

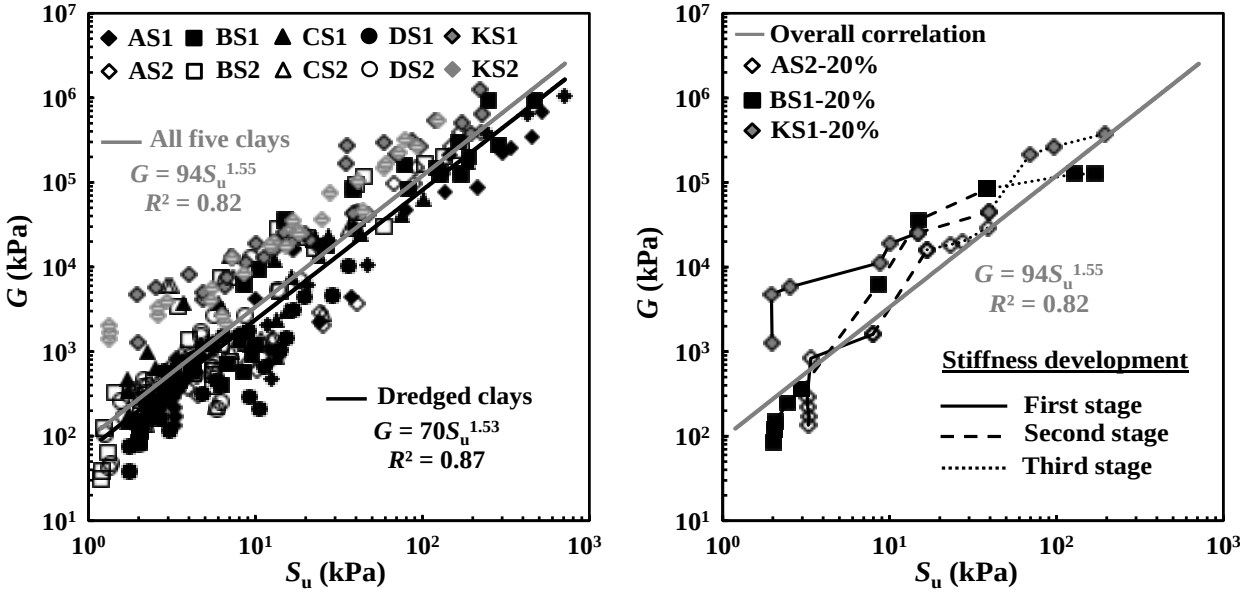
4.5.1 Overall correlation for the whole set of data

The correlation between strength and stiffness for cement or lime-mixed soils at relatively high levels of strength has been studied by many researchers (**Lee et al., 2005**; **Åhnberg and Holmén, 2008**; **Flores et al., 2010**). In this work, the strength and stiffness correlation of steel slag-mixed dredged clays was examined from early to intermediate curing range, i.e., from 0.5 hours to 28 days. **Fig.4.9** shows the correlation between G and S_u derived from the present study. As given in **Fig.4.9(a)**, The two separate regressions were applied to dredged clays and all the five clays. The linear relationships between log G and log S_u may be considered;

$$G=70S_u^{1.53} \quad (4.1)$$

$$G=94S_u^{1.55} \quad (4.2)$$

where G and S_u are in kPa.



(a) Two correlations of dredged clays and all the five clays

(b) Three typical paths during stiffness and stiffness mobilization

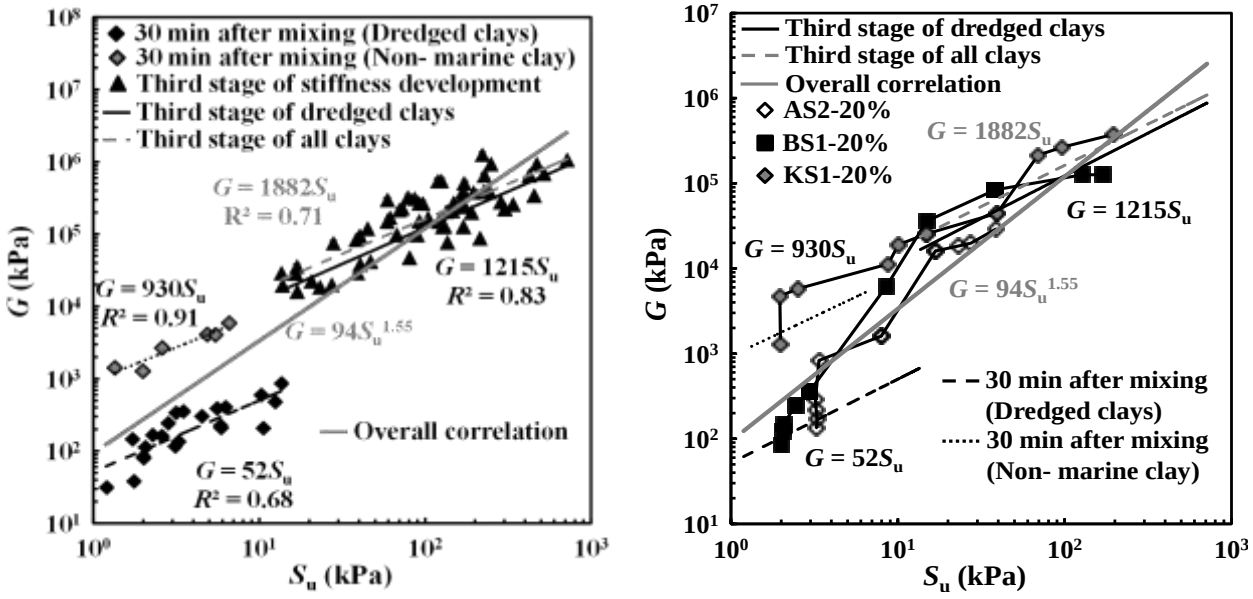
Figure 4. 9: Correlations between shear modulus (G) and shear strength, S_u

Eq.4.1 and 4.2 are identified with fare regression coefficients for dredged clays and all the five clays respectively. For these relationships, the measured G values range over six orders, from 0.05 MPa to 1060 MPa. Although the two linear relationships are nearly same, a slight difference may be caused by the 10 times greater stiffness of Kasaoka clay mixture compared to the other mixtures. In this interpretation, there are widely outlying points at medium strength levels for all the clays, because the clear differences were seen between the periods for each strength and stiffness development stage, i.e., strength and stiffness evolution was not completely concurrent. For example, the paths followed by three mixtures, AS2-20%, BS1-20% and KS1-20%, are shown in **Fig.4.9(b)** alongside the overall regression line to illustrate a typical observed path pattern during the stiffness and strength mobilization. The individual paths are initially vertical in this plot, as S_u remains

broadly constant as shown in **Fig.4.1** and **4.5**, and then lurch rightward as the second stage of strength mobilization is reached. Representing the family of paths followed by all the mixture by a single line is, therefore, misleading and inaccurate when it is taken as an averaged, typical path.

4.5.2 Identification of an alternative interpretation by considering the evolution of strength and stiffness in the second stage of curing

By considering the dramatic evolution of the strength and stiffness seen in the second stage of curing, an alternative interpretation is proposed, as shown in **Fig.4.10(a)**. Four parallel lines are drawn here, each representing (i) the state immediately (30 minutes) after mixing of dredged clays (the lowermost line; Eq.(4.3)), (ii) the state immediately after mixing of Kasaoka (non-marine clay) mixtures (Eq.(4.4)), (iii) only the third stage of stiffness mobilization in the dredged clays (Eq.(4.5)) and (iv) only the third stage of stiffness mobilization in all clays (the uppermost line; Eq.(4.6);



(a) Four correlations based on stiffness and on strength evolution stages

(b) Three typical paths superposed different correlation lines

Figure 4. 10: Correlations between shear modulus (G) and shear strength, S_u

$G=52S_u$ (4.3)

$G=930S_u$ (4.4)

$G=1215S_u$ (4.5)

$G=1882S_u$ (4.6)

Two parallel lines separately for the dredged clays mixtures and the Kasaoka clay mixtures are introduced to the state of immediately after mixing. The reason for these two lines is the stiffness in the Kasaoka clay mixtures at the first stage, more than 10 times greater than those for the dredged clays, as shown in **Fig.4.8.** Although the two upper lines at the third stage are parallel, the whole correlation is nearly 1.5 times greater than that for the dredged clays only. This discrepancy can be anticipated by the lower strength and high stiffness at 20% and 30% mixtures in Kasaoka clay compared to the other clays as illustrated in **Fig.4.6** and **4.8.**

A clear offset is seen between the lower and upper lines, and the accelerated mobilization in the second stage represents the leap from the lower to the upper line. The paths of mixtures D, which did not exhibit accelerated mobilization of the strength within 28 days of curing, also started from the lower line but did not reach the upper line except in a few cases. As seen in **Fig.4.10(b)**, the parallelism to the upper line shown by the last part of the AS2-20% , BS1-20% and KS1-20% paths confirms that the upper line is more representative of a mixture's eventual stiffness – strength relationship when the mixture has a potential to solidify to a meaningful level in engineering. More specifically, the data points of the G>5MPa cluster close to the upper line. It follows that, if G is measured in a sampled core or in the field and if it is greater than approximately 5MPa, the strength is better estimated by Eq.(4.5) and (4.6) than Eq.(4.1) and (4.2), as it is not biased by the initial 'no strength development' stage. In the meantime, the strength immediately after mixing, which is also an important factor when pipeline transportation, hopper discharge, etc. is designed, can be estimated by Eq.(4.3) and (4.4), and a quick shear wave probe. This is a useful finding, as the clay-slag mixtures' viscosity is generally too great even immediately after mixing to be evaluated by simple conventional methods, such as the

flow value test or the slump test. The flow values, obtained on 80mm-diameter and 80mm-high specimens (a de facto standard method in Japan), were all zero in all the 24 mixtures of dredged clays in this study.

Eqs.(4.3), (4.4), (4.5) and (4.6) are in linear forms, and this makes the expressions independent of the unit for G and S_u. **Seng and Tanaka, (2011)**, who studied cement-treated soils over a wide G and S_u range, also proposed a linear relationship $G=310S_u$ for their materials. This expression, with the coefficient of 310, falls between Eqs.(4.3) and (4.6). In fact, the data by **Seng and Tanaka, (2011)** also indicate that the G–S_u relationships initially show vertical portions, just as shown for the slag-clay mixtures in this study. Discarding these initial data will make their correlation line closer to Eq.(4.5) and (4.6).

Due to the limitation of time and resource, the present study could not extend the observation beyond the 28 days of curing. Questions remain as to whether (i) Eq.(4.5) and (4.6) are valid for longer curing periods and (ii) clays with lower amount of amorphous silica and hence a smaller potential for solidification, such as clay D, will eventually join the line by Eq.(4.5) and follows it in longer curing periods.

4.6 SUMMARY

Characteristics of strength and stiffness mobilization in steel slag-mixed dredged clays and non-marine clay were investigated in this chapter based on results from series of direct shear tests and bender element tests. The main focus was on the property changes in short to medium curing time, the possible relationship between physical and chemical properties of the steel slag-mixed clays, and potential correlation between stiffness and strength. Several conclusions are drawn as follows.

1. The very different strength and stiffness evolution patterns were identified for the 30 mixtures, with 5 clays and 2 steel slags at 3 different mixing ratios. For dredged clay mixtures, stiffness and strength mobilization patterns can be clearly categorized into distinct stages according to curing time. The most significant changes of the mechanical properties of dredged clays occurred between 4 hours and 3 days at earliest in some

mixtures, while this was significantly delayed or not observed in the others. The evolution of the shear strength and stiffness was no completely concurrent.

2. Even though the Kasaoka clay mixtures showed the distinct stages of stiffness and strength mobilization with curing time, the variation of the development rates.

3. The stiffness and strength increase rates, quantified as coefficients, in the second stage of evolution in different dredged clay-slag mixtures were found to be loosely correlated to the amorphous silica amount, of non-biogenic origin in particular. The correlation was probably also influenced by the Portlandite ($Ca(OH)_2$) amount in slag. The clays having the very small total amorphous silica amount (less than 10 mg/g) are hard to solidify and screened out at initial stages of investigation and design as mother soil for the slag-soil mixture.

4. By comparing the strength and stiffness mobilization of Kasaoka clay mixtures with those in clays A and D mixtures, it may further reveal that solidification can enhance by the influence of the amorphous silica content.

5. A correlation between the stiffness and strength was explored in two ways. A conventional approach of considering the whole dataset was fairly correlated by a linear function. However, subdividing the dataset by considering the three distinct stiffness and strength evolution stages led to more accurate and meaningful multiple correlation lines. These correlations represent the observed property paths better and may be used to estimate the strength at different stages based on non-destructive stiffness probes in practice.

CHAPTER 5 – FURTHER INVESTIGATION OF THE FACTORS AFFECTING MEASURED STRENGTH AND STIFFNESS

5.1 INTRODUCTION

This chapter discusses effect of additional factors on strength and stiffness development in steel slag-clay mixtures. The strengths obtained by direct shear tests were further investigated by comparing them to strengths obtained for similar mixtures by unconfined compression tests to understand effects of different test methods. It is still unknown what kind of mixing water leads to greater strength and stiffness development in terms of pore water salinity, and this issue needs to be experimentally addressed. Since the various grain size of steel slag may result in a difference in strength and stiffness mobilization, two types of steel slags with different grain sizes and properties were compared in this study.

In this chapter, the strengths obtained from 3-day to 28-day curing time between direct shear and unconfined compression tests were compared by using four different dredged clay mixtures and a non-marine clay, Kasaoka clay mixtures. Effects of pore water salinity, i.e., distilled water and seawater for mixing, and variation of grain sizes in steel slags on strength and stiffness mobilization were investigated by unconfined compression and bender elements tests. In addition to that a variation of grain shapes in steel slags was understood. From them, factors that should be taken into account in design are identified.

5.2. COMPARISON OF STRENGTHS OBTAINED BY DIRECT SHEAR AND UNCONFINED COMPRESSION TESTS

By using clays A, B and C mixtures, a comparison of the undrained shear strength obtained by the direct shear tests (DSTs) and the unconfined compression tests (UCTs) was made for curing time of 3 to 28 days. As given in **Table 3.6**, two different curing time ranges were adopted for specimens of non-marine Kasaoka clay mixtures in unconfined compression test, i.e., 3 days and 14 days for 20 % and 40 % slag content mixtures and 3 days to 28 days curing condition for 30 % slag content mixtures. These data were also

included in this discussion. The comparison is shown in **Fig.5.1**. For the most data points, S_u measured by the UCT is higher than that from DST.

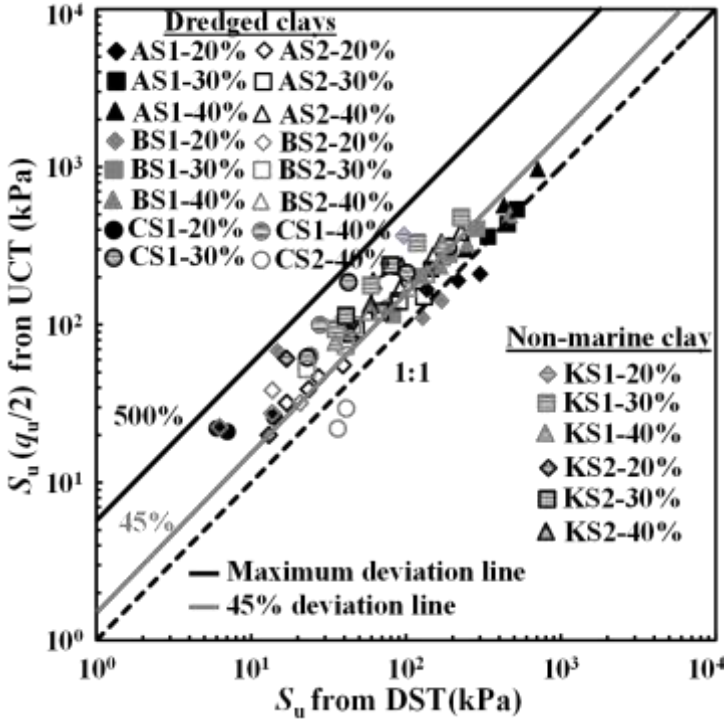


Figure 5. 1: Correlation between undrained shear strengths obtained by direct shear and unconfined compression tests

In this figure, two deviation lines from 1.1 ratios were introduced; the maximum deviation line for the data with the strength less than 400 kPa (difference within 500 %) and 45 % deviation line of strength approximately greater than 400 kPa. This significant variation at low to medium strength level (S_u less than 400 kPa) can be due to, (i) the undrained strengths obtained by DSTs was defined at first mobilization of the maximum stress ratio, as discussed in **Fig.3.13(c)**, and the undrained strengths obtained by UCTS was defined as the half of maximum value σ, which coincided with the maximum force measurement. The former does not reflect the significant dilatancy that led to shear stress increase after reaching the failure envelope, seen for the mixtures with lower strength (ii) the systematically larger UCT strength may be attributed to the specimens' anisotropic properties and the difference in the loading rates between the UCT and the DST.

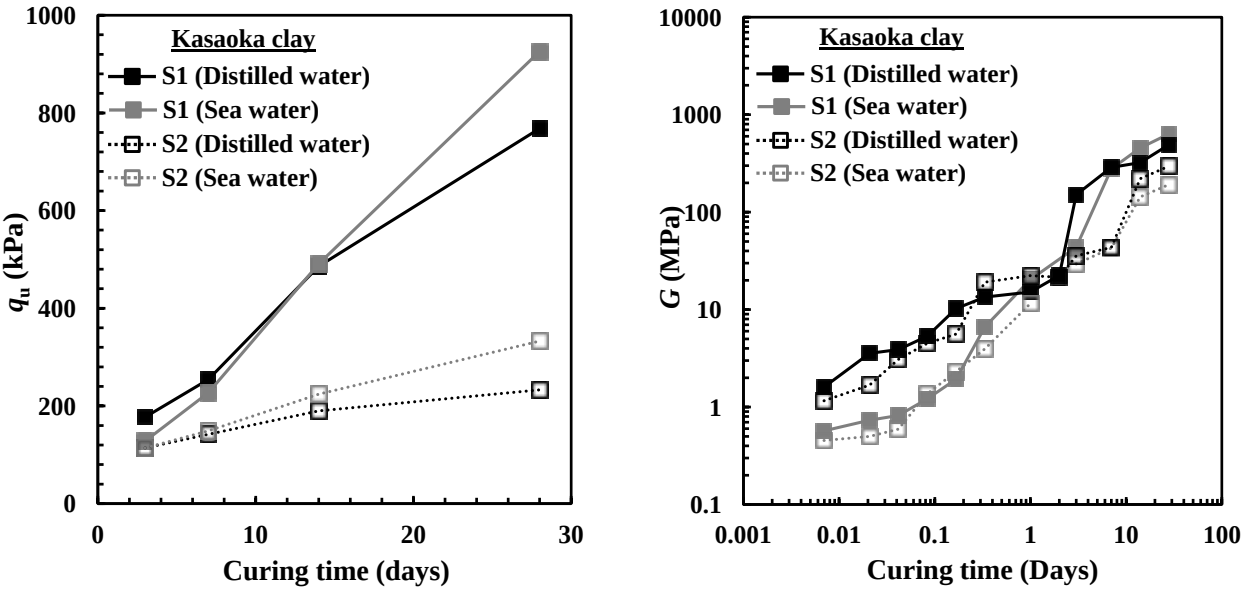
The mixtures having the strength greater than 400 kPa gives comparable agreement between UCTs and DSTs as reflected by the difference within 45 % shown in **Fig.5.1**. For many of the clay-slag combinations at high strength level, the peak strength is well

defined in DST at the curing age as shown in **Fig.3.13(d)**. For these cases, S_u was defined by the initial peak strength, which was not followed by the significant dilatancy seen for S_u obtained from UCTs. Therefore, the undrained strength obtained by direct shear and unconfined compression tests showed the different degree of agreement of strength comparison at low and high strength levels.

5.3 INFLUENCES OF PORE WATER SALINITY ON NON-MARINE KASAOKA CLAY MIXTURES

5.3.1 Effect of pore water salinity on the strength and stiffness mobilization in Kasaoka clay mixtures

As shown in **Fig.5.2**, the influence of pore water salinity on unconfined compressive strength, q_u obtained by UCTs and stiffness mobilization was studied, i.e., distilled water and seawater. From **Fig.5.2(a)**,it can be clearly noticed that until 14 days curing time, there is no significant difference in strengths between mixing distilled water and seawater. This can be expected by the formation of same C-S-H hydrates, as reflected in the similar declining pH in between Kasaoka clay mixed with distilled water and seawater, as shown in **Fig.3.10.**



(a) Strength with curing time **(b)** Stiffness with curing time

Figure 5. 2: Strength and stiffness mobilization with curing time for Kasaoka clay-slag mixture prepared with both distilled water and seawater

At 28-day curing time for slags S1 and S2, the seawater mixed specimens showed higher strength compared to distilled water mixed specimens. Such a difference in strengths may occur by the behavior of the dissolution of Ca from steel slag and Si from the clay-slag mixture under the distilled water and seawater mixing condition. For example, **Zhang et al. (2012)** found that the CaO/SiO_2 ratio of slag is the main factor on the dissolution behavior of elements. As well as the dissolution of Si increases with the slag/seawater ratio. In addition to that **Matsuura et al. (2016)** reported that the mixing of dredged soils with slag increased the dissolution concentration of Si and Ca in seawater.

As illustrated in **Fig.5.2(b)**, the distilled water mixed specimens show greater stiffness than seawater mixed specimens from immediately after mixing to 1 day curing time. There are two factors that may influence the difference in stiffness at initial curing condition. The first factor is that the rheological properties of the clay differ due to the various influence of pore water of the clay in distilled water and seawater mixtures. The consumption of Ca and Si cannot be observed until 1 day curing as reflected in no pH declining for both of distilled water and sweater mixing condition at initial curing. The second factor may be the influence of the pore water salinity on the stiffness mobilization at initial curing. After 1 day curing time, stiffness in four mixtures show significant development as reflected in C-S-H formation by declining pH for both distilled water and seawater mixing condition. There is no considerable difference in the overall stiffness mobilization rate between distilled water and seawater in contrast to the strength. The reason for this behavior may be the accuracy of reading the bender element test data.

5.4 INVESTIGATION OF EFFECT OF STEEL SLAG GRAIN SIZE ON STRENGTH AND STIFFNESS MOBILIZATION

5.4.1 Adjustment of different grain size of steel slags

In order to understand the influence of slag grain size on strength and stiffness mobilization, S1 slag was split into three different grain size ranges. The dredged clays having two different solidification responses were selected for the assessment of the effect of grain size, i.e., clay A with clear strength and stiffness development, and clay C with relatively low degree of developing.



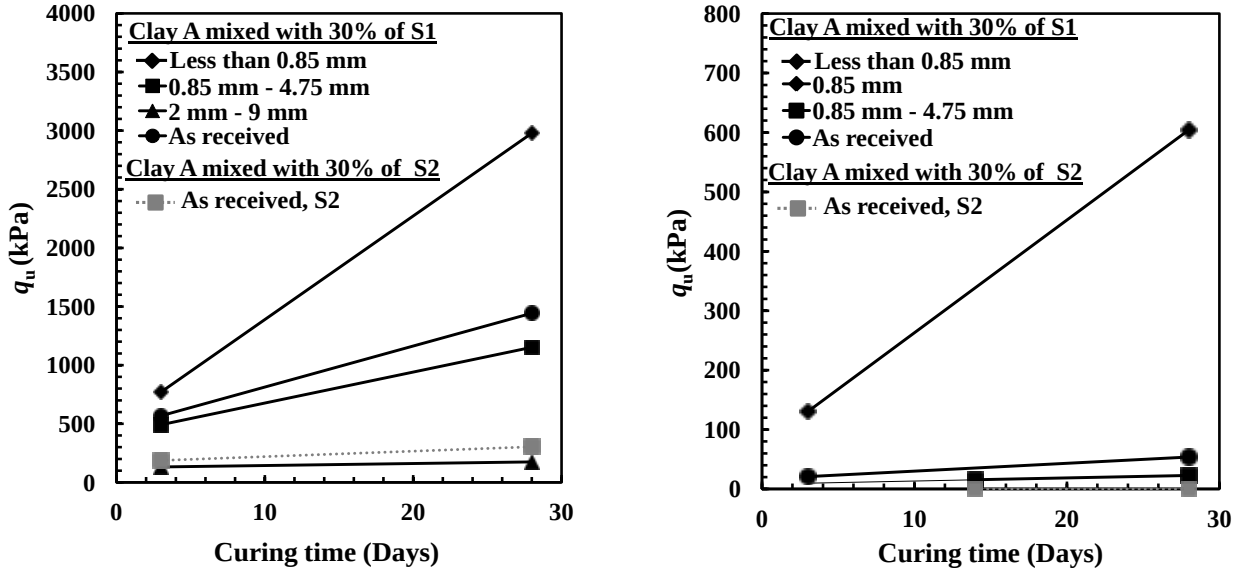
(a) <0.85 mm **(b)** 0.85 mm - 4.75 mm **(c)** 2 mm – 9 mm **(d)** As received

Figure 5. 3: Adjustment of grain size of S1 steel slag

As can be seen in **Fig.5.3**, four different grain size ranges were set; less than 0.85 mm, 0.85 mm- 4.75 mm, 2 mm-9 mm and as received. The slag content was set at 30% in the series. The unconfined compression tests were carried out for four different grain size ranges at two different curing times, i.e., 3 days and 28 days. The bender elements tests were conducted on same grain size ranges at 30 min after mixing to 28 days curing time.

5.4.2 Influence of different slag gradation on strength mobilization

Fig.5.4 shows the strength mobilization in the clays mixed with slags in four slag grain size ranges with curing time and further comparison of the strength obtained with S2 slag in the received form.



(a) Clay A mixed with slag 1 **(b)** Clay C mixed with slag 1

Figure 5. 4: Strength mobilization with curing time, according to different grain sizes of slag

From the very first look in the figure, it can be clearly identified the finest slag grain range, i.e., slag grain size less than 0.85 produced significantly higher strength compared to the other grain size ranges. This is attributed to the larger specific surface of the finer particle promoting the chemical reaction for formation of C-S-H hydrates. The similar tendency was found in solidification in dredged marine clay with steel slag by **Chan et al. (2012)**.The strength increment rates in clays A and C mixtures for the specimens having slag grain size less than 0.85 mm are considerably higher than specimens prepared with as-received form of slag, i.e., 2.1 times and 11 times respectively at 28 days curing. Since S2 slag in as-received form has grain size range of 0.85 mm-4.75 mm, it can be compared with S1 slag under same grain size rage to observe the difference in the strength mobilization between S1 and S2.Under the same slag gradation, the strength increase rates induced by S1 and S2 were more different, i.e., 3.8 times for clay A mixtures at 28 days curing and 22 times for clay C mixtures at 28 days curing. It suggests that the gradation is not the cause of the observed difference between the strength development with S1 and S2 at as-received gradations. However this factor is further discussed clearly in the next section.

5.4.3 Investigation of strength mobilization under the same gradation in both steel slag types

For understanding of the effect on strength mobilization under the same gradation in S1 and S2, original samples of two steel slags were sieved to obtain grain size of 0.85 mm-4.75 mm. To see a clear difference in strength mobilization, the clay A, which shows the strongest strength development, was mixed by adding these gradation-adjusted steel slags.

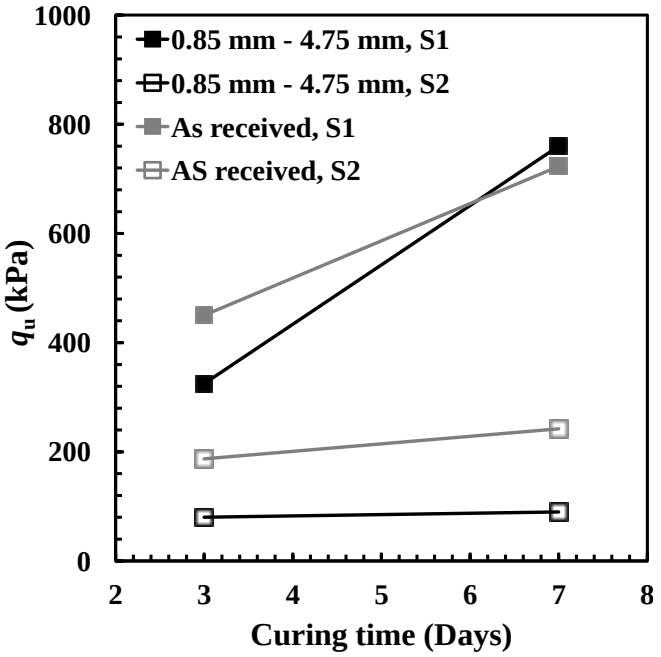
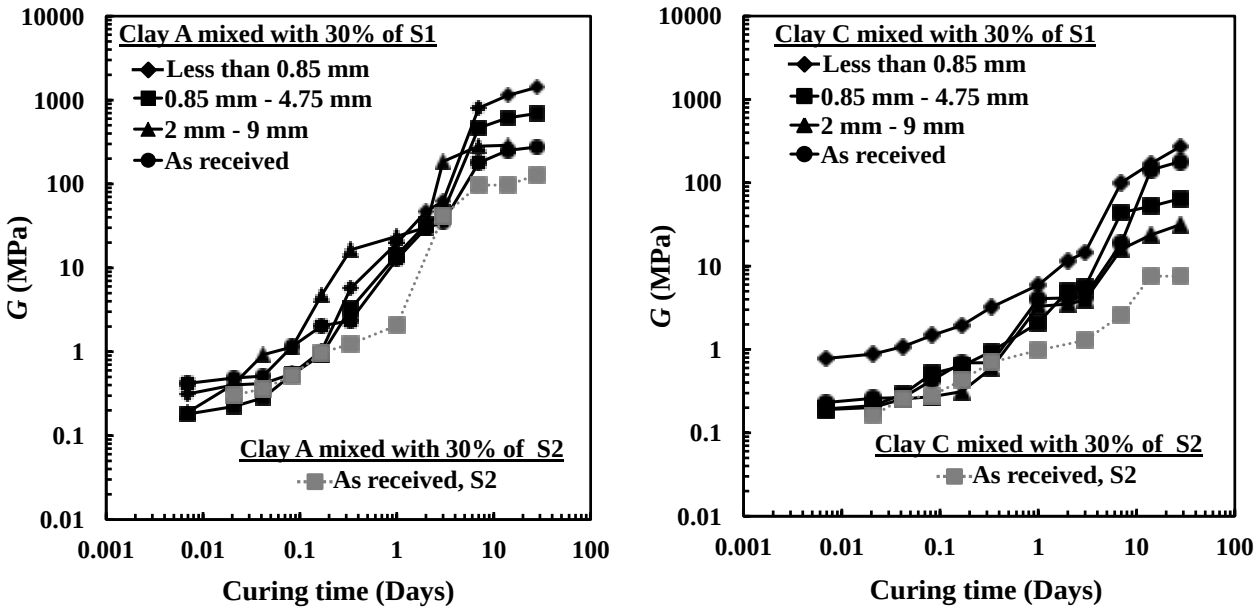


Figure 5. 5: Strength mobilization in clay A with curing time for similar gradation of slags S1 and S2

Unconfined compression tests were carried out on the specimens cured for 3 days and 7 days. **Fig.5.5** presents a variation of unconfined compressive strength with curing time for the adjusted slag grain size of S1 and S2. In a similar way as shown in **Fig.5.4**, S1 slag mobilized higher strength with a significant increment rate than S2 slag, i.e., 44 times greater than S2. Even if the grain size of the slag is same, the surface area of the slag can change by the different grain shape, which may affect the chemical reaction of the mixture for the C-S-H formation. In chapter 4, the amount of $Ca(OH)_2$ presences in S1 and S2 was identified as a key factor for different strength mobilization between S1 and S2. But this discussion leads to further investigation of slag grain shape variation between S1 and S2.

5.4.4 Influence of different slag gradation on stiffness mobilization

Fig.5.6 shows the stiffness mobilization in the mixture with S1 slag prepared in four grain size ranges with curing time, in comparison with stiffness values obtained with S2 slag in as-received form. Clay A does not give much difference in stiffness at the early stage of curing (before 1 day curing) between different grain size ranges. However, clay C shows a considerable increase in stiffness for the specimens of slag grain size less than 0.85 mm at initial curing and it is greater compared to same slag grain size specimen in clay A.



(a) Clay A mixed with slag 1 **(b)** Clay C mixed with slag 1

Figure 5. 6: Stiffness mobilization with curing time, according to different grain sizes of slag

The clay C has the lowest liquid limit and hence low water content among the four dredged clays. Therefore the higher surface area in finer slag grain size specimen with low water content may accelerate the water absorption effect resulting in such change of stiffness. As another reason, the accuracy of interpreting the bender elements test data may influence the final result. Similar to strength, finer grain size specimen produces higher stiffness with increasing curing time (greater than 1 day) and stiffness values under the same gradation have significant difference between S1 and S2, suggesting that the gradation is not the sole cause of the observed difference between the stiffness development with S1 and S2 at as-received gradations.

5.5 IDENTIFICATION OF STEEL SLAG GRAIN SHAPE IN S1 AND S2

5.5.1 Analysis of slag grain shape

In order to quantify the shape of the slag grains in S1 and S2, four different diameters were selected for taking images, i.e., 0.5, 1, 2 and 4 mm. From each slag grain size, five grains were randomly extracted for quantifying grain shapes in the slag sample. The grain sizes of 0.5, 1 and 2 mm were examined by using an optical microscope. Slag grains of 4 mm size were photographed by a digital camera. The two-dimensional projection plane

was selected by considering the plane where slag grain showing the larger slag grain area.



Figure 5. 5: Image processing for circularity calculation by ImageJ application

D (mm)	No. 1	No. 2	No.3	No. 4	No. 5	Average circularity
0.2						0.710
	0.685	0.721	0.759	0.747	0.636	
1						0.663
	0.597	0.674	0.726	0.694	0.624	
2						0.632
	0.653	0.578	0.591	0.654	0.682	
4						0.537
	0.433	0.504	0.67	0.55	0.53	

(a) Random 5 samples of S1

D (mm)	No. 1	No. 2	No.3	No. 4	No. 5	Average circularity
0.2						0.709
	0.607	0.730	0.690	0.759	0.758	
1						0.695
	0.716	0.758	0.684	0.674	0.669	
2						0.645
	0.602	0.606	0.666	0.681	0.670	
4						0.534
	0.499	0.569	0.586	0.474	0.540	

(b) Random 5 samples of S2

Figure 5. 6: Circularity of slag grains according to four different of grain diameters

The ImageJ application was used to binarize all images and get the perimeter of the grain as given in **Fig.5.7**. The circularity of the grain can be calculated by the Eq. 5.1.

$$\text{Circularity} = \frac{4\pi A}{p^2} \tag{5.1}$$

where *A* is the area of the grain and *p* is the perimeter of the grain. When a grain is exactly circle, circularity becomes 1. The calculated circularities of the two steel slags are shown in **Fig.5.8** along with the image of each grain. As shown in **Fig.5.8(a)** and **(b)**, when the grain size is larger, circularity becomes smaller in both slag. There is no significant difference in average circularities between S1 and S2 slags. It implies that any difference in the slag grain shape between the two slags is unlikely to be a critical factor affecting the different solidification seen for the mixtures prepared with the two slags. Therefore it can be confirmed that the amount of $Ca(OH)_2$ presence in between S1 and S2 is the key factor for getting difference solidification behavior with the two steel slags. The determination of the sphericity and roundness of slag grains provides further understanding of this factor.

5.6 SUMMARY

The comparison of strength obtained by using two different test methods such as direct shear test (DST) and unconfined compression test (UCT) was carried out on the specimen cured from 3 days to 28 days. Further study was made on potential factors affecting the stabilization processes, such as the influence of water salinity and the grain size and shape. Several conclusions are drawn as follows.

1. For strength less than 400 kPa, significant difference of undrained strength obtained by direct shear test (DST) and unconfined compression test (UCT) was identified due to changes in specimens' anisotropic properties and the difference in the loading rates between the UCT and the DST, and based on S_u definition.

2. Although there is no significant influence of pore water salinity on strength, stiffness at

initial curing may differ in seawater compared to the distilled water. This difference in initial curing may be depend on the different rheological properties of the clay in distilled water and seawater mixtures, and the delaying the arrival time of shear wave under the seawater mixing condition at initial curing.

3. The finer gradation in steel slag, which leads to larger specific area provides a greater degree of solidification by enhancing the strength and stiffness. Under the same gradation, the strength increase rates induced by S1 and S2 were even more different, suggesting that the original difference between S1 and S2's gradation is not the cause of the observed difference.

4. There is no significant difference in average circularities between S1 and S2 slags. It implies that the grain shape is not the cause for observed the difference degree of solidification between two slags. Therefore it can be confirmed that the amount of $Ca(OH)_2$ presence in between S1 and S2 is the key factor for explaining different solidification behavior in the two steel slags.

CHAPTER 6 – ASSESMENT OF INTERNAL MICRO-STRUCTURE BY THE X-RAY COMPUTED TOMOGRAPHY (X-Ray CT) ON DIRECT SHEAR SPECIMENS

6.1 INTRODUCTION

The mechanical behavior of soils is highly dependent on the soil microstructure. The microstructure is commonly referred to the soil fabric, which includes the shape, distribution, and arrangement of grains and void space (**Matsushima et al., 2006**; **Mokwa et al., 2011)**. Because of the inherent difficulties in measuring soil properties on a micro scale, geotechnical engineers use macro properties to estimate, or predict, the response of soil when subjected to changes in the state of stress. These macro properties (void ratio, porosity, density, uniformity, etc.) are used to represent gross or average measures of the soil microstructure in terms of engineering behavior; i.e., strength, compressibility, and permeability (**Alshibli et al., 2000**; **Mokwa et al., 2011**).

The non-destructive nature of CT scanning allows the granular soil or rock sample (geomaterials) to be scanned multiple times. Because the soil structure is not affected by the procedure, CT scanning provides an opportunity to investigate particle and pore characteristics at any time and location within a sample. High-quality digital images can be obtained of the microstructure during loading or during environmental changes, such as fluctuations in temperatures or moisture. Tomographic studies on geomaterials conducted during the past two decades (**Otani et al., 2004**; **Alramahi and Alshibli, 2006**; **Mokwa and Nielsen, 2006**) indicate that X-ray CT technology provides a viable means for nondestructively observing, measuring, and quantifying the internal microstructure of geomaterials. The gray-scale in the CT image provides a measure of total attenuation, which is a combination of the mass attenuation and mass density of the material. As explained in **Phillips and Lannutti (1997)**, this attenuation is quantified using the linear attenuation coefficient. In terms of CT imaging technology, the linear attenuation coefficient is related to the density of a pixel and is useful for distinguishing and quantifying different constituents of a specimen.

This chapter focuses on the investigation of the internal micro-structural characteristics in the steel slag-mixed clay specimen. Since the steel slag-mixed clay sample was tapped in three-layer for the preparation of the specimen for the direct shear test, the uniformity of the specimen needs to be confirmed. As a result of tapping the sample, the segregation of the particles in the mixed soil fabric may occur to cause an inhomogeneous distribution of the mixed soil. In addition to observing the initial state, tracking the formation of cracks provides a much better understanding of an internal failure mechanism during shearing. Therefore image-based analysis of failure patterns was performed aided by X-Ray Computed Tomography (X-Ray CT) tests.

6.2 INTERNAL SLAG GRAIN DISTRIBUTION PATTERN OBSERVED BY X-RAY COMPUTED TOMOGRAPHY (X-RAY CT)

6.2.1 Direct shear apparatus with X-Ray Computed Tomography scanning technology

The dredged clay A, showing the strongest solidification under many conditions, was selected for observation the mechanism of micro-structural behavior in the specimen during shearing. Since 30% is a standard ratio often adopted in practice, the two specimens having 30% slag content of S1 mixed with dredged clay A were prepared and cured for separately 1 hour and 14 days before conducting the direct shear test with X-Ray CT scanning.

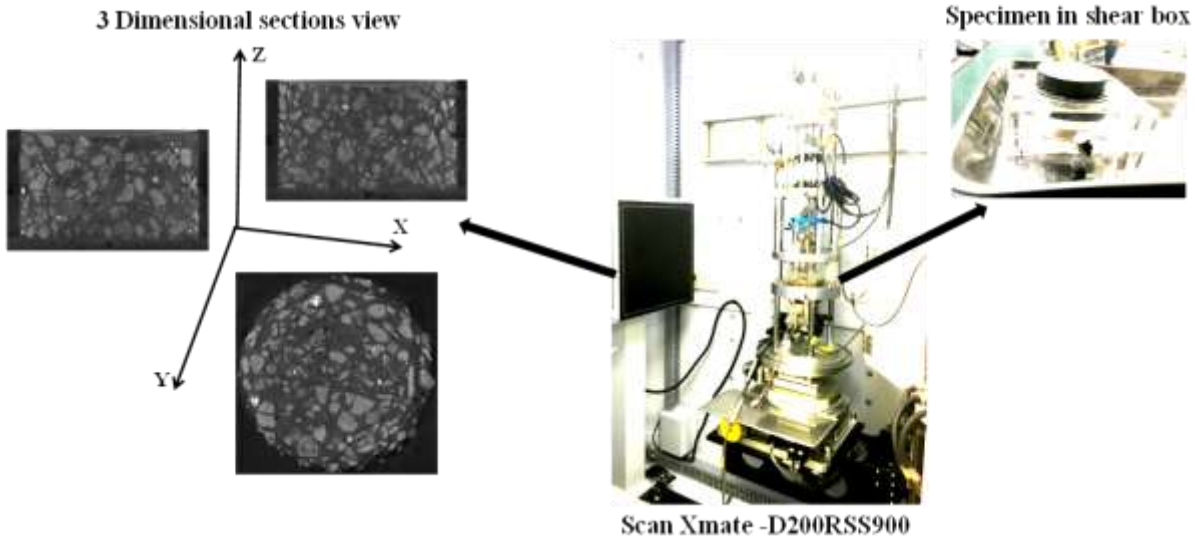


Figure 6. 1: Diagram of direct shear apparatus with X-Ray CT scanning technology

In this study, the two separate direct shear tests were carried on the 1 hour and 14 days cured specimens while it is scanned by the scan Xmate-D200RSS900, which is in the Port and Airport Research Institute in Kanagawa, Japan. The 1 hour cured specimen was prepared in the shear box in a similar way as the previous direct shear tests to represent a soft mixture. The specimen was scanned at every 1 mm shear displacement by interrupting the displacement and rotating the whole direct shear apparatus on the roundtable by 360˚. The shear was continued until the displacement reached while 7 mm. Two-dimensional section views were scanned and three-dimensional data was reconstructed, as shown **Fig.6.1**.

A typical X-Ray equipment configuration is shown in **Fig.6.2**. After scanning a specimen, the recorded data is assimilated into a meaningful digital representation using computer-based algorithms. As one of the primary functions of computed tomography, the recorded X-Ray data is converted into a digital image. Each pixel of a scanned image represents the average density of a voxel (volumetric unit representing a physical space (x, y, z). Image processing can be conducted using a variety of commercially available software packages.

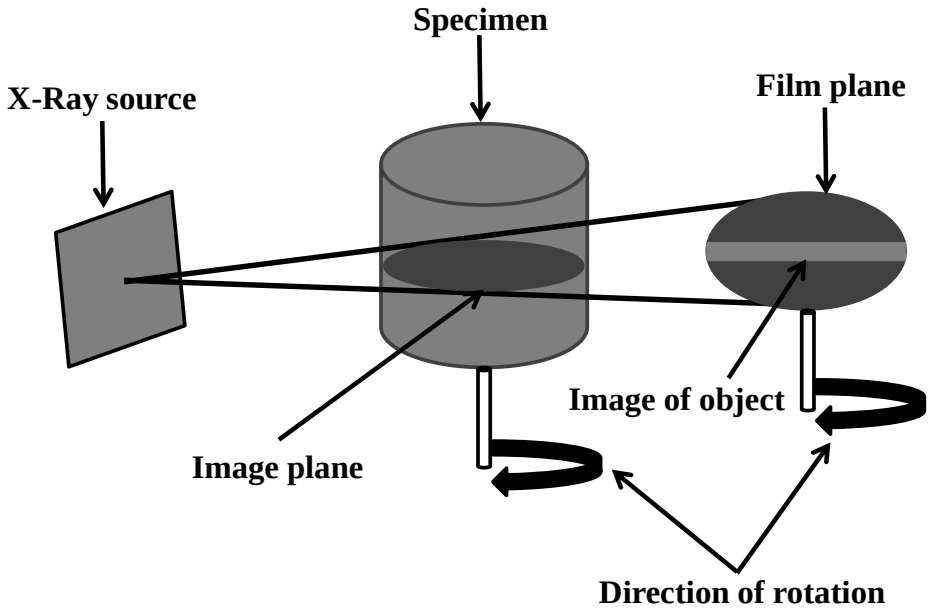


Figure 6. 2: Diagram of typical X-Ray configuration

The approaches described in this study utilized the open source software titled ImageJ, which is an image analysis program originally developed by scientists from the

National Institutes of Health in the United States (**Collins et al., 2007; Schneider et al., 2012**). The software can be downloaded from the developer's website along with numerous 'plug-in' subroutines that provide enhanced image reconstruction and processing applications. Digital images suitable for collecting information about the internal structure of a soil specimen can be used for making quantifiable measurements of basic properties such as grain area, grain size, grain distribution histogram, void ratio and density.

6.2.2 Assessment of uniformity of the specimen

This section focuses on the investigation of the quantitative assessment of the distribution pattern to confirm the initial homogeneity of the specimen. As a basic parameter for quantifying the distribution pattern, number of pixels in each grain and X and Y coordinates of the center of grains are calculated from a raw X-Ray CT image using a series of steps that can be categorized under the following sequence as shown in **Fig.6.3**.

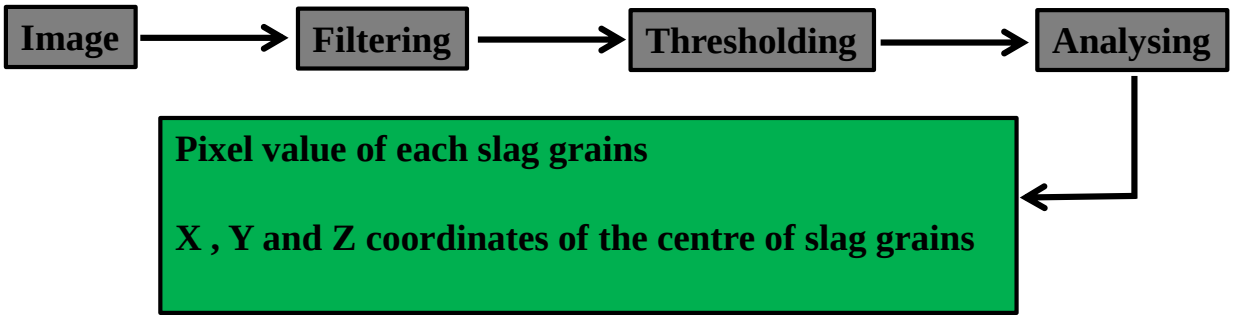


Figure 6. 3: Steps sequence conducted in ImageJ application

Image- In this study, two-dimensional sectional images are selected for calculating grains sizes of each section, i.e., horizontal plane of XY, and vertical planes of YZ, and ZX. The conversion of voxel scale to physical scale (in mm) was conducted by referring to a known length in the image, typically the diameter and height of the specimen.

Filtering- This removes background noise from the image by applying a pixel shading correction and a smoothing feature. For optimizing the filtering, the large structures are filtered down to 40 pixels. The small structures are up to 3 pixels.

Thresholding- This is known as a technique for dividing an image into two (or more)

classes of pixels, which are typically called "foreground" and "background". One of thresholding works by selecting a value cutoff, such that every pixel less than that value is considered one class, while every pixel greater than that value is considered the other class. Therefore to get better thresholding, the threshold value was chosen such that the proportion of pixel representing the slag particle (higher material density and hence the degree of X-ray absorption) coincided with the adopted slag content, 30 %, in the mixture.

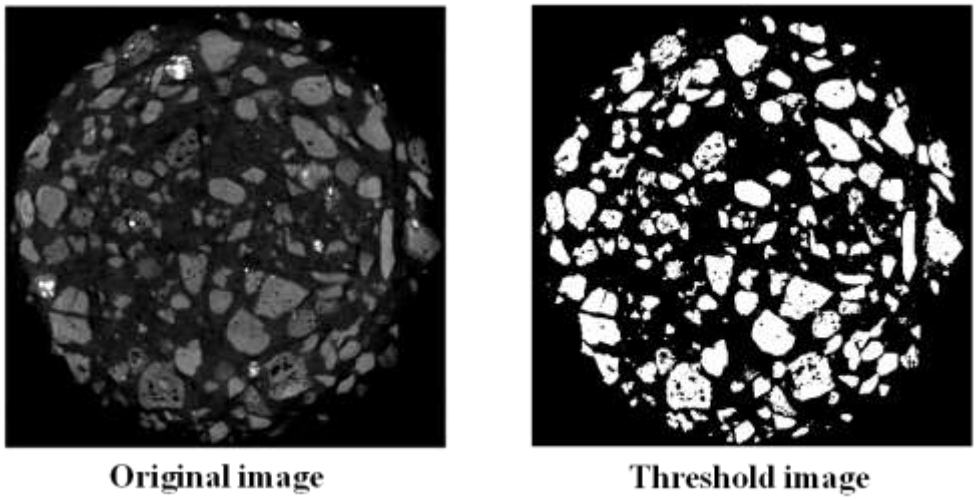


Figure 6. 4: A typical example of an image processed by ImageJ application

Analyzing- From this, the required measurements can be set such as X-Y, X-Z, and Y-Z coordinates of the slag grains, coordinates of center in the slag grains, and the pixel value of the slag grains.

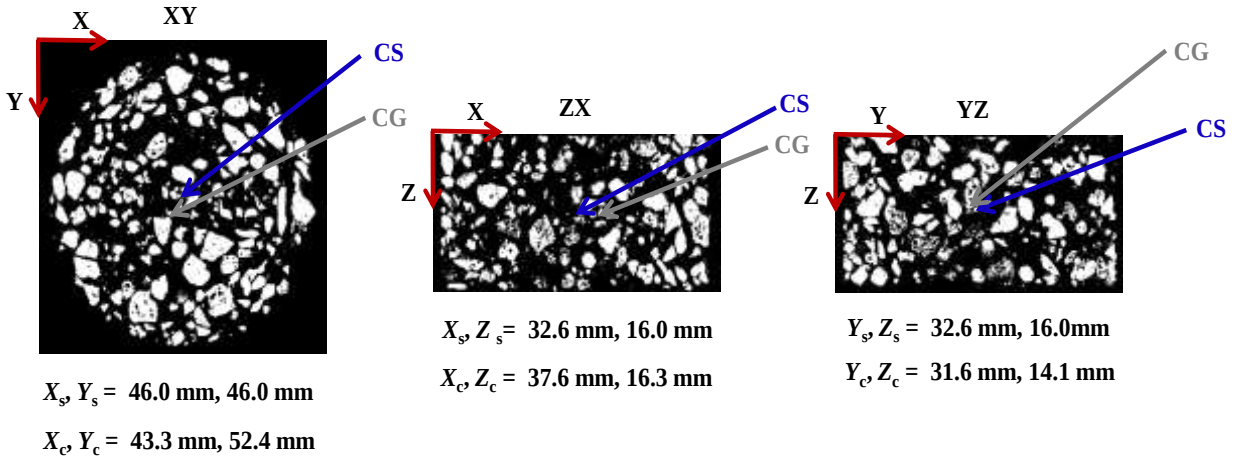
For quantitative assessment of the uniformity of the specimen, the image-based analysis was performed on each plane. The above-mentioned sequence was followed during the ImageJ processing. From the binary images, the center of the specimen domain (CS) coordinates of each plane can be easily determined such as X_s, Y_s, and Z_s. The centre of the geometry of grain assembly (CG) in each plane was calculated based on Eq.6.1 to 6.3.

$$X_c = \frac{\sum_{i=1}^{n} N_i X_i}{\sum_{i=1}^{n} N_i} \quad (6.1)$$

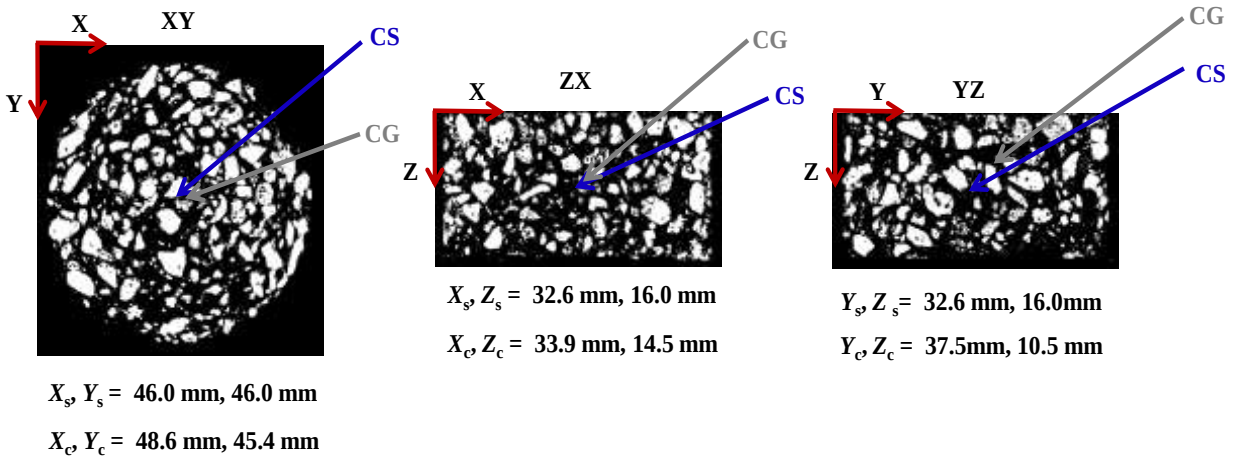
$$Y_c = \frac{\sum_{i=1}^{n} N_i Y_i}{\sum_{i=1}^{n} N_i} \quad (6.2)$$

$$Z_c = \frac{\sum_{i=1}^{n} N_i Z_i}{\sum_{i=1}^{n} N_i} \quad (6.3)$$

where X_c, Y_c, and Z_c are the X, Y and Z coordinate of the center of geometry of grain assembly, n is a number of slag grains, N_i is the pixel value of each slag grain, X_i, Y_i and Z_i are the X, Y and Z coordinate of the center of each slag grain.



(a) 1-hour curing



(b) 14-day curing

Figure 6. 5: Coordinates of center in three-dimensional sectional views for AS1-30%

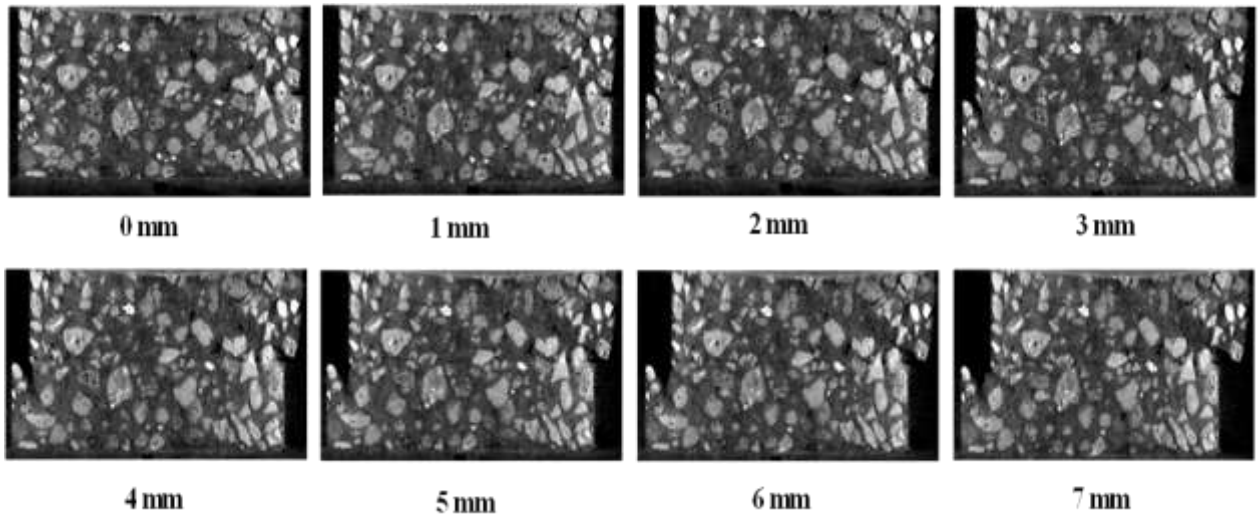
Fig.6.5 shows the coordinates of the center of the specimen domain and the center of geometry of grain assembly of each plane for AS1-30% mixture in 1-hour and 14-day curing. As a qualitative measure, it can confirm the uniform distribution even by visual eye. Although the maximum difference in coordinates between the center of the specimen domain and the center of geometry of grain assembly is less than 6.5 mm, based on the coordinates both center most closely coincide with each other. Therefore, according to this

geometrical interpretation, it implies that three sectional views show no bias of slag grains to a particular edge of the specimen.

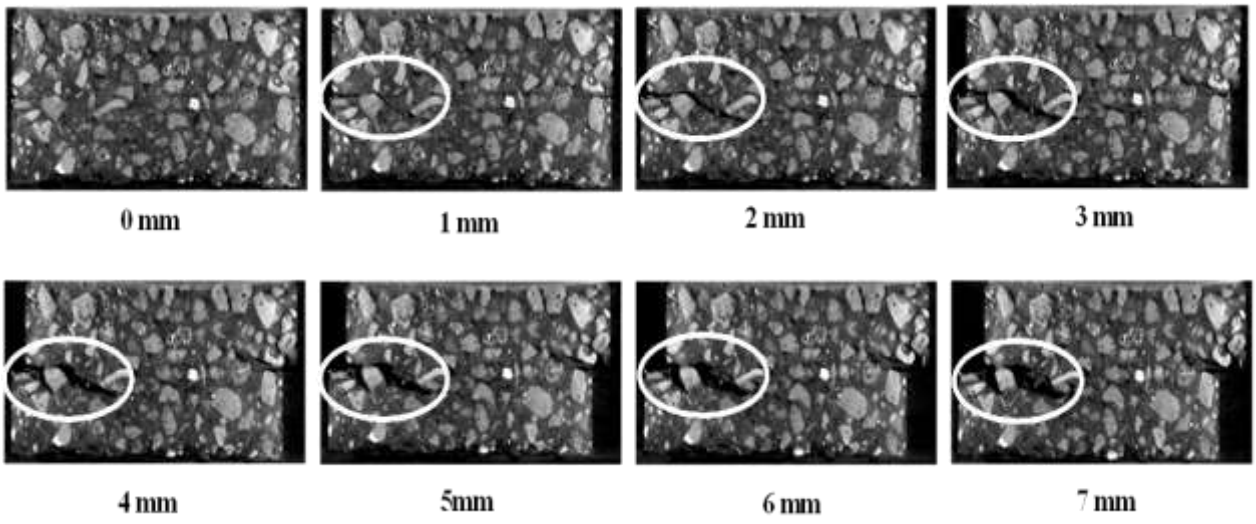
6.3 X-RAY COMPUTED TOMOGRAPHY DURING DIRECT SHEARING OF THE SPECIMEN

6.3.1 Identification of formation of crack during shearing

Materials' ductility/brittleness is governed by both the external conditions around the material and the internal conditions sample. The external conditions include temperature, confining pressure, the pressure of fluids, etc.

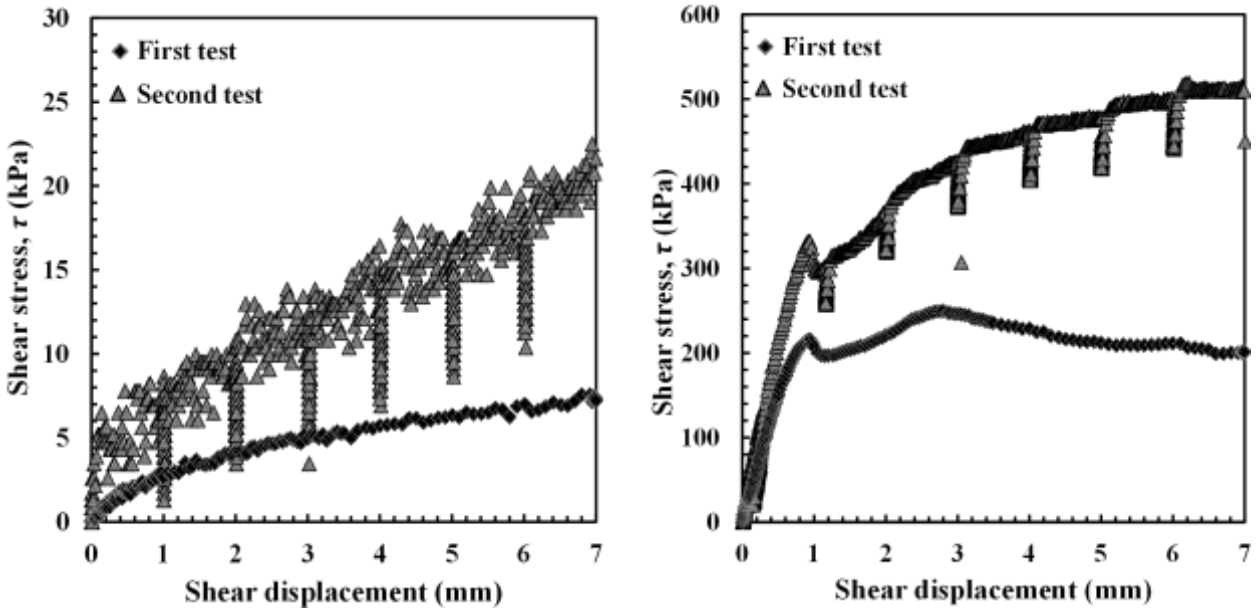


(a) 1-hour curing of AS1-30%



(b) 14-day curing of AS1-30%

Figure 6. 6: Formation of cracks during shearing from 0 mm to 7 mm



(a) 1-hour curing of AS1-30% **(b)** 14-day curing of AS1-30%

Figure 6. 7: Relationship between shear stress and shear displacement obtained by direct shear test discussed in chapter 3 (First test) and X-Ray CT direct shear test in Port and Airport Research Institute (Second test)

In this study, S1 slag mixed specimen shows clear granular soil skeleton as shown in **Fig.6.6(a)** and **(b)**. **Fig.6.7** illustrates X-Ray CT scanned images during shearing from 0 mm to 7 mm for 1-hour and 14-day curing specimens in AS1-30% mixture. It can be obviously noticed that 1-hour cured, soft specimen undergoes ductile behavior. However, 14-day cured specimen clearly shows brittle tendency as circled in **Fig.6.7 (b)**. In spite of constant volume condition during the shearing, there is an open crack on the specimen. The reason can be explained by; the failure of restraining the movement caused by top loading platen of direct shear apparatus due to dilation of coarser materials.

In addition to observing the crack formation, the relationship between shear stress and shear displacement was obtained for two specimens. **Fig.6.8** gives the comparison of shear stress and shear displacement in 1-hour and 14-day curing specimens obtained by the direct shear test discussed in Chapter 3 (First test) and X-Ray CT direct shear test in Port and Airport Research Institute (Second test). The shear stress in the second test shows some relaxation at every 1 mm shear displacement. This behavior is due to the scanning at every 1 mm shear displacement by interrupting the displacement. The shear stress

obtained by the second test is greater than those obtained by the first test. The reason for this variation may be the difference between two direct shear tests, friction and losing the water content of the specimen in the second test. However, the first test can be the most appropriate direct shear test, since it undergoes perfect constant volume condition by restraining the movement of the top loading platen.

6.4 SUMMARY

This chapter focused on the further investigation of the internal micro-structural characteristics in the steel slag-mixed clay specimen. Image-based analysis of failure patterns was performed aided by X-Ray Computed Tomography (X-Ray CT) tests in the Port and Airport Research Institute (PARI) in Kanagawa, Japan. The soft and stiff specimens were scanned during the shearing.

1. The visual observation let in identifying the uniform distribution of the specimen. As a quantitative assessment, the adopted mathematical method shows the coincidence of the center of the specimen domain and the center of geometry of the slag grain assembly of each plane. It implies that three sectional views show no bias of grain concentration to a particular edge of the specimen. This understanding further confirmed that the specimen preparation method adopted in this study was effective in allowing no segregation or grain separation in the specimen.

2. It can be obviously noticed that 1-hour curing specimen, soft specimen underwent ductile behavior. But 14-day cured specimen clearly showed brittle tendency by the formation of clear cracks. Although a similar tendency of shear stress mobilization was observed between two sets of direct shear apparatus, different magnitudes of strength were detected by the two, possibly due to a variety of differences between two direct shear tests, friction and the movement of the top loading platen in the direct shear test of PARI.

CHAPTER 7 – CONCLUSIONS AND RECOMMENDATIONS

Characteristics of strength and stiffness mobilization in steel slag-mixed dredged clay were discussed in this research based on results from series of laboratory mechanical tests and geochemical analyses. The main focus was on the property changes in short to medium curing time, with a purpose of developing a method/criterion for screening out unfavorable mixing conditions and estimating mid-term, 28-day strength, at earlier stages. The strength and stiffness mobilization characteristics of four dredged clays, named A, B, C and D from Japan mixed with two steel slags, S1 and S2 were continuously investigated from immediately after mixing to 28 days of curing in this study by using direct shear apparatus and bender elements. In addition to dredged clays, one of non-marine clay was used: Kasaoka (K) to further investigate the strength and stiffness mobilization. Unlike in more conventionally adopted unconfined compression testing, these tests could be applied to mixed specimens since initial uncemented states, and are useful in detecting the transition of the slurry-like states to more solid states.

The stiffness and strength increase rates in the second, main stage of evolution in the clay-slag mixtures were found to be loosely correlated to the amorphous silica amount. The correlation was also influenced by the $Ca(OH)_2$ amount in slag. The results can be used to screen out clays that are hard to solidify in the medium term, based on quick on-site measurement of amorphous silica amount. For quality control in practice, the strength–stiffness relationship was critically examined as means to assess the strength with non-destructive stiffness probes. A close observation revealed that representing a wide range of curing time and mixing conditions by a single line, as proposed in existing studies, could be misleading. A new interpretation of the relationship is proposed.

The comparison of strength obtained by using two different tests method such as direct shear test (DST) and unconfined compression test (UCT) was carried out on the specimen cured from 3 days to 28 days. The strength greater than 400 kPa shows fair agreement between strength obtained by direct shear test and unconfined compression test. Further study was made on potential factors affecting the stabilization processes, such as the

influence of pore water salinity, and the grain size and shape. There is no significant influence of pore water salinity on strength and stiffness mobilization after 1-day curing. The studying of grain size and shape more convince that the strength development of steel slag can be evaluated to a certain degree by quantifying the amount of $Ca(OH)_2$ in slag by X-Ray diffraction analysis. This study also focused on the further investigation of the internal micro-structural characteristics in the steel slag-mixed clay specimen. The uniform distribution of the slag grains within a direct shear test specimen was identified to confirm the homogeneity of the specimen. The soft specimen which is immediately after mixing (1-hour cured specimen) showed ductile behavior while a stiff specimen having longer curing days (14-day cured specimen) showed brittle tendency by the formation of the cracks.

In this study, only two types of slag were used throughout all experiments. Similar tests on other types of slag will support to understand the possible role played by the slag-derived $Ca(OH)_2$ amount in hydration. From them, the correlations between amorphous silica amount with strength and stiffness increment coefficients can be improved based on the $Ca(OH)_2$ amount. The correlations between stiffness and strength can be modified by introducing additional marine clays. This will help to further understand the validity of proposed correlations between stiffness and strength. The investigation can be continued by mixing artificially silica into clays that are hard to solidify with steel slags. This study provides further the influence of amorphous silica amount on the hydration process in solidification and the possible enhancement of the solidification in weak clay like clay D.

REFERENCES

Ahmari, S., & Zhang, L. (2012). Production of Eco-Friendly Bricks from Copper Mine Tailings through Geopolymerization. *Construction and Building Materials,* 29, 323-331.

Åhnberg, H., & Holm, G. (1999). Stabilization of some Swedish organic soils with different types of binders. *Proceeding of Dry Mixed Methods for Deep Soil Stabilization*, Stockholm, Balkema, 101-108.

Åhnberg, H., & Holmén, M. (2008). Laboratory determination of small-strain moduli in stabilized soils. *Proceedings of the 4 th International Synposium on Deformation Characteristics of Geomaterials, Atlanta (eds S.E. Burns, P.W. Mayne and J.C.Santamarina)*, Amsterdam, the Netherlands: IOS Press., 291-297.

Al Bakri, A. A., Kamarudin, H., Omar, A. K., Norazian, M. N., Ruzaidi, C. M., & Rafiza, A. R. (2011). The effect of alkaline activator ratio on the compressive strength of fly ash-based geopolymers. *Australian Journal of Basic and Applied Sciences*, 5, No.9, 1916-1922.

Alramahi, B., & Alshibli, K. (2006). Application of CT to characterize the internal structure of geomaterials: Limitaions and Challengess. *ASCE Geotechnical Special Publication, Site and Geomaterial Characterization*, 149, 88-95.

Alshibli, K. A., Batiste, S. N., Swanson, R. A., Sture, S., Costes, N. C., & Lankton, M. R. (2000). Quantifying void ratio in sand using Computed Tomography. *ASCE Geotechnical Special Publication*, 106, 30-43.

Al-Tabbaa, A., & Evans, W. C. (2005). Stabilization-Solidification Treatment and Remediation: Part I: Binders and Technologies-Basic Principal. *Proceedings of the International Conference on Stabilization/Solidification Treatment and Remediation* , Cambridge, UK: Balkerma, 367-385.

Aoyagi, K. (1985). Origin of the Miocene Carbonate reservoir rocks, Fukubezawa oil field, Akita province, Northeast Honshu, Japan. In P. O. Roehl, & P. W. Choquette, *Carbonate Petroleum Reservoirs*, 561-571.

Arulrajah, A., Mohammadinia, A., Phummiphan, I., Horpibulsuk, S., & Samingthong, W. (2016). Stabilization of recycled demolition aggregates by geopolymers comprising Calcium Carbide residue, fly ash and slag precursors. *Construction and Building Materials,* 114, 864-873.

Association of Japan Port and Harbor (1999). *Technical standard for port facilities.*

ASTM-D593. (2011). Standard specification for fly ash and other Pozzolanas for use with

lime for soil stabilization. In *In Annual Book of ASTM Standard.* West Conshohocken, PA.

ASTM D3080-98. (2003). Standard test method for direct shear test of soils under consolidated drained conditions. In *Anunual Book of ASTM Standards,* Vol. 04.08, West Conshohocken, PA, 347-352.

ASTM C1437-15. (2015). Standard test method for flow of hydraulic-cement motars. In Anunual Book of ASTM Standards, Vol. 0.4.01, West Conshohocken, PA.

Bădănoiu, A. I., Al-Saadi, T. H., & Voicu, G. (2015). Synthesis and Properties of New Materials Produced by Alkaline Activation of Glass Cullet and Red Mud. *International Journal of Mineral Processing,* 135, 1-10.

Bergado, D., Anderson, L., Miura, N., & Balasubramaniam, A. (1996). *Soft ground improvement in lowland and other environment.* New York: ASCE press.

Brils, J., Boer, P. d., Mulder, j., & Boer, E. d. (2014). Reuse of dredged material as a way to tackle societal challenges. *Journal of Soils Sediments,* 14, 1638-1641.

Chan, C. M. (2014). On the reuse of dregded marine sediments: no dumping, reuse please. *International Journal of Enviromental Engineering,* 1, No.2, 1-9.

Chan, C. M., & Abdul Jalil, A.N. (2014). Some insights to the reuse of dredged marine soils by admixing with activated steel slag, *Advances in Civil Engineering*, Research article.

Chan, C. M. (2015). Pseudo- solidification of Dredged Marine Soils with Cement-Fly Ash for Reuse in Coastal Development. *Journal of WSEAS Transaction on Environemnt Development,* 11, 173-181.

Chan, C. M., & Shahri, Z. (2017). Geo-characterisation of dredged marine soils from Malaysian waters for potential reuse assessment. *ARPN Journal of Engineering and Applied Sciences,* 12, No.14, 4229-4235.

Chan, C. M., Mizutani, T., & Kikuchi, Y. (2012). Solidification of dregded marine clay for sustainable civil engineering applications: a laboratory study. *International conference on Eco-systems and Biological Sciences*, Penang, 27-33.

Chan, C. M., Mizutani, T., & Kikuchi, Y. (2011). Reusing dredged marine clay by solidification with steel slag: a study of Compressive strength. *International Journal of Civil and Structural Engineering,* 2, No.1, 270-279.

Chan, C. M., Pun, K. H., & Ahmad, F. (2013). A Fundamental Parametric Studyon the Solidification of the Malayasian Dredged marine Soils. *World Applied Sciences Journal,* 24, No.6, 784-793.

Cheng, T., & Chiu, J. (2003). Fire-Resistant Geopolymer Produced by Granulated Blast

Furnace Slag. *Minerals Engineering,* 16, 205-2010.

Chiu, C. F., Zhu, W., & Zhang, C. L. (2008). Yielding and shear behavior of cement-treated dredge materials. *Engineering Geology,* 103, No.1, 1-12.

Chrysochoou, M., Grubb, D. G., Drengler, K. L., & Malasavage, N. E. (2010). Stabilized dredged material. III: Mineralogical perspective. *Journal of Geotechnical and Geoenvironemntal Enginnering,* 136, No.8, 1037-1050.

Cokrell, C. F., Muter, R. B., Leonard, J. W., & Anderson, R. E. (1970). *Application of floatation for recovery of calcium constituents from limestone modified fly ash.* Virginia University, Coal Resource Bureau and School of Mines.

Collins, T. J. (2007). ImageJ for microscopy. *BioTechqniques,* 43, No.1, 25-30.

Conley, D. J., Schelske, C. L., & Stoermer, E. F. (1993). Modification of the biogeochemical cycle of silica with eutrophication. *Marine Ecology Progress Series*, 101, 179-192.

Consoli, N. C., Fonseca, A. V., Cruz, R. C., & Heineck, K. S. (2009). Fundermental Parameters for the Stiffness and Strength Control of Artificially Cemented Sand. *Journal of Geotechnical and Geoenvironmental Engineering*, 1347-1353.

Consoli, N. C., Rotta, G. V., & Prietto, P. D. (2000). Influence of curing under stress on the triaxial response of cemented soils. *journal of Geotechnique,* 1, No.50, 99-105.

Cui, H., Kaufman, A. J., Xiao, S., Zhou, C., & Liu, X. M. (2017). Was the Ediacaran Shuram Excursion a globally synchronized early diagenetic event? Insights from methen-derived authigenic carbonates in the uppermost Doushantuo Formation, South China. *Chemical Geology,* 450, 59-80.

Das, B. M. (1990). *Principle of foundation engineering.* Boston: PWS-KENT publishing company.

Davidovits, J. (1991). Geopolymers. *Journal of Thermal Analysis,* 37, 1633-1656.

Deng, Y. F., Zhang, T. W., Zhao, Y., Liu, Q. W., & Wang, Q. (2017). Mechanical behavior and microstructure of steel slag-based composite and its application for soft clay stabilization. *European Journal of Environmental and Civil Engineering*.

Dong, Y., Li, D., Fatahi, B., Zhang, X., & Khabbaz, H. (2017). Small- strain shear modulus of soft clay treated with Saccharomyces cerevisiae and cement. *proceedings of the 19th International Conference on Soil Mechanics and Geotechnical Engineering*, Seoul, 2507-2510.

Essink, K. (1999). Ecological effects of dumping of dredged sediments; options for management. *Journal of Coastal Conservation,* 5, 60-80.

Fakhimi, A., & Hosseinpour, H. (2011). Experimental and numerical study of the effect of an oversize particle on the shear strength of mined-rock pile material. *Geotechnical Testing Journal*, 34, No.2, 131-138.

Ferguson, G. (1993). *Use of self cementing fly ashes as a soil stabilization agent*. American Society of Civil Engineer.

Flores, R. D., Emidio, G. D., & Impe, W. F. (2010). Small-strain shear modulus and strength increase of cement-treated caly. *Geotchnical Testing Journal*, 33, No.1, 62-71.

Gao, X., Yu, Q. L., & Brouwers, H. J. (2015). Properties of alkali activated slag-fly ash blends with limestone addition. *Cement and Concrete Composites*, 59, 119-128.

Geiman, C. M. (2005). Stabilization of soft clay subgrades in Virginia phase I laboratory study. *Master thesis* .

Green, V. G. (2000). Ground and great: Soil stabilization with slag. *Buliding Reasearch and Information* , England, 28, 70-72.

Grubb, D. G., Chrysochoou, M., Smith, C. J., & Malasavage, N. E. (2010). Stabilized Dredged Material. I: Parametric Study. *Journal of Geotechnical and Geoenvironmental Engineering*, 1011-1024.

Ho, L. S., Nakarai, K., Ogawa, Y., Sasaki, T., & Morioka, M. (2017). Strength development of cement-treated soils: Effect of water content, carbonation, and pozzolanic reaction under drying curing condition. *Construction and Building Materials*, 134, 703-712.

Horpibulsuk, S., Rachan, R., Suddeepong, A., & Chinkulkijniwat, A. (2011). Strength development in cement admixed Bangkok clay. *Soils and Foundations*, 51, No.2, 239-251.

Kamon, M., & Nontananandh, S. (1991). Combining industrial wastes with lime for soil stabilization. *Journal of Geotechnical Engineering*, 117, No.1, 1-17.

Kang, G., Tsuchida, T., & Athapaththu, A. M. (2015). Strength mobilization of cement-treated dredged clay during the early stages of curing. *Soils and Foundations*, 55, No.2, 375-392.

Kang, G., Tsuchida, T., Wakioka, H., & Kim, Y. (2015). Strength mobilization of cement-treated marine clays with various curing time. *The 15th Asian Regional Conference on Soil Mechanics and Geotechnical Engineering*, Kyushu: JGS special publication, 2047-2052.

Kasama, K., Zen, K., & Iwataki, K. (2006). Undraine shear strength of cement-treated soils. *Soils and Foundations.*, 46, No.2, 221-232.

Kassim, K. A., Hamir, R., & Kok, K. (2005). Modification and stabilization of Malaysian cohesive soils with lime. *Geotechnical Engineering* ,36, No.2, 123-132.

Kavak, A., & Bilgen, G. (2016). Reuse of ground granulated blast furnace slag (GGBFS) in lime stabilized embankment materials. *IACSIT International Journal of Engineering and technology,* 8, No.1, 11-14.

Kawamura, M., & Diamond, S. (1975). Stabilization of clay soils against erosion loss. *Clay and Clay Minerals,* 443-451.

Kiso, E., Tsujii, M., Ito, K., Nakagawa, M., Gomyo, M., & Nagatome, T. (2008). Method of dredged soil improvement by mixing with converter steel-making slag. *Proceeding of ocean development*, Japan, 327-332.

Kodama, H. (1995). Analysis of Soil Inorganic Amorphous Substances Identification and Determination by One-Seperation Extraction method. *Geological News*, 26-35.

Kodama, H., & Ross, G. J. (1991). Tiron disolution method used to removeand characterize inorganic components in soils. *Soil Science Society of America*, 55, 1180-1187.

Kodama, H., Kotlyar, L. S., & Ripmeester, J. A. (1989). Quntification of crystaline and noncrystaline material in ground kaolinite by X-ray powder diffraction, infrared,solid-staet nuclear magnetic resonance, and chemical dissolution analysis. *Clay Minerals*, 37, 364-370.

Larsson, S. (2001). Binder distribution in lime-cement columns. *Ground Improvement*, 5, No.3, 111-122.

Lee, F. H., Lee, Y., Chew, S. H., & Yong, K. Y. (2005). Strength and Modulus of Marine Clay-Cement Mixes. *Journal of Geotechnical and Geoenvironmental Engineering,* 131, No.2, 178-186.

Locat, J., Berube, M. A., & Choquette, M. (1990). Laboratory investigations on the lime stabilization of sensitive clays: Shear strength Development. *Canadian Geotechnical Journal*, 27, No.3, 294-304.

Lorenzo, G. A., & Bergado, D. T. (2004). Fundamental Parameters of Cement-Admixed Clay-New Approach. *Journal of Geotechnical and Geoenvironemntal Engineering,* 130, No.10, 1042-1050.

MacLaren, D. C., & White, M. A. (2003). Cement: Its Chemistry and Properties. *Journal of Chemical Education,* 80, No.6, 623-635.

Mallela, J. P., Quintus, H. V., & Smith, K. L. (2004). *Consideration of lime-stabilized layers mechanistic-empirical pavement design.* The National Lime Association, Arlington, Virginia, USA.

Mateos, M. (1964). Soil lime research at Iowa State University. *Journal of Soil Mechanics and Foundation Division, ASCE,* 90, No.2, 127-153.

Matsushima, T., Katagiri, J., Uesugi, K., Nakano, T., & Tsuchiyama, A. (2006). Micro X-ray CT at SPring-8 for granular mechanics. *Soil Stress-Strain Behavior: Measurement, Modeling and Analysis Geotechnical Symposium* , Roma, 1-10).

Matsuura, H., Zhou, Q., Katabe, F., Zang, L., Zhang, G., & Tsukihashi, F. (2016). Dissolution mechanism of nutrient elements from steel making slag into seawater. *Advances in Molten Slags, Fluxes, and Salts: Proceedings of the 10th International Conference on Molten Slags, Fluxes, and Salts (MOLTEN16)*, Washington, USA 829-836.

Miki, H., Iwabuchi, J., & Chida, S. (2005). New soil threatment methods in Japan. *The 2nd International Symposium Threatment and Recycling of Materials for Transport Infrastructure*, 1-10.

Mitarai, Y., Nakamura, Y., & Otani, J. (2008). Evaluation of effect of tire chips in the cement stabilized soil using X-ray CT,. *Procedings of the International Workshop on Scrap Tire Derived Geomaterials-Opertunities and Challenges*, London, 224-229.

Mitchell, J.K., Veng, T.S., Monishith, C.L. (1974). Behavior of stabilized soils under repeated loading, Performance evaluation of cement-stabilized soil layers and its relationship to pavement design, *Department of Civil Engineering. University of California*, Berkeley, California.

Miura, N., Taesiri, Y., Koga, Y., & Nishida, K. (1988). Practical of improvement of Ariake clay by mixing admixtures. *Proceeding of International Symposium on shallow sea and low land*,Saga,159-168.

Moh, Z. C. (1962). Soil stabilization with cement and Sodium additives. *Journal of Soil Mechanics and Foundation Division, ASCE*, 88, No.6, 81-105.

Mokwa, R. L., Morris, Z. L., & Lutey, W. A. (2011). *X-Ray computed tomography: A new pedagogical tool for studying micro and macro geomaterial properties.* Montana State University. American Society for Engineering Education.

Mokwa, R., & Nielsen, B. (2006). Characterization of soil porosity using X-ray Computed Tomography. *ASCE Geotechnical Special Publication, Site and Geotchnical Characterization* , 149, 96-103.

Mortlock, R. A., & Froelich, P. N. (1989). A simple method for the rapid determination of biogenic opal in pelagic marine sediments. *Deap-Sea Research,* 36, No.9, 1415-1426.

Nakarai, K., & Yoshida, T. (2015). Effect of carbonation on strength development of cement-treated Toyoura sand . *Soils and Foundations,* 55, No.4, 857-865.

Nanri, M., & Onitsuka, K. (1996). Utility effect by ark shell ash for improving surplus soft construction work. *Environmental Geotechnics,* Kamon, Balkema, Rotterdam, 845-850.

Nelson, D. M., Treguer, P., Brzezinski, M. A., Leynaert, A., & Queguiner, B. (1995). Production and dissolution of biogenic silica in the ocean: revised global estimates, comparison with regional data and relationship to biogenic sedimentation. *Global Biogeochemical Cycles,* 9, 359-372.

Onitsuka, K., & Shen, J. N. (1998). Evaluation of lime-treated Ariake clay with flyash as road materials. *Journal of Pavement Engineering,* 3, 157-164.

Onitsuka, K., & Shen, J. N. (2000). Evaluation of lime-treated Ariake clay with foaming waste glass as road materials. *International Journal of Pavement Engineering* , 1, 35-47.

Otani, J. (2004). State of the art report on geotechnical X-ray CT research at Kumamoto University. *Proceedings of the International Workshop on X-Ray CT for Geomaterials,* Kumamoto, Japan: Balkema, 43-77.

Palmer, A. N., & Palmer, M. V. (1995). Geochemistry of capillary seepage in Mammoth Cave. *Proceedings of the 4th Mammoth Cave Science Confererence*, Mammoth Cave, KY, 119-133.

Phetchuay, C., Horpibulsuk, S., Suksiripattanapong, C., Chinkulkijniwat, A., Arulrajah, A., & Disfani, M. M. (2014). Calcium carbide residue: Alkaline activator for clay-fly ash geopolymer. *Construction and Building Materials,* 69, 285-294.

Phillips, D. H., & Lannutti, J. J. (1997). Measuring physical densitiy with X-Ray Computed Tomography. *NDT and E international,* 30, No.6, 339-350.

Poh, H. Y., Ghataora, G. S., & Ghazireh, N. (2006). Soil stabilization using basic oxygen steel slag fines. *Journal of Materials in Civil Engineering,* 18, No.2, 229-240.

Rajasekaran, G., Kurali, K., & Srinivasaraghavan, R. (1997). Effect on chlorides and sulphates on lime treated marine clays. *Soils and Foundation,* 37, No.2, 105-115.

Reish, J. (1980). Marine and estuarine pollution. *Journal of Water Pollution Control Federation,* 52, 1533-1575.

Reish, J. (1981). Marine and estuarine pollution. *Journal of Water Pollution Control Federation,* 53, 925-949.

Rogers, C. D., & Glendinning, S. (1993). Modification of clay soils using lime. *Proceeding of the Seminar held at Loughborough University on Lime Stabilization*, London: Thomas Telford, 99-114.

Rotta, G. N., Cosoli, N. C., Prietto, P. D., Coop, M. R., & Graham, J. (2003). Isotropic yielding in an artificially cemented soil cured under stress. *Journal of Geotechnique,* 5, No.53, 493-501.

Sarmiento, J., & Gruber, N. (2006). Silicate Cycle. In *Ocean Biogeochemical Dynamics*, 270-313.

Sasanian, S., & Newson, T. A. (2014). Basic parameters governing the behavoir of cement-treaded clays. *Soils and Foundations,* 54, No.2, 209-224.

Schneider, C. A., Rasband, W. S., & Eliceiri, K. W. (2012). NIH image to ImageJ: 25 years of image analysis. *Nat Methods,* 9, No.7, 671-675.

Seng, S., & Tanaka, H. (2011). Properties of cement-treated soils during initial curing stages. . *Soils and Foundations,* 51, No.5, 775-784.

Sherwood, P. (1993). Soil stabilization with cement and lime. *State of the Art Review.* London.

Sherwood, P. T. (1958). *Effect of sulphates on cement-stabilized soils.* National research Council, Washington.

Sherwood, P. T. (1962). *Effect of sulphates on cement and lime-stabilized soils.* National research council, Washington D.C.

Shi, C. (2004). Steel slag-its production, processing, characteristics and cementitious properties. *Journal of Materials in Civil Engineering,* 16, No.3, 230-236.

Solanki, P., & Zaman, M. (2012). Microstructural and Mineralogical CharacteriZation of Clay Stabilized Using Calcium-Based Stabilizers. In *Scanning Electron Microscopy*, 771-798.

Sun, K., Nakano, M., Yamada, E., & Asaoka, A. (2009). Elasto-plastic description of mechanical behaviour on treated soils of the dredged soil of Nagoya port. *Journal of Applied mechanics,* 12, 413-420.

Tang, Y. X., Miyazaki, Y., & Tsuchida, T. (2001). Practices of reused dredging by cement treatment. *Soils and Foundations,* 41, No.5, 129-143.

Temuujin, J., Van Riessen, A., & MacKenzie, K. (2010). Preparation and Characterisation of Fly Ash Based Geopolymer Mortars. *Construction and Building Materials,* 24, 1906-1910.

Terashi, M., Tanaka, H., Mitsumoto, T., Homma, S. and Ohashi, T. (1983). Fundamental properties of lime and cement treated soils (3rd report), *Report of Port and Harbor*

Research Institute, 22, No.1, 69-96, in Japanese.

Thompson, M. R. (1966). Lime reactivity of Illinois soils. *Journal of Soil Mechanics and Foundation Division, ASCE,* 92, No.5, 67-92.

Thompson, M. R. (1966). Shear strength and elastic properties of lime-soil mixtures. *Highway Research Record*, Washington D.C, 139, 1-14.

Toda, K., Otake, T., Sato, T., Sato, H., Weerakoon, N., & Nishimura, S. (2018). Key factors affecting strength development of steel slag-dredged soil mixtures. *Minerals*, 8, No.174, 1-16.

Toohey, M. N., Mooney, M. A., Asche, M., & Bearce, R. G. (2013). Stress-Strain-Strength Behaviour of Lime-Stabilized Soils during Accelerated Curing. *Journal of Materials in Civil Engineering,* 25, No.12, 1880-1886.

Tsuchida, T., & Egashira, K. (2004). The lightweight threated soil method. *New Geomaterials for Soft Ground Engineering in Coastal Areas*.

Tsuchida, T., Tang, T.X., 2012. A consideration on estimation of strength of cement-treated marine clays. *Japanese Geotechnical Society Journa*l. 7, No. 3, 435–447, in Japanese.

Wang, S. D., Scrivener, K. L., & Pratt, P. (1994). Factors Affecting the Strength of Alkali-Activated Slag. *Cement and Concrete Research*, 24, 1033-1043.

Watabe, Y., & Sassa, S. (2015). History of land reclamation using dredged soils at Tokyo Haneda Airport. *The 15th Asian Regional Conference on Soil Mechanics and Geotechnical Engineering*, Fukuoka, 1784-1789.

Wild, S., Abdi, M. R., & Ward, G. L. (1993). Sulphate expansion of lime-stabilized Kaolinite: II. Reaction products and expansion . *Clay Minerals,* 28, No.4, 569-583.

Wild, S., Kinuthia, J. M., Jones, G. I., & Higgins, D. D. (1999). Suppression of swelling associated with ettringite formation in lime stabilized sulphate bearing clay soils by partial substitution of lime with G.G.B.S. *Engineering Geology,* 51, 257-277.

Wild, S., Kinuthia, J. M., Robinson, R. B., & Humphreys, I. (1996). Effects of Ground Granulated Blaster Furnace Slag (GGBS) on the Strength and Swelling Properties of Lime-Stabilized Kaolinite in the Presence of Sulphates. *Clay minerals,* 31, 423-433.

Xiao, H. W., Lee, F. H., & Chin, K. G. (2014). Yielding of cement treated marine clay. *Soils and Foundations*, 54, No.3, 488-501.

Xiao, H., Lee, F. H., & Goh, S. H. (2017). Small strain shear modulus of high cement-admixed marine clay with fibers. *Proceedings of the 19th International Conference of Soil Mechanics and Geotechnical Engineering*, Seoul, 533-536.

Yamagoshi, Y., Kitano, Y., Kosugi, C., Nakagawa, M., Akashi, Y., Kiso, E., & Hata, K. (2015). *Basic characteristics of CaO-improved soil*. Kimitsu: Nippon Steel and Sunitomo Metal Technical Report.

Yamashita, S., Kawaguchi, T., Nakata, Y., Mikami, T., Fujiwara, T., & Shinuya, S. (2009). Interpretation of international parallel test on the measurement of Gmax using bender element. . *Soils and Foundations*, 49, No.4, 631-650.

Zhang, X., Matsuura, H., & Tsukihashi, F. (2012). Dissolution mechanism of various elements into seawater for Recycling the steelmaking slag. *ISIJ International*, 5, No.5, 928-933.